

ELECTRO-WEAK INTERACTIONS  
IN LIGHT NUCLEI

THESIS SUBMITTED FOR THE DEGREE OF  
"DOCTOR OF PHILOSOPHY"

BY  
DORON GAZIT

SUBMITTED TO THE SENATE OF THE HEBREW UNIVERSITY  
OCTOBER 2007

THIS WORK WAS CARRIED OUT UNDER THE  
SUPERVISION OF:  
PROF. NIR BARNEA

To my beloved wife Shani,  
my strength and guide in life.

# ABSTRACT

---

In this thesis, conducted in the field of few-body nuclear physics, I studied low energy inelastic reactions of electro-weak probes on light nuclei.

Such interactions hold experimental and theoretical attention in recent years because of the role they play in various fields of physics, stretching from checking the standard model limits; through nuclear structure and dynamics research; up to microscopic interaction in astrophysical phenomena, such as supernova explosion and the nucleosynthesis of the elements.

The reactions considered in this work are:

- (i) Neutrino interaction with  $A = 3$  and  ${}^4\text{He}$  nuclei, in energies typical to core-collapse supernova. For  ${}^4\text{He}$  both the neutral and charged current reactions were calculated, whereas only neutral current reactions are calculated for  $A = 3$  nuclei.
- (ii) Photoabsorption on  ${}^4\text{He}$ . This long standing problem has been the attraction of theoretical and experimental efforts in the last three decades.

A complete theoretical description of these reactions holds many obstacles. The most significant one arises from the fact that light nuclei are weakly bound and as such they have few, if any, excited states. Thus, evaluation of the nuclear dynamics usually includes a transition between the nucleus ground state and a resonance in the continuum, namely fragments of the initial nucleus interacting with each other in what is commonly known as final state interaction (FSI). As a result, a theoretical study of the reaction should contain both the ground state and the final state interaction. In order to avoid a calculation of a continuum final state, which is currently out of reach

already for  $A = 4$ , I used an integral transform with a lorentzian kernel. This novel method, the Lorentz integral transform (LIT) method allows a reduction of the full scattering problem into a Schrödinger like equation with boundary conditions of a bound state. This equation is solved using the recently developed method of effective interaction hyperspherical harmonics (EIH). The combination of these two methods has been applied in the literature for electro-magnetic and strong reactions. In my thesis, the approach was applied for the first time for weak reactions, and results in a percentage level numerical accuracy.

Photon reactions on nuclear targets are a common experimental method for investigating the nuclear structure and dynamics. In electromagnetic processes, the nuclear forces manifest themselves also as exchange currents, due to gauge invariance. However, one does not have to explicitly calculate their contribution. The conservation of the electromagnetic current allows an application of the Siegert theorem, which in low energy suggests that these currents are included in the single nucleon charge operator. Thus, the scattering operators are model independent. This makes photonuclear processes ideal for experimental study of the nuclear force and structure.

A fundamental example of electromagnetic response which drew continuous interest in the last three decades, both in theory and in experiment, is the  $^4\text{He}$  photodisintegration process. The  $\alpha$ -particle is drawing such a great attention because it has some typical features of heavier systems (e.g. binding energy per nucleon), which make it an important link between the classical few-body systems, viz deuteron, triton and  $^3\text{He}$ , and more complex nuclei. For example in  $^4\text{He}$  one can study the possible emergence of collective phenomena typical of complex nuclei like the giant dipole resonance. Furthermore,  $^4\text{He}$  is the ideal testing ground for microscopic two- and three-body forces, which are fitted in the two- and three-body systems. One expects that the 3NF is of considerably greater relevance in the four-body system, as the number of triplets is bigger, and due to its higher density.

The microscopic calculation of the  $^4\text{He}$  photoabsorption process presented here is the first evaluation of the cross-section which includes realistic NN potential, Argonne  $v_{18}$ , and 3NF, Urbana IX, and full final state interaction, taken into account via the

LIT method. The resulting cross-section is characterized by a pronounced peak, due to a dipole excitation. We have found that the 3NF only slightly lowers the peak (by about 6%). This effect is much smaller than the 20% effect on the binding energy, and than the influence expected when compared to the  ${}^3\text{H}/{}^3\text{He}(\gamma)$  processes. The effect of the 3NF grows at higher energy transfer to about 35%.

The comparison to experiments is unclear, mainly due to the poor status of the experimental data, in which the differences reach a factor of 2. However, close to threshold the theoretical cross section agrees quite well with all experiments. In the giant resonance region of the cross-section, where there are several experimental evaluations of the cross-sections which in some cases do not agree, the theoretical results are in good agreement with the majority of the available data.

The photoabsorption process can be used to infer properties of the ground state. In fact, moments of the total photoabsorption cross-section lead to known sum-rules, which are indicative for different characteristics of the ground state, such as the charge radius and the nucleon-nucleon distance. In particular, the configuration tetrahedral symmetry of  ${}^4\text{He}$  is tested, and this symmetry is found to be slightly broken. This observation, which can be tested in experiments, suggests that the mean distance between identical nucleons is slightly (6%) larger than the mean distance between proton and neutron.

The second branch of the work investigates inelastic neutrino scattering on  $A = 3$  and  ${}^4\text{He}$  nuclei in core-collapse supernova scenario. Inelastic neutrino interaction with nuclei can potentially influence several properties of the physics in the supernova. Firstly, they may change the structure of the neutrino signals. Secondly, they can deposit energy in the matter behind the stalled shock, thus might change its temperature and even revive the shock. Finally, they change the chemical composition of the star by breaking nuclei to fragments. The high abundance of  ${}^4\text{He}$  nuclei both in the shocked area and in the outer layers of the star, may result in an effect on these processes.

Lately, we have discovered that a substantial amount of trinuclei can exist in the neutrinosphere of the newly born proto-neutron star. This is a result of the previously

neglected interaction between nuclei in that area. Thus, neutrino interaction with these nuclei may affect the neutrino spectra.

These facts motivate evaluation of the cross-sections. In this work, the first *ab-initio* calculation of the inelastic reactions is given, with realistic forces: AV18 NN potential and UIX 3NF. By using the LIT method, all break-up channels are considered. The vector meson exchange currents are implicitly calculated using the Siegert theorem. The contribution of the (non-conserved) axial meson exchange currents to the cross sections has to be calculated explicitly. I cope with this by using effective field theory of QCD at low energy, with the nucleons and pions as explicit degrees of freedom. The axial currents are calibrated to reproduce the triton half-life, within this nuclear Hamiltonian, thus enabling parameter-free prediction of the cross-sections. This calculation procedure, known in the literature as EFT\*, has been tested successfully in the calculation of numerous weak reactions, e.g. Park *et. al* calculated *pp*-fusion and *hep* process. The current work is the first application of the method for the calculation of complete inelastic processes, not only on-threshold.

The contribution of the exchange currents to the  $\nu - \alpha$  scattering process is negligible, due to the “closed shell” character of this nucleus. However, the effect of meson exchange currents in the case of neutrino scattering on mass-three nuclei is about 20% of the cross-section for low neutrino temperature. As neutrino temperature increases, the effect reduces to less than 2% for neutrino temperatures above 5 MeV.

The error estimation, for both  $\alpha$  and the trinuclei, due to the effective theory cutoff dependence of the cross-section is less than a percent, for neutrino temperatures higher than 2 MeV. This is a strong validation of the calculation.

The neutrino scattering cross-section is found to be rather sensitive to the properties of the force model. Thus, the predicted neutrino scattering cross-sections are considered to be of 5% accuracy.

The reactions calculated in this thesis make an important step towards more precise predictions made by nuclear physics. These predictions have the ability to check the properties of the nuclear forces on the one hand, and on the other hand to be used as accurate and reliable microscopic input for simulations of astrophysical phenomena.

# CONTENTS

---

<b>Abstract</b>	<b>iv</b>
<b>1 Introduction</b>	<b>1</b>
1.1 Photodisintegration of ${}^4\text{He}$ . . . . .	4
1.2 Neutrino Scattering on Light Nuclei in Supernova . . . . .	6
1.3 About this thesis . . . . .	8
<b>2 Scattering of electro-weak probes on Nuclei</b>	<b>10</b>
2.1 Neutrino Scattering . . . . .	11
2.1.1 Cross section calculation for neutrino scattering processes . . . . .	13
2.2 Relations Between Multipoles and the Siegert theorem . . . . .	16
2.2.1 Siegert Theorem . . . . .	18
2.3 Photoabsorption on Nuclei Up To Pion Threshold . . . . .	18
<b>3 Chiral Effective Field Theory</b>	<b>20</b>
3.1 QCD symmetries at low energy . . . . .	20
3.2 Power Counting of Chiral Perturbation Theory . . . . .	23
3.3 Effective Lagrangian . . . . .	24
3.3.1 Pion Lagrangian . . . . .	24
3.3.2 Pion–Nucleon Interaction Lagrangian . . . . .	25
3.3.3 Nucleon Contact terms in the Lagrangian . . . . .	26
3.4 Currents in the Nucleus . . . . .	27
3.5 Nuclear Currents Operators . . . . .	29
3.6 Standard Nuclear Physics and EFT . . . . .	33

<b>4</b>	<b>Lorentz Integral Transform Method</b>	<b>35</b>
4.1	Integral Transformations . . . . .	36
4.2	Integral Transform with a Lorentzian Kernel . . . . .	37
4.2.1	Calculation of LIT using the Lanczos Algorithm . . . . .	39
4.3	Inversion of the LIT . . . . .	40
<b>5</b>	<b>Nuclear Wave functions</b>	<b>43</b>
5.1	Few-Body problems in terms of the Hyperspherical Harmonics . . . . .	43
5.1.1	Hyperspherical Coordinates . . . . .	44
5.1.2	The Hyperspherical Harmonics Functions . . . . .	46
5.1.3	The Hyperspherical Formalism with Internal Degrees of Freedom . . . . .	50
5.1.4	Matrix Elements within the Hyperspherical Formalism . . . . .	53
5.2	Effective Interaction with the Hyperspherical Harmonics . . . . .	54
5.2.1	Lee-Suzuki Approach for Effective Interactions . . . . .	55
5.2.2	EIHH method . . . . .	57
<b>6</b>	<b>Photoabsorption on <math>^4\text{He}</math> with a realistic nuclear force</b>	<b>59</b>
6.1	Photoabsorption Calculation . . . . .	59
6.1.1	The Unretarded Dipole Approximation . . . . .	59
6.1.2	Calculation of The Response Function . . . . .	60
6.1.3	Results and Discussion . . . . .	63
6.2	Photonuclear Sum Rules and the Tetrahedral Configuration of $^4\text{He}$ . . . . .	67
6.2.1	SR and the Nucleus Ground State . . . . .	69
6.2.2	Calculation of SR using the LIT method . . . . .	72
6.2.3	Results and Discussion . . . . .	73
<b>7</b>	<b>Neutrino Scattering on Light Nuclei in Supernovae</b>	<b>78</b>
7.1	Core-collapse Supernovae . . . . .	78
7.1.1	Shock revival and Light Nuclei . . . . .	80
7.1.2	Nucleosynthesis and $\nu - \alpha$ Interaction . . . . .	82
7.2	Weak Interaction Observable – Beta Decay Rate . . . . .	84
7.3	Neutrino Scattering Cross-sections Calculation . . . . .	87

7.3.1	Leading Multipole Contributions . . . . .	88
7.3.2	Inelastic Cross-sections and Energy-transfer . . . . .	89
7.3.3	Neutrino scattering on ${}^4\text{He}$ nucleus . . . . .	90
7.3.4	Neutrino scattering on $A = 3$ nuclei . . . . .	94
7.3.5	Neutrino energy loss due to inelastic scattering . . . . .	95
<b>8</b>	<b>Conclusions</b>	<b>98</b>
8.1	Photoabsorption on ${}^4\text{He}$ . . . . .	98
8.2	Neutrino Interaction with ${}^4\text{He}$ and $A=3$ nuclei in Supernova . . . . .	99
<b>A</b>	<b>Weak Currents In the Standard Model</b>	<b>101</b>
<b>B</b>	<b>Lepton Current</b>	<b>103</b>
<b>C</b>	<b>Non-relativstic expansions of Dirac spinors expressions</b>	<b>106</b>
<b>D</b>	<b>Feynman Diagrams for <math>\chi\text{PT}</math></b>	<b>107</b>
D.1	Leading Order Diagrams . . . . .	107
D.2	Next-to Leading Order Diagrams . . . . .	108
D.3	Example: Single Nucleon Operators For Neutrino Scattering . . . . .	109
D.4	Example: Axial MEC Operators For Neutrino Scattering . . . . .	110
<b>E</b>	<b>Reduced Matrix Elements of different opearators</b>	<b>114</b>
E.1	2-Body Matrix Elements . . . . .	117
	<b>Bibliography</b>	<b>119</b>
	<b>Acknowledgements</b>	<b>127</b>

# LIST OF TABLES

---

6.1	Convergence of HH expansion for the ${}^4\text{He}$ binding energy $E_b$ [MeV] and root mean square matter radius $\langle r^2 \rangle^{\frac{1}{2}}$ [fm] with the AV18 and AV18+UIX potentials. Also presented are results of other methods (see text). . . . .	61
6.2	Convergence in K of the SR for AV18+UIX potentials. The converged AV18 results are also shown. The last two lines of the table show the convergence in $\bar{\omega}$ of the various moments. . . . .	74
7.1	Binding energies of ${}^3\text{H}$ and ${}^3\text{He}$ calculated using AV18/UIX Hamiltonian model compared to the same calculation done by using FY equations and expansion on correlated hyperspherical harmonics (CHH) basis (Nogga et al., 2003). For the EIH calculation, the number in parenthesis indicates the numerical error. Also shown are the experimental values. . . . .	86
7.2	Temperature averaged neutral current inclusive inelastic cross-section per nucleon as a function of neutrino temperature. The last column is the calculation in Woosley et al. (1990). . . . .	93
7.3	Temperature averaged inclusive inelastic cross-section (upper part) and energy transfer cross-section (lower part) per nucleon as a function of temperature. . . . .	93

7.4 Averaged neutrino- and anti-neutrino- $^3\text{H}$  and  $^3\text{He}$  neutral-current inclusive inelastic cross-sections per nucleon ( $A=3$ ),  $\langle\sigma\rangle_{T_\nu} = \frac{1}{2A}\langle\sigma_\nu + \sigma_{\bar{\nu}}\rangle_{T_\nu}$  (left columns), and energy transfer cross-sections,  $\langle\omega\sigma\rangle_{T_\nu} = \frac{1}{2A}\langle\omega\sigma_\nu + \omega\sigma_{\bar{\nu}}\rangle_{T_\nu}$  (right columns), as a function of neutrino temperature  $T_\nu$ , in units of  $10^{-42}\text{ cm}^2$  and  $10^{-42}\text{ MeVcm}^2$  respectively. . . . 95

# LIST OF FIGURES

---

2.1	Neutrino scattering processes and their kinematics: (a) charged current $e^+$ production; (b) charged current $e^-$ production; (c) neutral current process . . . . .	12
2.2	Effective vertex for low energy weak interactions. . . . .	12
6.1	Convergence of $\mathcal{L}_{K_m}$ with $\sigma_I = 10$ MeV (AV18+UIX). . . . .	62
6.2	Convergence of $\Delta_{K_m} = (\mathcal{L}_{K_m} - \mathcal{L}_{19})/\mathcal{L}_{19}$ (AV18+UIX). . . . .	63
6.3	Convergence of $\sigma_{\gamma, K_m}$ (AV18+UIX), also shown $\sigma_{\gamma, 17}^\infty$ and $\sigma_{\gamma, 19}^\infty$ . . . . .	64
6.4	Total ${}^4\text{He}$ photoabsorption cross section: (a) $\sigma_\gamma$ (MT, AV18) and $\sigma_{\gamma, 19}^\infty$ (AV18+UIX); experimental data from (Arkatov et al., 1979). (b) as (a) but also included upper/lower bounds and various experimental data (see text), area between dotted lines (Berman et al., 1980; Feldman et al., 1990), dotted box (Wells et al., 1992), squares (Nilsson et al., 2005), and circles (Shima et al., 2005). . . . .	65
7.1	Density profile of $11M_\odot$ star, 120 milliseconds after bounce. The black line is the total density, and the red line is the $\alpha$ mass fraction. One can view the accretion shock at about 200 km off center. . . . .	81
7.2	Mass fractions of nucleons and $A = 3, 4$ nuclei in chemical equilibrium as a function of temperature $T$ . The top and bottom rows correspond to a density of $10^{11}$ g/cm $^3$ and $10^{12}$ g/cm $^3$ respectively, and from left to right the proton fractions are $Y_p = 0.1, 0.3$ and $0.5$ . . . . .	82

7.3	Relative error in the sum-rule of the leading response functions with respect to the hyper-angular momentum quantum number $K$ (for ${}^4\text{He}$ ). Calculated using the AV8' NN potential model. The error bars reflect the uncertainty in inverting the LIT. . . . .	91
7.4	Convergence of $\mathcal{L}_{\hat{O}_1\hat{O}_2}/q$ for the leading operators, as a function of the HH grand angular momenta $K$ (for ${}^4\text{He}$ ). . . . .	92
7.5	Temperature averaged inelastic cross-sections at temperature $T = 10$ MeV for ${}^4\text{He}$ . The solid line is the differential cross-section, $\langle \frac{d\sigma}{d\omega} \rangle_T = \frac{1}{2} \frac{1}{A} \langle \frac{d\sigma_\nu}{d\omega} + \frac{d\sigma_\pi}{d\omega} \rangle_T$ , (left scale). The dashed line is the differential energy transfer cross-section, $\langle \omega \frac{d\sigma}{d\omega} \rangle_T = \frac{1}{2} \frac{1}{A} \langle \omega \frac{d\sigma_\nu}{d\omega} + \omega \frac{d\sigma_\pi}{d\omega} \rangle_T$ , (right scale). . . . .	94
7.6	Relative contribution of MEC to the energy transfer, i.e. $\frac{\langle \omega \sigma \rangle_{T_\nu}^{MEC} - \langle \omega \sigma \rangle_{T_\nu}^{No\ MEC}}{\langle \omega \sigma \rangle_{T_\nu}^{No\ MEC}}$ . The width of the line indicates the error in the theoretical estimate, due to the cutoff dependence. . . . .	96
7.7	Neutrino total energy transfer cross-section a function of the neutrino temperature $T_\nu$ for $A = 3, 4$ nuclei. . . . .	97
7.8	Neutrino energy loss $dE_\nu/dx$ for inelastic excitations of $A = 3, 4$ nuclei as a function of the matter temperature $T$ at a density of $10^{12}$ g/cm $^3$ . We assume that the neutrino energies are characterized by a Fermi-Dirac distribution with a temperature $T_\nu = 6$ MeV. The contributions from ${}^3\text{H}$ , ${}^3\text{He}$ and ${}^4\text{He}$ nuclei, and the total neutrino energy loss are shown for proton fractions $Y_p = 0.1, 0.3$ and $0.5$ . . . . .	97
D.1	The lowest order pion - nucleon Feynman diagrams. Nucleons are indicated by solid lines, whereas pions are indicated by dashed lines. . . . .	107
D.2	Vertices in the axial current. Crossed circles indicate the attachment to the external probe. . . . .	108
D.3	Contact axial vertex in NLO. . . . .	109
D.4	Leading order 1-body axial vector current. . . . .	110
D.5	Pion-production on a nucleon. . . . .	111
D.6	Pion exchange contribution to the scattering amplitude . . . . .	112
D.7	Pion production contribution from NLO lagrangian. . . . .	113

# 1 INTRODUCTION

---

The physics of the atomic nucleus has drawn a large amount of attention since the dawn of quantum mechanics, fascinating physicists in its diversity and complexity. Understanding the nuclear world has led to many practical uses, the examples stretch from medical application, where radioactive and nuclear magnetic resonance mappings are already standard procedures; through nuclear reactors, in which one makes use of the energy released in stimulated nuclear decays as a power source; and finally to the destructive power of nuclear weapons.

The nucleus is a complex entity, built of nucleons held together by the strong force. A nucleon is a common name for both neutrons and protons, emphasizing the approximated symmetry of their response to the strong force, and their similar mass. Determining the properties of the strong force was, and still remains, a scientific challenge. It is accepted today that the strong force is the low energy appearance of quantum chromodynamics (QCD). However, deriving the nuclear force from the fundamental theory is an open question, due to the non-perturbative character of QCD in low energy.

The modern nuclear physics has two main approaches to meet this problem, a semi-phenomenological approach and an effective field theory (EFT) approach. In the semi-phenomenological approach the potential includes all functional shapes and operators allowed by Poincarè and isospin symmetry of QCD. The parameters for this potential are calibrated by experimental scattering phase shifts. A clear disadvantage is that the fit of the parameters is not unique as the theory lacks a clear connection to the underlying theory, a fact which leads to a questionable predictive measure. However, the approach has many successes. One of its important consequences is identifying the need of adding attractive three nucleon forces (3NF) to fit the spectra of  $A \geq 3$  nuclei. The realistic semi-phenomenological potentials combined with 3NFs

successfully reproduce the low lying spectra of  $A < 12$  nuclei.

The EFT approach uses the chiral symmetry of QCD to describe the force among nucleons. The approach leads to a consistent perturbative expansion of the interaction, with numerical coefficients which contain information about higher energy degrees of freedom. These coefficients can be in principal calculated from QCD, but due to the aforementioned difficulties are usually calibrated using low energy experiments. Among obvious advantages, in this approach the 3NF are predicted and appear at higher order of perturbation theory, thus less important - as also found phenomenologically. However, in order to reach the accuracy achieved in describing the entirety of problems as the semi-phenomenological approach one has to expand the potentials up to next-to-next-to-next-to leading order ( $N^3LO$ ). Such potentials are still not completely available (see however (Epelbaum et al., 2000; Entem and Machleidt, 2003)).

It is of great interest to check the success of both approaches in predicting dynamical observables of nuclei. This is not a simple task. The problem arises from the need to solve the Schrödinger equation in  $3A - 3$  dimensions, with substantial inter-particle correlations. Without any further approximations, this is an example of the few-body quantum problem, which explores the response of  $A$  bodies to the forces between them. Even today, this problem lacks a general mathematical solution, mainly in cases of scattering to continuum states. For bound state problems, the last decade has brought immense progress, due to theoretical advances and increasing available computer power. A variety of methods solving the nuclear problem microscopically (for bound states) have evolved, among which are the No Core Shell Model (Navrátil and Barrett, 1996), Green Function Monte Carlo (Wiringa et al., 2000), Stochastic Variational Method (Suzuki and Varga, 1998) and the Effective Interaction Hyper-spherical Harmonics approaches, which have been used for calculations of nuclei in the medium range ( $A > 4$ ).

Contrary to this, calculations of reactions have not met this success. Specifically, light nuclei are weakly bound and as such they have few, if any, bound excited states. Thus, experiments designed to study nuclear dynamics include a transition between the nucleus ground state and the continuum. The latter are essentially fragments

interacting with each other in final state interaction (FSI). It is clear that a complete theoretical evaluation of the reaction should include an accurate description of both the ground state and the final state interaction. An exact calculation of a final state in the continuum for all break-up channels is out of reach already for  $A = 4$ . In order to avoid a calculation of a continuum final state one can use an integral transform with a lorentzian kernel. This novel method, the Lorentz integral transform (LIT) method (Efros et al., 1994) reduces the full scattering problem to a Schrödinger like equation with bound state boundary conditions. This equation can be solved using the above mentioned few-body methods, and in this thesis the modern method of effective interaction hyperspherical harmonics (EIHH) method (Barnea et al., 2000, 2001b; Barnea and Novoselsky, 1997) is used for solving the LIT equations.

The combination of the LIT and EIHH methods allows nuclear theory to describe reactions of complex nuclei with  $A \geq 3$  which were previously unreachable in *ab initio* calculations. The methods have proven successful for the calculation of the total photoabsorption cross-section (Orlandini, 2004) and inclusive electron-scattering process of  $A = 3$  nuclei (Efros et al., 2004), with realistic nucleon-nucleon potential and 3NF. Calculations of photoabsorption and electron scattering processes using semi-realistic forces were done for  $A = 4 - 7$  body systems, giving quite realistic results in comparison with experiments (Bacca et al., 2004, 2002; Efros et al., 1997b,c).

The focus of this thesis is the accurate modeling and calculation, feasible by using the LIT and EIHH methods, of electro-weak interaction with light nuclei, specifically neutrino scattering and photoabsorption on nuclei. Electro-weak reactions are of central importance not only due to their use in experiments which probe nuclear structure and force properties. Their importance stems also from the role they play in cosmic and stellar events. This research field, “nuclear astrophysics”, evolved in the last century from the understanding that in many astrophysical phenomena the typical thermodynamic conditions are so extreme that nuclear reactions can be induced thermally. By this observation, nuclear physics has turned to be the microscopic ingredient used to address astrophysical mysteries. For example, energy released in nuclear fusion has been discovered to be the fuel of stars, thus nuclear theory sets the main properties of a star, i.e. its composition, evolution and way of death. Another

key question addressed in nuclear astrophysics is the origin of the variety of elements in nature. Big-bang nucleosynthesis, i.e. the synthesis of light elements in the early stages of the universe, provides a hatch to physics in the first three minutes of the universe. The rest of the elements are believed to be produced during the evolution of a star and mainly in the extreme conditions of its death, in a supernova. In this work, neutrino reactions with  $A = 3$  and  ${}^4\text{He}$  are calculated. These reactions are of interest in the description of the exploding death of a massive star, and in the nucleosynthesis within, as will be explained.

In the next two sections we will elaborate on the specific processes addressed in this thesis.

## 1.1 Photodisintegration of ${}^4\text{He}$

Photonuclear reactions are a common experimental method for investigating the nuclear structure and dynamics. In these processes, a real photon excites a nucleus. The perturbative character of the electromagnetic interaction, dictated by the fine structure constant  $\frac{e^2}{\hbar c} \ll 1$ , makes it possible to separate the scattering process and the nuclear properties affecting the process. The photon, as a result, is ideal for experimental study of nuclei.

A fundamental example of an electromagnetic response which drew a continuous interest in the last three decades, both in theory and in experiment (see (Nilsson et al., 2005; Shima et al., 2005) and references therein), is the  ${}^4\text{He}$  photodisintegration process. The  $\alpha$ -particle is drawing such a great attention because it has some typical features of heavier systems (e.g. binding energy per nucleon), which make it an important link between the classical few-body systems, viz deuteron, triton and  ${}^3\text{He}$ , and more complex heavy nuclei. For example, in  ${}^4\text{He}$  one can study the possible emergence of collective phenomena typical of complex nuclei. Such a phenomenon is the giant dipole resonance, an enhanced cross section in the range 10 – 30 MeV found in heavy nuclei, due to an  $E^1$  dipole excitation. Furthermore,  ${}^4\text{He}$  is the ideal testing ground for microscopic two- and three-body forces, which are fitted in the two- and three-body systems. At present the 3NF is not yet well determined, thus

it is essential to search for observables where it plays an important role. Because of gauge invariance, in electromagnetic processes nuclear forces manifest themselves also as exchange currents, which have turned out to be very important in photonuclear reactions and hence 3NF effects might become significant. For the three-nucleon systems photonuclear processes have already been studied (Efros et al., 2000; Golak et al., 2002, 2005), e.g. in Efros et al. (2000) it was found that the 3NF leads to an almost 10% reduction of the electric dipole peak and up to 15% enhancement at higher energy. One expects that the 3NF is of considerably greater relevance in the four-body system, since it involves six nucleon pairs and four triplets, compared to three pairs and just one triplet in the three-nucleon systems. In addition, the higher density of  ${}^4\text{He}$  might enhance the importance of the 3NF.

The  ${}^4\text{He}(\gamma)$  reaction represents a very challenging theoretical problem due to the fact that the nucleus has no bound excited states, so the full four-body continuum dynamics and all possible fragmentation have to be considered. It is of no surprise that the current theoretical situation of the  ${}^4\text{He}$  photodisintegration is not sufficiently settled. Calculations with realistic nuclear forces have not yet been carried out, and exist only for semi-realistic nucleon-nucleon (NN) potentials. In Refs. (Efros et al., 1997b; Barnea et al., 2001a; Quaglioni et al., 2004) it has been shown that such models lead to pronounced peak cross sections, in rather good agreement with the data of Nilsson et al. (2005) and much different from what was calculated earlier (Ellerkmann et al., 1996).

A similar status holds for the experimental research of the process, as most of the experimental work has concentrated on the two-body break-up channels  ${}^4\text{He}(\gamma, n){}^3\text{He}$  and  ${}^4\text{He}(\gamma, p){}^3\text{H}$  in the giant resonance region, but a large disagreement still exists in the peak. In fact in two very recent  $(\gamma, n)$  experiments (Nilsson et al., 2005; Shima et al., 2005) one finds differences of a factor of two.

It is evident that the experimental and theoretical situations are very unsatisfactory. In this thesis I present an important step forward on the theory side performing a calculation of the total photoabsorption cross section  $\sigma_\gamma$  of  ${}^4\text{He}$  with a realistic nuclear force, namely Argonne V18 (AV18) NN potential (Wiringa et al., 1995) and the Urbana IX (UIX) 3NF (Pudliner et al., 1997).

## 1.2 Neutrino Scattering on Light Nuclei in Supernova

Core-collapse supernovae (SN) are giant explosions of massive stars, above 9 solar masses, that radiate 99% of their energy in neutrinos. The current theory of core collapse supernova holds some open questions regarding the two important phenomena related to the event, i.e. the explosion mechanism and the synthesis of complex nuclei.

The extreme conditions within the supernova make nuclear reactions important microscopic phenomena which govern the equation of state. Therefore, the dynamics and neutrino signals can be sensitive to the details of neutrino interactions with nucleonic matter. In order to analyze the mentioned questions, a better understanding of the involved microscopic processes is needed. In particular, due to the high abundance of  $\alpha$  particles in the supernova environment, the inelastic neutrino- ${}^4\text{He}$  reaction has drawn attention in recent years. This interest yielded a number of studies trying to estimate the cross-section and the role of neutrino- ${}^4\text{He}$  reactions in the described phenomena (Haxton, 1988; Epstein et al., 1988; Meyer, 1995; Yoshida et al., 2005, 2006; Ohnishi et al., 2006; Suzuki et al., 2006; Woosley et al., 1990). However to date, a full *ab-initio* calculation that includes a realistic nuclear Hamiltonian is still missing. Moreover, the contribution of meson exchange currents (MEC) to this particular scattering process was never estimated.

Core collapse supernovae are believed to be neutrino driven explosions of massive stars. As the iron core of the star becomes gravitationally unstable it collapses until the nuclear forces halt the collapse and drive an outgoing shock. This shock gradually stalls due to energy loss through neutrino radiation and dissociation of the iron nuclei into a mixture of  $\alpha$  particles and free nucleons.

At this stage, the proto-neutron star (PNS) cools mainly by emitting neutrinos in enormous numbers. These neutrinos are a result of thermal pair production, and thus are produced in flavor equilibrium. The characteristic temperatures of the emitted neutrinos are about 6 – 10 MeV for  $\nu_{\mu,\tau}$  ( $\bar{\nu}_{\mu,\tau}$ ), 5 – 8 MeV for  $\bar{\nu}_e$ , and 3 – 5 MeV for  $\nu_e$ . The difference in temperature originates from the large cross-sections for  $\nu_e, \bar{\nu}_e$

electron scattering and charge current reactions, thus  $\nu_{\mu,\tau}$  ( $\bar{\nu}_{\mu,\tau}$ ) decouple deeper within the star, where the temperature is higher. Interactions of neutrino with nuclei in this location, called *neutrinosphere*, can change neutrino temperature and spectra. Clearly, it is essential to estimate the abundances of nuclei in that region.

Abundances of nuclei are usually predicted using nuclear statistical equilibrium (NSE) models based on binding energies and the quantum numbers of nuclei. However, NSE models only treat approximately (or neglect) strong interactions between nuclei, and consequently break down near the *neutrinosphere*. In a recent work (O'Connor et al., 2007), we have shown this results in a substantial amount of  $A = 3$  nuclei near the newly born proto-neutron star (PNS), an effect forehand unnoticed.

The hot dilute gas above the PNS and below the accretion shock contains up to 70%  ${}^4\text{He}$  nuclei. The high temperature of heavy flavored neutrinos migrating out of the PNS leads to a considerable amount of  $\mu$  and  $\tau$  neutrinos (and anti-neutrinos) which carry more than 20 MeV, hence may dissociate the  ${}^4\text{He}$  nucleus through inelastic neutral current reactions. If these reactions deposit enough energy in the matter behind the shock, they can eventually reverse the flow and revive the shock. This delayed shock mechanism, originally introduced by Colgate and White (1966), has not yet been proven in full hydro-reactive simulations. Haxton (1988) has suggested that inelastic neutral reactions of neutrinos with  ${}^4\text{He}$  can lead to an enhanced neutrino energy deposition. This effect is usually ignored (see however (Ohnishi et al., 2006; Woosley et al., 1990)) and was not considered in full hydrodynamic simulations.

The energy deposition also creates the needed conditions for the *r*-process, nucleosynthesis by rapid capture of free neutrons, believed to occur in the material ejected from the PNS. The break-up of  ${}^4\text{He}$  by neutrinos is part of the chain of reactions which determines the amount of free neutrons (Fuller and Meyer, 1995) needed for a successful *r*-process.

A different nucleosynthesis process which is influenced by  $\nu - \alpha$  interaction is  $\nu$ -nucleosynthesis in the outer layers of the star. A knock out of a nucleon from a  ${}^4\text{He}$  nucleus in the helium rich layer, creates the seed to light element nucleosynthesis in the supernova environment (Woosley et al., 1990). Followed by a fusion of the remaining trinucleus with another  $\alpha$  particle, this will result in a 7-body nucleus.

This process is an important source of  ${}^7\text{Li}$ , and of  ${}^{11}\text{B}$  and  ${}^{19}\text{F}$  through additional  $\alpha$  capture reactions. Due to the high dissociation energy of the  $\alpha$ , this mechanism is sensitive to the high-energy tail of the neutrinos. Thus a correct description of the process must contain an exact, energy dependent cross-section for the neutral inelastic  $\alpha - \nu$  reaction, which initiates the process. The relatively low temperature of the  $\nu_e$ 's and  $\bar{\nu}_e$ 's emitted from the core of the star suppress the probability for inelastic reactions of these neutrinos with  ${}^4\text{He}$  in the supernova scenario. Oscillations of the  $\mu$  and  $\tau$  (anti) neutrinos can yield a secondary source of energetic electron neutrinos. The resulting charge current reactions, which have larger cross-sections than the neutral cross-sections, would affect the discussed yields (Yoshida et al., 2006).

The work in this thesis predicts, to a percentage level accuracy, the cross-sections for neutrino interactions with  $A = 3$  and  ${}^4\text{He}$  nuclei. This removes the uncertainty, which exists today, in the microscopic information needed for a correct evaluation of the aforementioned processes.

### 1.3 About this thesis

The work presented in this thesis summarizes the results published in a series of papers written during my PhD. studies.

Two of these papers investigated the photoabsorption process on  ${}^4\text{He}$ :

- P1** “Photoabsorption on  ${}^4\text{He}$  with a Realistic Nuclear Force”, D. Gazit, S. Bacca, N. Barnea, W. Leidemann, G. Orlandini, *Phys. Rev. Lett.* **96**, 112301 (2006).
- P2** “Photonuclear sum rules and the tetrahedral configuration of  ${}^4\text{He}$ ”, D. Gazit, N. Barnea, S. Bacca, W. Leidemann, G. Orlandini, *Phys. Rev.* **C 74**, 061001(R) (2006).

A substantial mass of the work was done on the subject of low-energy neutrino scattering on light nuclei, namely triton,  ${}^3\text{He}$  and  ${}^4\text{He}$ , published in:

- P3** “Neutrino neutral reaction on  ${}^4\text{He}$ : Effects of final state interaction and realistic  $NN$  force”, D. Gazit and N. Barnea, *Phys. Rev.* **C 70**, 048801 (2004).

- P4** “Low-Energy Inelastic Neutrino Reactions on  ${}^4\text{He}$ ”, D. Gazit and N. Barnea, *Phys. Rev. Lett.* **98**, 192501 (2007).
- P5** “Neutrino breakup of  $A = 3$  nuclei in supernovae”, E. O’Connor, D. Gazit, C. J. Horowitz, A. Schwenk, N. Barnea, *Phys. Rev. C* **75**, 055803 (2007).
- P6** “Few body Calculation of Neutrino Neutral Inelastic scattering on  ${}^4\text{He}$ ”, D. Gazit and N. Barnea, *Nucl. Phys. A* **790**, 356 (2007) .
- P7** “Low energy inelastic neutrino reactions on light nuclei”, D. Gazit and N. Barnea, *in prep.*

The structure of the thesis is as follows. The first part, chapters 2-5, contains a detailed description of the underlying physics and the methods of calculations. Chap. 2 explains the quantum formalism of electro-weak probes scattering on nuclei. The next chapter uses EFT approach to derive the scattering operator. The LIT method is discussed in Chap. 4, followed by a description in Chap. 5 of the nuclear wave functions used to solve the LIT equations.

The second part of the thesis presents the calculated cross-sections and their physical application. In Chap. 6 the photoabsorption on  ${}^4\text{He}$  process is analyzed, based on the work published in **P1** and **P2**. Chap. 7 a complete calculation is given for neutrino inclusive scattering on  $A = 3$  and  ${}^4\text{He}$  nuclei, as was first presented in **P3-P7**.

The thesis concludes with a summary.

# SCATTERING OF ELECTRO-WEAK PROBES ON NUCLEI

---

The unification of the electro-magnetic and weak forces is considered one of the biggest accomplishments of physics in the twentieth century. In the forty years since the pioneering work by Weinberg, Salam and Glashow, the standard model has been a matter of constant interest and ongoing research.

The application of this theory to the description of photon and neutrino scattering off matter is a key ingredient in experiments checking the limits of the standard model or exploring the structure of baryonic matter. These reactions are also the microscopic engines of many stellar phenomena, from star evolution to supernova explosion.

The weakness of the electro-weak interaction, in comparison to the strong force, makes a perturbative treatment of scattering processes on nuclei a good approximation. Consequently the interaction between electro-weak probes and nuclei targets reduces to a current-current type, as shown in the first section of this chapter.

An important result, presented in this chapter, is that the observables directly relate to the nuclear matrix element. Not only does this simplify calculations, but also provides an experimental separation of the electro-weak effects and the strong force effects. One cannot overemphasize the importance of the latter fact in the experimental research of the strong force, as reflected in the nuclear structure and dynamics. From the point of view of a theoretician, a construction of the electromagnetic and weak currents within the nucleus is needed. Chap. 3 is dedicated to meeting this challenge.

An additional simplification is achieved by using a multipole decomposition of the nuclear currents. This breaks the current into a series of operators, each characterized by known parity and angular momentum  $J^\pi$ . For low energy probes, whose wavelength  $q^{-1}$  is much larger than the typical size of a nucleus  $R$ , the multipole decomposition provides a polynomial dependence in the small parameter  $qR$ . In the

following discussion, the multipole decomposition technique is rigorously reviewed for the electro-weak interaction.

## 2.1 Neutrino Scattering

Neutrino scattering processes on elementary particles can be easily calculated using the Feynman diagrams of the standard model. Nuclei, however, are not elementary particles. On the contrary, they are built of protons and neutrons, that are built of quarks.

A possible way to cope with this problem, which is common in the literature, is to treat the nucleons as point fermions, with form factors indicating their complex quark structure.

The weak coupling constant  $G = 1.166 \times 10^{-11} \text{ MeV}^{-2}$  provides a small parameter, so the relevant neutrino scattering processes include one boson exchange. The first order Feynman diagrams for neutrino scattering off nucleon appear in Walecka (1995). The neutrino scattering processes of interest appear in Fig. 2.1. A neutrino with momentum  $k_i^\mu$  interacts with a nucleus of initial momentum  $P_i^\mu$ , through the exchange of heavy boson with momentum  $q^\mu = (\omega, \vec{q})$ . The result of the interaction is the emergence of a lepton with momentum  $k_f^\mu$ , and nuclear fragments with momentum  $P_f^\mu$ . Energy momentum conservation implies:  $q^\mu = k_i^\mu - k_f^\mu = P_f^\mu - P_i^\mu$ .

The lepton could be either neutrino of the same flavor in the case of neutral current reaction, or an electron, muon or tau, for charged current reactions. In the low energy regime typical to supernova environment, the possible charged reaction is the creation of an electron or a positron.

Thus, for all neutrino scattering processes, one can write the general form of the transition matrix for both charged and neutral currents (with one boson exchange):

$$T_{fi} = (\text{neutrino current})^\mu \cdot \frac{g_{\mu\nu} + \frac{q_\mu q_\nu}{M_B^2}}{q^2 + M_B^2} \cdot (\text{nuclear current})^\nu. \quad (2.1)$$

For low energy reactions with respect to the boson masses –  $M_{Z^0} \approx 92 \text{ GeV}$  and

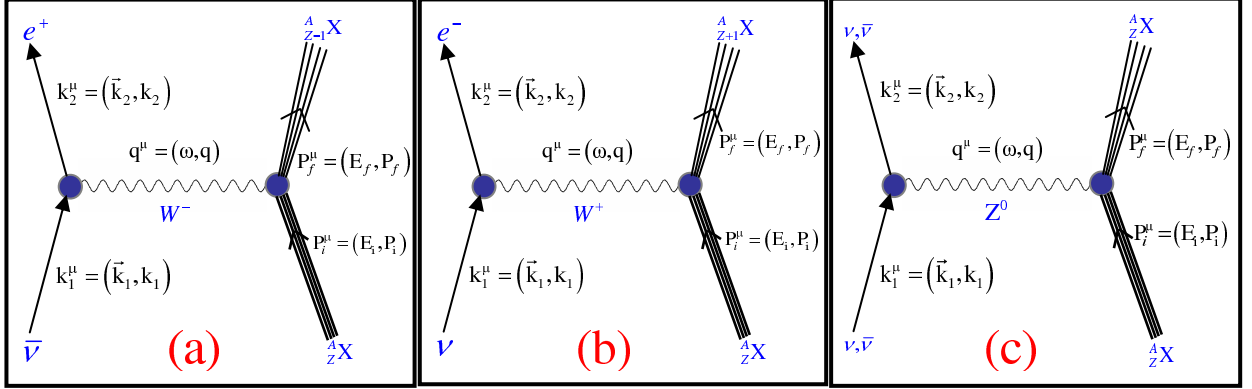


Figure 2.1: Neutrino scattering processes and their kinematics: (a) charged current  $e^+$  production; (b) charged current  $e^-$  production; (c) neutral current process

$M_{W\pm} \approx 80 \text{ GeV}$  – the momentum dependent terms are negligible. The boson propagator is constant in this limit  $\sim g_{\mu\nu}/M_B^2$ , and acts as an effective coupling constant (which explains the weak scale of weak interaction). This effective vertex, demonstrated in Fig. 2.2, leads to the famous current–current Hamiltonian density:  $\mathcal{H}_W \sim j^\mu \mathcal{J}_\mu$  ( $j^\mu$  is the lepton current, and  $\mathcal{J}_\mu$  is the nuclear current). The standard

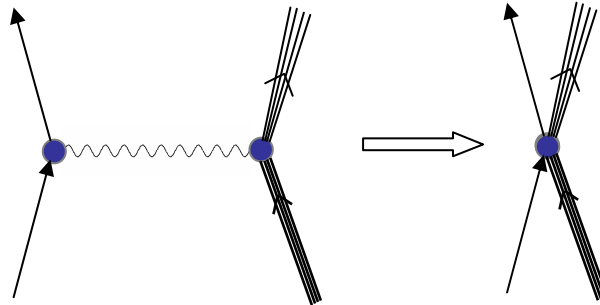


Figure 2.2: Effective vertex for low energy weak interactions.

model gives additional information regarding the formal structure of the currents. It is shown in Appendix A, that the weak neutral current takes the form,

$$\begin{aligned} \mathcal{J}_\mu^{(0)} &= (1 - 2 \cdot \sin^2 \theta_W) \frac{\tau_0}{2} J_\mu^V + \frac{\tau_0}{2} J_\mu^A - 2 \cdot \sin^2 \theta_W \frac{1}{2} J_\mu^V \\ &= \frac{\tau_0}{2} (J_\mu^V + J_\mu^A) - 2 \cdot \sin^2 \theta_W J_\mu^{em} \end{aligned} \quad (2.2)$$

Where  $J_\mu^V$  and  $J_\mu^A$  have vector and axial symmetry, respectively. The second equality takes advantage of the conserved vector current hypothesis, by which the weak-vector current is an isospin rotation of the electro-magnetic current ( $J_\mu^{em} = \frac{1+\tau_3}{2} J_\mu^V$ ).

A similar calculation for the charged current yields:

$$\mathcal{J}_\mu^{(\pm)} = \frac{\tau_\pm}{2} (J_\mu^V + J_\mu^A) \quad (2.3)$$

The vector and axial currents include not only a sum over all nucleons. It is well known, and will be shown in the next chapter, that in order to keep consistent with the chiral symmetry one has to include not only one nucleon currents but also meson exchange currents, which hold the nucleons bound in the nucleus.

### 2.1.1 Cross section calculation for neutrino scattering processes

In order to evaluate the probability for a scattering, the starting point is the Golden Rule (by Fermi). Taking into account the recoil of the nucleus, the differential cross-section takes the form,

$$d\sigma = 2\pi \int d\epsilon \delta(\epsilon - \omega + \frac{q^2}{2M_A}) \frac{d^3\vec{k}_f}{(2\pi)^3} \sum_f |\langle f | \hat{\mathcal{H}}_W | i \rangle|^2 \delta(E_f - E_i - \epsilon) \quad (2.4)$$

Here  $M_A$  is the initial nucleus mass,  $|i\rangle$  ( $|f\rangle$ ) is the initial state of the system, and  $E_i$  ( $E_f$ ) is the initial (final) energy of the nuclear system. In the previous chapter it was shown that, in the limit of low energy-momentum transfer with respect to the heavy gauge bosons  $W^\pm$  and  $Z^0$  mass, a proper approximation for the weak interaction between leptons and baryons is,

$$\hat{\mathcal{H}}_W = \frac{G}{\sqrt{2}} \int d^3\vec{x} \hat{j}_\mu(\vec{x}) \hat{\mathcal{J}}^\mu(\vec{x}). \quad (2.5)$$

The calculation of the matrix element of the Hamiltonian needed in Eq. (2.4) is divided accordingly. Keeping the theory to first order in the weak interaction constant, the

lepton current  $\hat{j}_\mu(\vec{x})$  is composed only of one lepton, which is a point Dirac particle. Thus, its matrix element is  $\langle f|j_\mu(x)|i\rangle = l_\mu e^{-i\vec{q}\cdot\vec{x}}$ , where for neutrino reaction  $l_\mu = \bar{u}(k_1)\gamma_\mu(1 - \gamma_5)u(k_2)$ , and for anti-neutrino reaction  $l_\mu = \bar{v}(-k_2)\gamma_\mu(1 - \gamma_5)v(-k_1)$ . Consequently,

$$\langle f|\hat{\mathcal{H}}_W|i\rangle = \frac{G}{\sqrt{2}} \int d^3\vec{x} e^{-i\vec{q}\cdot\vec{x}} [l_0 \mathcal{J}_{fi}^0(\vec{x}) - \vec{l} \cdot \vec{\mathcal{J}}_{fi}(\vec{x})]. \quad (2.6)$$

To continue, it is useful to choose the  $\hat{z}$  direction parallel to the momentum transfer  $\vec{q}$ , so the plane wave can be expanded as

$$e^{-i\vec{q}\cdot\vec{x}} = \sum_J i^J \sqrt{4\pi(2J+1)} j_J(qx) Y_{J0}(-\hat{x}), \quad (2.7)$$

where  $j_J(x)$  is the spherical bessel function of order  $J$ , and  $Y_{JM}(\hat{x})$  are the spherical harmonics.

Since the vector  $\vec{l}$  is written in the same spherical orthonormal coordinate system  $\hat{e}_{\pm 1}, \hat{e}_0 = \frac{\vec{q}}{q}$  it is useful to invert the definition of the vector spherical harmonics:  $\vec{Y}_{JLM} \equiv [Y_L \otimes \hat{e}]_M^{(J)}$ , to get  $Y_{Lm} e_\lambda = \sum_{JM} (Lm1\lambda|JM) \vec{Y}_{JLM}$ .

For the nuclear current  $\hat{\mathcal{J}}^\mu(\vec{x})$ , a multipole analysis of the current provides natural expansion and some insight in low energy regime. We define the multipole operators, viz the Coulomb, electric, magnetic and longitudinal operators:

$$\hat{C}_{JM}(q) = \int d\vec{x} j_J(qx) Y_{JM}(\hat{x}) \hat{\mathcal{J}}_0(\vec{x}) \quad (2.8)$$

$$\hat{E}_{JM}(q) = \frac{1}{q} \int d\vec{x} \vec{\nabla} \times [j_J(qx) \vec{Y}_{JJM}(\hat{x})] \cdot \hat{\mathcal{J}}(\vec{x}) \quad (2.9)$$

$$\hat{M}_{JM}(q) = \int d\vec{x} j_J(qx) \vec{Y}_{JJM}(\hat{x}) \cdot \hat{\mathcal{J}}(\vec{x}) \quad (2.10)$$

$$\hat{L}_{JM}(q) = \frac{i}{q} \int d\vec{x} \vec{\nabla} [j_J(qx) Y_{JM}(\hat{x})] \cdot \hat{\mathcal{J}}(\vec{x}) \quad (2.11)$$

respectively.

For unoriented and unobserved targets, one has to sum over all possible final states, and average over all initial states. For the nuclear sector, this procedure gives

the following expression:

$$\begin{aligned}
& \sum_f \frac{1}{2J_i + 1} \sum_{M_i} \sum_{M_f} |\langle f | \hat{\mathcal{H}}_W | i \rangle|^2 \delta(E_f - E_i - \epsilon) = \frac{G^2}{2} \frac{4\pi}{2J_i + 1} \times \\
& \times \left\{ \sum_{J \geq 1} \left[ \frac{1}{2} (\vec{l} \cdot \vec{l}^* - l_3 l_3^*) (\mathcal{R}_{\hat{E}_J} + \mathcal{R}_{\hat{M}_J}) - \frac{i}{2} (\vec{l} \times \vec{l}^*)_3 2Re \mathcal{R}_{\hat{E}_J \hat{M}_J^*} \right] + \right. \\
& \left. + \sum_{J \geq 0} \left[ l_3 l_3^* \mathcal{R}_{\hat{L}_J} + l_0 l_0^* \mathcal{R}_{\hat{C}_J} - 2Re(l_3 l_0^* \mathcal{R}_{\hat{C}_J \hat{L}_J^*}) \right] \right\}
\end{aligned} \tag{2.12}$$

$J_i$  is the total angular momentum of the initial nuclear state (which is usually the ground state). We use here the nuclear response functions

$$\mathcal{R}_{\hat{O}_1 \hat{O}_2} \equiv \sum_f \delta(E_f - E_i - \epsilon) \langle f | \hat{O}_1^\dagger | i \rangle \langle f | \hat{O}_2 | i \rangle, \tag{2.13}$$

which should be calculated using a model for the nucleus. The  $\sum$  sign in the response function is a sum over discrete bound states, and an integral over final states which are in the continuum. For brevity we use the notation  $\mathcal{R}_{\hat{O}} \equiv \mathcal{R}_{\hat{O} \hat{O}}$ .

For the lepton sector, one sums over all possible helicities of the ejected lepton. In the case of neutrino scattering, there is no need in averaging on initial helicities as there is only one (anti) neutrino helicity in nature that interacts via the electro-weak force. The lepton summation is simply converted to the calculation of traces of Dirac spinors, as explained in Appendix B.

An additional effect, which needs to be taken into account for charged lepton production, is the deformation of the lepton wave function due to the long-range electromagnetic interaction with the nucleus. This is done in an approximated way using the Fermi function (Fermi, 1934).

The final result for the differential cross section of a beam of neutrinos scattering

on unpolarized and unobserved targets, into solid angle  $d\Omega$  is thus:

$$\begin{aligned} \frac{d\sigma^{(a)}}{d\Omega dk_f} &= \frac{2G^{(a)2}}{2J_i + 1} F^{(a)}(Z_f, k_f) k_f^2 \times \\ &\times \left\{ \left[ 1 - (\hat{k}_i \cdot \hat{q})(\vec{\beta}_f \cdot \hat{q}) \right] \sum_{J \geq 1} (\mathcal{R}_{\hat{E}_J} + \mathcal{R}_{\hat{M}_J}) \mp \hat{q} \cdot (\hat{k}_i - \vec{\beta}_f) \sum_{J \geq 1} 2Re\mathcal{R}_{\hat{E}_J \hat{M}_J^*} + \right. \\ &\left. + \sum_{J \geq 0} \left[ \left[ 1 - \hat{k}_i \cdot \vec{\beta}_f + 2(\hat{k}_i \cdot \hat{q})(\vec{\beta}_f \cdot \hat{q}) \right] \mathcal{R}_{\hat{L}_J} + \left( 1 + \hat{k}_i \cdot \vec{\beta}_f \right) \mathcal{R}_{\hat{C}_J} - 2\hat{q} \cdot (\hat{k}_i + \vec{\beta}_f) Re\mathcal{R}_{\hat{C}_J \hat{L}_J^*} \right] \right\} \end{aligned} \quad (2.14)$$

where  $Z_f$  is the charge of the final nucleus, and  $\vec{\beta}_f = \frac{\vec{k}_f}{\sqrt{m_f^2 + k_f^2}}$  is the outgoing lepton velocity ( $m_f$  is the mass of the lepton). The  $-$  sign is for neutrino scattering, and the  $+$  sign is for anti-neutrino. The superscript  $(a) = 0, \pm 1$  indicates the process:

$a = 0$  Neutral current, for which the  $G^{(0)} = G$  and the screening function  $F^{(0)}(Z_f, k_f) = 1$ .

$a = \pm 1$  Charge changing current.  $G^{(\pm)} = G \cos \theta_C \approx 0.974G$  ( $\theta_C$  is the Cabibbo angle, mixing the  $u$  and  $d$  quarks) and the screening function is the Fermi function (Fermi, 1934):

$$F^{(\pm)}(Z_f, k_f) = 2(1 + \gamma_0)(2k_f R_f)^{2(\gamma_0 - 1)} \frac{|\Gamma(\gamma_0 + i\rho)|^2}{|\Gamma(2\gamma_0 + 1)|^2} e^{\pi\rho} \quad (2.15)$$

with  $\alpha \approx 1/137$  is the fine structure constant,  $R_f$  is the radius of the final nucleus,  $\rho = \mp \alpha Z_f / \beta_f$ , and  $\gamma_0 = \sqrt{1 - (\alpha Z_f)^2}$  ( $\Gamma(x)$  is the Gamma function).

## 2.2 Relations Between Multipoles and the Siegert theorem

The multipole decomposition is a systematic expansion in the possible angular momenta exchange in a reaction. This makes it a powerful and intuitive tool to analyze reactions, in which the quantum numbers of the final state are given. On a different perspective, one can view the multipole decomposition essentially as expansion in

powers of the momentum transfer, since  $j_J(\rho) \simeq \frac{\rho^J}{(2J+1)!!}$  for  $\rho \ll 1$ . Thus, it provides a tool when investigating low energy reactions with  $qR < 1$  ( $R$  is the radius of the nucleus), for which a finite number of multipoles are sufficient to estimate the cross-section to given accuracy.

The electro-weak reactions discussed in the scope of this work are investigated up to pion threshold  $\sim 140$  MeV, thus the multipole decomposition is applicable and efficient.

In this section we will discuss some important properties of the multipole operators and relations between multipoles, helpful in calculations. It is useful to understand that the longitudinal, Coulomb and electric multipoles are of normal parity, i.e. if one denotes the parity of the current by  $\pi$  then their parity is  $\pi \cdot (-)^J$ . The magnetic operator parity is  $\pi \cdot (-)^{J+1}$

An important relation exists between the electric and the longitudinal operators. In order to find it, one uses the following formulas,

$$\begin{aligned}\vec{\nabla}_\rho [j_J(\rho)Y_{JM}(\hat{\rho})] &= \sqrt{\frac{J+1}{2J+1}}j_{J+1}(\rho)\vec{Y}_{JJ+1M}(\hat{\rho}) + \sqrt{\frac{J}{2J+1}}j_{J-1}(\rho)\vec{Y}_{JJ-1M}(\hat{\rho}) \\ \vec{\nabla}_\rho \times [j_J(\rho)\vec{Y}_{JJM}(\hat{\rho})] &= -i\sqrt{\frac{J}{2J+1}}j_{J+1}(\rho)\vec{Y}_{JJ+1M}(\hat{\rho}) + i\sqrt{\frac{J+1}{2J+1}}j_{J-1}(\rho)\vec{Y}_{JJ-1M}(\hat{\rho}).\end{aligned}$$

This leads to,

$$\vec{\nabla}_\rho \times [j_J(\rho)\vec{Y}_{JJM}(\hat{\rho})] = i\sqrt{\frac{J+1}{J}}\vec{\nabla}_\rho [j_J(\rho)Y_{JM}(\hat{\rho})] - i\sqrt{\frac{2J+1}{J}}j_{J+1}(\rho)\vec{Y}_{JJ+1M}(\hat{\rho}). \quad (2.16)$$

Thus,

$$\hat{E}_{JM} = \sqrt{\frac{J+1}{J}}\hat{L}_{JM} - i\sqrt{\frac{2J+1}{J}} \int d\vec{x} j_{J+1}(qx)\vec{Y}_{JJ+1M}(\hat{x}) \cdot \hat{\mathcal{J}}(\vec{x}). \quad (2.17)$$

One notes that since the leading order in  $\hat{E}_{JM}$  (and  $\hat{L}_{JM}$ ) is  $O((qR)^{J-1})$ , then the second term is smaller by a factor of  $(qR)^2$ . Finally, this leads to the following relation

for low momentum transfer:

$$\hat{E}_{JM} \approx \sqrt{\frac{J+1}{J}} \hat{L}_{JM}. \quad (2.18)$$

### 2.2.1 Siegert Theorem

An additional relation between multipole operators exists for conserved currents, *inter alia* the electro-magnetic current and the vector part of the weak current. For a conserved current  $\vec{\nabla} \cdot \hat{\mathcal{J}} = -i[\hat{\mathcal{H}}, \hat{\mathcal{J}}_0]$ , and thus its matrix element (between eigen-states of the Hamiltonian) satisfies:  $\vec{\nabla} \cdot \vec{\mathcal{J}} = -i\omega \mathcal{J}_0$ . Let us first look at the longitudinal operator:

$$\hat{L}_{JM}(q) = \frac{i}{q} \int d\vec{x} \vec{\nabla} [j_J(qx) Y_{JM}(\hat{x})] \cdot \hat{\mathcal{J}}(\vec{x}) = -\frac{i}{q} \int d\vec{x} [j_J(qx) Y_{JM}(\hat{x})] \cdot \vec{\nabla} \cdot \hat{\mathcal{J}}(\vec{x}) = -\frac{\omega}{q} \hat{C}_{JM}(q) \quad (2.19)$$

We use Eq. (2.17) to connect the electric multipole to the Coulomb multipole,

$$\hat{E}_{JM} = -\frac{\omega}{q} \sqrt{\frac{J+1}{J}} \hat{C}_{JM} - i \sqrt{\frac{2J+1}{J}} \int d\vec{x} j_{J+1}(qx) \vec{Y}_{J+1M}(\hat{x}) \cdot \hat{\mathcal{J}}(\vec{x}). \quad (2.20)$$

These relations are called the Siegert theorem (Siegert, 1937). In low energy, the second term in Eq. (2.20) is negligible with respect to the first one.

The strength of the Siegert theorem is in the connection it makes between currents and charge. It implies that for conserved currents in low energy, one can calculate all the corrections due to meson exchange currents by calculating the single-nucleon Coulomb operator. This not only simplifies calculation, but also keeps the operators model-independent.

## 2.3 Photoabsorption on Nuclei Up To Pion Threshold

Photoabsorption is the process in which a real photon is absorbed in a nucleus. The process can result in excitation of the nucleus to a bound state, but can also result

in a break up of the nucleus, a process called photodisintegration. The latter is the case for all photoabsorption processes of  ${}^4\text{He}$ , since it has no bound excited states.

The interaction Hamiltonian of an electro-magnetic process can be found by looking at minimal substitution of the momentum in the kinetic energy operator:  $(\hat{\vec{p}} - e\hat{\vec{A}}(r))^2 = \hat{p}^2 + e^2\hat{A}^2 - e\{\hat{\vec{p}}, \hat{\vec{A}}\}$ . The first two terms are the kinetic energies of the nucleus and the photon field, and the last is the interaction term. Hence, it is clear that the interaction Hamiltonian is,

$$\hat{\mathcal{H}}_{EM} = \frac{4\pi\alpha}{\sqrt{2}} \int d^3\vec{x} \hat{A}_\mu(\vec{x}) \hat{\mathcal{J}}^\mu(\vec{x}). \quad (2.21)$$

where  $\alpha$  is the fine structure constant,  $\hat{A}_\mu$  is the photon field, and  $\hat{\mathcal{J}}^\mu$  is the nuclear electro-magnetic current. The photon field in the Coulomb gauge (i.e.  $\vec{\nabla} \cdot \hat{\vec{A}}_\mu(\vec{x})$ ) is given by,

$$\hat{\vec{A}} = \sum_{\vec{k}} \sum_{\lambda=\pm 1} (2\omega_k)^{-1/2} \left[ \hat{e}_{\vec{k}\lambda} \hat{a}_{\vec{k}\lambda} e^{i\vec{k}\cdot\vec{x}} + h.c. \right] \quad (2.22)$$

Due to the gauge only the transverse polarizations,  $\lambda = \pm 1$ , participate.

The analogy to the weak Hamiltonian is clear (cf. Eq. 2.5), so the calculations are in analogy, but the kinematics is different.

Let us consider a photon of momentum  $\vec{q}$  and energy  $\omega = |q|$ , as the photon is absorbed. The initial (final) nucleus state is denoted by  $|i/f\rangle$ , with energies  $E_{i/f}$  respectively (by definition  $\omega = E_i - E_f$ ). The photon is absorbed, thus the surviving matrix element is  $\langle \vec{k}\lambda | \hat{a}_{\vec{k}'\lambda'}^\dagger | 0 \rangle = \delta_{\vec{k}\vec{k}'} \delta_{\lambda\lambda'}$ .

Due to the possible polarizabilities, only the magnetic and electric enter in the calculation. By using the golden rule, we get the final result for the total photoabsorption cross-section:

$$\sigma(\omega) = 4\pi^2\alpha\omega \sum_J [\mathcal{R}_{\hat{E}_J}(\omega) + \mathcal{R}_{\hat{M}_J}(\omega)]. \quad (2.23)$$

# 3 CHIRAL EFFECTIVE FIELD THEORY

---

Nuclear theory is believed to be the low-energy reflection of quantum chromodynamics (QCD). Though QCD properties are well known, deriving the nuclear forces is not possible directly, as QCD is non-perturbative in low energy.

Two seminal ideas proposed by Weinberg (1979) have pointed the way to a solution to the problem. The first idea suggests that a Lagrangian which includes all possible terms consistent with the symmetries of the underlying theory, would result in the most general S-matrix consistent with the theory. The second idea introduces a scheme which organizes the terms to dominant and less dominant contributions to the S-matrix. This way, the anticipated low energy expansion for QCD becomes possible. These ideas were used in the last 15 years to construct a nuclear Lagrangian based on an effective field theory for low-energy QCD, named chiral perturbation theory ( $\chi$ PT) (see for example (Ordóñez et al., 1994; van Kolck, 1994; Epelbaum et al., 2000; Entem and Machleidt, 2003)).

In this chapter, the application of effective field theory to QCD is presented, and used to get a description of the currents in a nucleus. In turn, these currents interact with electro-weak probes, determining their coupling with matter. The effective field theory is constructed to describe nuclear electro-weak processes of typical energy of up to 100 MeV. Thus the relevant degrees of freedom are pions and nucleons.

## 3.1 QCD symmetries at low energy

QCD, as a field theory, describes the interaction among quarks and gluons. Its underlying gauge symmetry is the non-abelian color  $SU(3)$  Lie algebra. The masses of the up and down quarks, which are the building blocks of nucleons, are small (Yao et al., 2006):  $m_u = 2 \pm 1$  MeV and  $m_d = 5 \pm 2$  MeV. Thus, these masses are negligible

with respect to the QCD mass scale ( $\sim 1$  GeV). In the context of nuclear physics, it is natural to treat QCD in the limit of zero quark masses, with restriction to the up and down quarks.

Following these restrictions, one writes the quark field composed of two components:  $\begin{pmatrix} u \\ d \end{pmatrix}$ . The massless quark field enters in the QCD Lagrangian as,

$$\mathcal{L}_{QCD}^q = i\bar{q}\gamma_\mu\mathcal{D}^\mu q. \quad (3.1)$$

The quark field has a left and right symmetry. We define right and left handed components of the quark field:  $q_{R,L} = \frac{1}{2}(1 \pm \gamma_5)q$ , respectively. Using the properties of the  $\gamma$  matrices (see Appendix B), the Lagrangian can be separated,

$$\mathcal{L}_{QCD}^q = i\bar{q}_R\gamma_\mu\mathcal{D}^\mu q_R + i\bar{q}_L\gamma_\mu\mathcal{D}^\mu q_L. \quad (3.2)$$

One may check that this Lagrangian is invariant under the global transformations:

$$q_R = \begin{pmatrix} u_R \\ d_R \end{pmatrix} \mapsto \exp\left(-i\vec{\Theta}^R \cdot \frac{\vec{\tau}}{2}\right) \begin{pmatrix} u_R \\ d_R \end{pmatrix} \quad (3.3)$$

and,

$$q_L = \begin{pmatrix} u_L \\ d_L \end{pmatrix} \mapsto \exp\left(-i\vec{\Theta}^L \cdot \frac{\vec{\tau}}{2}\right) \begin{pmatrix} u_L \\ d_L \end{pmatrix}, \quad (3.4)$$

where  $\vec{\tau}$  are pauli matrices generating the flavor symmetry between up and down. As right and left quarks do not mix, this implies the *chiral symmetry*  $SU(2)_R \times SU(2)_L$  of QCD. One can rewrite this to a symmetry on the original quark field:

$$q = \begin{pmatrix} u \\ d \end{pmatrix} \mapsto \exp\left[-i\frac{1}{2}(1 \pm \gamma_5)\vec{\Theta} \cdot \frac{\vec{\tau}}{2}\right] \begin{pmatrix} u \\ d \end{pmatrix}. \quad (3.5)$$

The chiral symmetry can be transformed linearly to a vector symmetry,

$$q = \begin{pmatrix} u \\ d \end{pmatrix} \mapsto \exp \left[ -i \vec{\Theta}^V \cdot \frac{\vec{\tau}}{2} \right] \begin{pmatrix} u \\ d \end{pmatrix}, \quad (3.6)$$

and axial symmetry,

$$q = \begin{pmatrix} u \\ d \end{pmatrix} \mapsto \exp \left[ -i \gamma_5 \vec{\Theta}^A \cdot \frac{\vec{\tau}}{2} \right] \begin{pmatrix} u \\ d \end{pmatrix}. \quad (3.7)$$

Nöther's theorem suggests the existence of conserved vector and axial currents:  $\vec{V}^\mu = \bar{q} \gamma^\mu \frac{\vec{\tau}}{2} q$  and  $\vec{A}^\mu = \bar{q} \gamma^\mu \gamma_5 \frac{\vec{\tau}}{2} q$ .

The problem is that this symmetry entails a degeneracy of ground states. A vector degeneracy is found, the *isospin symmetry*, which couples for example the proton and neutron to a single entity, the nucleon. This is not the case for the axial symmetry, as multiplets of opposite parities are not observed in nature. One concludes that in nature  $SU(2)_R \times SU(2)_L$  is broken to  $SU(2)_V$ .

This is an example of spontaneous breaking of symmetry, i.e. a symmetry of the Lagrangian which is not realized in the ground state. A consequent of this is the existence of Goldstone–Nambu bosons, massless particles that possess the quantum numbers of the broken generators. In the case of the chiral symmetry, the Goldstone bosons should be pseudoscalar. The pions, pseudoscalar isospin triplet, are considered to be the Goldstone bosons of the chiral symmetry. As a result of the non-vanishing up and down small masses, the pions obtain mass, but they are light  $\left(\frac{m_\pi}{m_N}\right)^2 \approx 0.02$ .

The appearance of Goldstone–Nambu bosons is a result of the Goldstone theorem (Goldstone et al., 1962). This theorem gives an additional information regarding the structure of the transformations. The pion field is defined by,

$$\xi = \exp \left( i \frac{\vec{\pi} \cdot \vec{\tau}}{2f_\pi} \right). \quad (3.8)$$

Goldstone theorem leads to the transformation rule for  $U \equiv \xi^2$

$$U = \exp\left(i\frac{\vec{\pi} \cdot \vec{\tau}}{f_\pi}\right) \mapsto LUR^\dagger, \text{ with } L \in SU(2)_L \text{ and } R \in SU(2)_R \quad (3.9)$$

Thus,  $U$  transforms as the  $(\bar{2}, 2)$  representation of  $SU(2)_R \times SU(2)_L$ . This is a non-linear realization of the symmetry, as  $U^\dagger U = 1$  and  $\det U = 1$ .

This implies the following transformation rules on the nucleon and pion fields:

$$N \mapsto hN \quad (3.10)$$

$$\xi \mapsto L\xi h^\dagger = h\xi R^\dagger \quad (3.11)$$

with  $h \in SU(2)_V$ , local matrix.

With these transformation laws, it is possible to build Lorentz invariant terms to include in the Lagrangian of the effective theory,

$$\mathcal{L}_{eff} = \sum_A c_A \mathcal{L}_A \quad (3.12)$$

This is an effective theory, thus renormalizability is inserted via the low energy coefficients. This sum however is infinite. Hence, a logic in deciding the order of a term in the expansion is needed.

## 3.2 Power Counting of Chiral Perturbation Theory

EFT of low energy QCD is called Chiral Perturbation Theory ( $\chi$ PT). The theory has a natural cutoff scale, the chiral symmetry breaking scale, which is of the order of the nucleon mass  $\Lambda \sim 1 \text{ GeV}$ . The expansion relies on the small momentum typical to the needed process  $Q$ , thus the expansion parameter is  $(Q/\Lambda)$ .

The contribution of an interaction is determined by its power:  $(Q/\Lambda)^\nu$ . Let a scattering process be described by a diagram. The diagram is built of  $C$  separately connected pieces,  $A$  nucleons,  $L$  loops. The diagram includes several vertices, each

involves  $n_i$  nucleon fields,  $d_i$  pion masses or derivatives. The order  $\nu$  is given by (Weinberg, 1996):

$$\nu = -2 + 2A - 2C + 2L + \sum_i \Delta_i \quad (3.13)$$

with  $\Delta_i \equiv d_i + \frac{n_i}{2} - 2$ .

One has to note that  $\nu$  is bounded from below, thus enabling systematic expansion. This counting holds not only for diagrams, but also for Lagrangian terms. The counting for a Lagrangian term is similar to a vertex:  $\nu_{\mathcal{L}} = d + \frac{n}{2}$ .

The power counting formalism introduced here is applicable when the choice of cutoff  $\Lambda$  is relevant for the energy-regime of the process (see discussions by Nogga et al. (2005); Epelbaum and Meissner (2006)).

### 3.3 Effective Lagrangian

As aforementioned, the chiral effective field theory takes into account pions and nucleons. Not surprisingly, the Lagrangian includes three parts, a pure pion, a pure nucleon and pion–nucleon interaction Lagrangian. In this section I will review the different parts of the Lagrangian, and emphasize those parts needed for deriving the currents within the nucleus. In general, Lagrangians to next-to-leading order (NLO) are considered, built using the formalism introduced in Coleman et al. (1969); Callan et al. (1969) and following the discussion in Ananyan et al. (2002).

#### 3.3.1 Pion Lagrangian

The Lagrangian has to be a Lorentz invariant scalar term. Thus, it should include even number of derivatives/pion masses. Since the expansion used here is up to NLO, the pion Lagrangian term is expanded to  $\nu = 2$ , in the power counting introduced previously. Thus,

$$\mathcal{L}_{\pi\pi}^{(2)} = \frac{f_\pi^2}{4} \text{Tr} [\partial^\mu U \partial_\mu U^\dagger + m_\pi^2 (U + U^\dagger)] \quad (3.14)$$

$f_\pi \approx 92.4 \text{ MeV}$  is the pion decay constant, calibrated from this process at low pion four momentum. The pion mass is taken as  $m_\pi = 139 \text{ MeV}$ .

### 3.3.2 Pion–Nucleon Interaction Lagrangian

The pion–nucleon interaction, to lowest order, arises from the nucleon free Dirac Lagrangian. The reason is that the Dirac Lagrangian  $i\bar{N}(\gamma_\mu\partial^\mu - M_0)N$  is not invariant under the transformation rules of Eq. (3.10). This is not surprising, as the Yang–Mills theory demands adding gauge term to the derivative. The additional term has to be of chiral order 1, equivalent to the derivative. It can be easily checked that this term is:

$$v_\mu \equiv -\frac{i}{2} (\xi\partial_\mu\xi^\dagger + \xi^\dagger\partial_\mu\xi). \quad (3.15)$$

The chiral covariant derivative is:  $\mathcal{D}_\mu = \partial_\mu + iv_\mu$ . The notation  $v_\mu$  indicates the vector–like parity of this term. Trivially, a term with axial–like parity of the same chiral order is,

$$a_\mu \equiv -\frac{i}{2} (\xi\partial_\mu\xi^\dagger - \xi^\dagger\partial_\mu\xi). \quad (3.16)$$

This leads to the leading order pion–nucleon Lagrangian,

$$\mathcal{L}_{\pi N}^{(2)} = \bar{N} \{i\gamma_\mu\mathcal{D}^\mu + g_A\gamma^\mu\gamma_5 a_\mu - M_0\} N \quad (3.17)$$

The low energy constant (LEC) introduced here is the axial coupling constant  $g_A = 1.2670 \pm 0.0035$  (Yao et al., 2006).  $M_0 \approx 890$  MeV is the nucleon bare mass.

Expanding Eq. (3.17) to leading order in the pion field, one gets the leading interaction Lagrangian:

$$\mathcal{L}_{int}^{(2)} = -\frac{1}{4f_\pi^2} \epsilon^{abc} \pi^a \bar{N} (\not{\partial}\pi^b) \tau^c N + \frac{g_A}{2f_\pi} \bar{N} (\not{\partial}\pi^a) \gamma_5 \quad (3.18)$$

Using this, one constructs the Feynman diagrams related to this interaction Lagrangian.

Constructing the next–to–leading order contribution to the pion–nucleon interaction is easier, as the building blocks are  $a_\mu$  and  $v_\mu$ , and  $U$ . It is easily shown that

there are two terms at this order:

$$\delta_1 \mathcal{L}_{\pi N}^{(3)} = \frac{2\hat{c}_3}{M_N} \bar{N} N \text{Tr}(a_\mu a^\mu) \quad (3.19)$$

$$\delta_2 \mathcal{L}_{\pi N}^{(3)} = i \frac{\hat{c}_4}{M_N} \bar{N} [a_\mu, a_\nu] \sigma^{\mu\nu} N, \quad (3.20)$$

Where  $\sigma^{\mu\nu} = \frac{i}{2}[\gamma^\mu, \gamma^\nu]$ . The LECs here are calibrated using  $\pi - N$  scattering data  $\hat{c}_3 = -3.66 \pm 0.08$ , and  $\hat{c}_4 = 2.11 \pm 0.08$  (Bernard et al., 1995).

In view of the need of Feynman diagrams, one gets to this order:

$$\mathcal{L}_{int}^{(3)} = \frac{i\hat{c}_4}{2f_\pi^2 M} \bar{N} \vec{\tau} \cdot (\partial_\mu \vec{\pi} \times \partial_\nu \vec{\pi}) \sigma^{\mu\nu} N + \frac{\hat{c}_3}{f_\pi^2 M} \bar{N} N \partial_\mu \pi^a \partial^\mu \pi^a \quad (3.21)$$

### 3.3.3 Nucleon Contact terms in the Lagrangian

Nucleon contact terms represent the short-range nuclear force, usually connected to the exchange of heavy mesons, such as the  $\omega(782)$ . This mass is too close to the QCD scale, so it cannot be described as a multi-pion interaction using  $\chi$ PT. The contact terms are important for the purpose of renormalization and dimensional regularization of pion-exchange. In case of infinities, the contact terms act as counter-terms.

The contact terms include two nucleons, without meson fields. Being the representative of higher energy modes, these terms are not constrained by chiral symmetry, and required to fulfill parity and time-reversal symmetries (Ordóñez et al., 1994). Parity suggests even numbers of derivatives. The LO has no derivatives, and the NLO consist of two derivatives/pion masses.

Contact terms appear also when pions, electro-weak leptons, photons or other probes couple to pairs of nucleons. This gives rise to a contribution of few nucleon terms to the nuclear force (Grdestig and Phillips, 2006), and two nucleon exchange currents. The leading effects are represented by a term in the chiral Lagrangian (van Kolck, 1994),

$$\mathcal{L}_4 = -2D_1 (\bar{N} \gamma^\mu \gamma_5 a_\mu N) (\bar{N} N). \quad (3.22)$$

In general, the LECs in the contact terms should be calibrated by nuclear matter experiments. In the current case the short-range LEC is calibrated using the triton

half life. This process is discussed and applied in Sec. 7.2.

### 3.4 Currents in the Nucleus

The axial and vector symmetries of the Lagrangian imply conserved Nöther currents. These Currents are,

$$\mathcal{J}^{a\mu} \equiv -\frac{\partial \mathcal{L}}{\partial(\partial_\mu \epsilon^a(x))} \quad (3.23)$$

where the superscript  $a$  indicates isospin components.  $\epsilon^a(x)$  are local, infinitesimal parameters of the symmetry transformation.

A vector transformation has to be invariant to parity. The definition of parity,  $P : L \rightleftharpoons R$ , means that for a vector transformation with infinitesimal group parameters  $\vec{\beta}$ ,

$$L = R = \exp\left(i\frac{\vec{\beta} \cdot \vec{\tau}}{2}\right). \quad (3.24)$$

The  $h(x)$  transformation field can be found using Eq. (3.10), to get  $h(x) = L = R$ .

For an axial transformation one gets

$$L = \exp\left(i\frac{\vec{\beta} \cdot \vec{\tau}}{2}\right), \quad R = L^\dagger = \exp\left(-i\frac{\vec{\beta} \cdot \vec{\tau}}{2}\right). \quad (3.25)$$

In this case  $h(x)$  should be solved from its definition in Eq. (3.10). Putting  $h(x) = \exp\left(i\frac{\vec{\gamma} \cdot \vec{\tau}}{2}\right)$ , one can find,

$$\vec{\gamma} = -2(\hat{\beta} \times \hat{\pi}) \arctan \left[ \frac{\tan \frac{\beta}{2} \tan \frac{\pi}{2f_\pi}}{1 - (\hat{\beta} \cdot \hat{\pi}) \tan \frac{\beta}{2} \tan \frac{\pi}{2f_\pi}} \right] = -(\vec{\beta} \times \hat{\pi}) \tan \frac{\pi}{2f_\pi} + O(\beta^2) \quad (3.26)$$

Using this, one can derive the currents corresponding to the Lagrangians of the

previous section. The vector currents:

$$\mathcal{V}_{\pi\pi}^{(2)a\mu} = -i\frac{f_\pi^2}{4}\text{Tr}\{\tau^a[U\partial^\mu U^\dagger + U^\dagger\partial^\mu U]\} = (\vec{\pi} \times \partial^\mu \vec{\pi})^a \text{sinc}^2\left(\frac{\pi}{f_\pi}\right) \quad (3.27)$$

$$= (\vec{\pi} \times \partial^\mu \vec{\pi})^a + O(\pi^3)$$

$$\mathcal{V}_{\pi N}^{(2)a\mu} = \frac{1}{4}\bar{N}\gamma^\mu[\xi\tau^a\xi^\dagger + \xi^\dagger\tau^a\xi]N + \frac{1}{4}g_A\bar{N}\gamma^\mu\gamma_5[\xi\tau^a\xi^\dagger - \xi^\dagger\tau^a\xi]N = \quad (3.28)$$

$$= \bar{N}\gamma^\mu\frac{\tau^b}{2}N[\cos(\frac{\pi}{f_\pi})(\delta^{ab} - \hat{\pi}^a\hat{\pi}^b) + \hat{\pi}^a\hat{\pi}^b] + g_A\epsilon^{abc}\hat{\pi}^b\sin(\frac{\pi}{f_\pi})\bar{N}\gamma^\mu\gamma_5\frac{\tau^c}{2}N =$$

$$= \bar{N}\gamma^\mu\frac{\tau^a}{2}N + \frac{g_A}{f_\pi}\epsilon^{abc}\hat{\pi}^b\bar{N}\gamma^\mu\gamma_5\frac{\tau^c}{2}N + O(\pi^2)$$

$$\mathcal{V}_{\pi N}^{(3)a\mu} = -\frac{i\hat{c}_4}{2M}\bar{N}\sigma^{\mu\nu}[\xi^\dagger\tau^a\xi - \xi\tau^a\xi^\dagger, a_\nu]N - \frac{2\hat{c}_3}{M}\bar{N}N\text{Tr}[\xi^\dagger\tau^a\xi - \xi\tau^a\xi^\dagger, a_\mu] \quad (3.29)$$

$$= \frac{\hat{c}_4}{Mf_\pi^2}\bar{N}\sigma^{\mu\nu}[\vec{\pi} \times (\partial_\nu \vec{\pi} \times \vec{\tau})]^a N$$

where  $\text{sinc}(x) = \frac{\sin x}{x}$ . The axial currents:

$$\mathcal{A}_{\pi\pi}^{(2)a\mu} = -i\frac{f_\pi^2}{4}\text{Tr}\{\tau^a[U\partial^\mu U^\dagger - U^\dagger\partial^\mu U]\} \quad (3.30)$$

$$= -f_\pi\partial_\mu\pi^b\left[\text{sinc}\left(\frac{2\pi}{f_\pi}\right)(\delta^{ab} - \hat{\pi}^a\hat{\pi}^b) + \hat{\pi}^a\hat{\pi}^b\right]$$

$$= -f_\pi\partial_\mu\pi^b + O(\pi^2)$$

$$\mathcal{A}_{\pi N}^{(2)a\mu} = \frac{1}{4}\bar{N}\gamma^\mu[\xi\tau^a\xi^\dagger + \xi^\dagger\tau^a\xi]N + \frac{1}{4}g_A\bar{N}\gamma^\mu\gamma_5[\xi\tau^a\xi^\dagger - \xi^\dagger\tau^a\xi]N = \quad (3.31)$$

$$= -\epsilon^{abc}\hat{\pi}^b\sin(\frac{\pi}{f_\pi})\bar{N}\gamma^\mu\frac{\tau^c}{2}N - g_A\bar{N}\gamma^\mu\gamma_5\frac{\tau^b}{2}N[\cos(\frac{\pi}{f_\pi})(\delta^{ab} - \hat{\pi}^a\hat{\pi}^b) + \hat{\pi}^a\hat{\pi}^b]$$

$$= -g_A\bar{N}\gamma^\mu\gamma_5\frac{\tau^a}{2}N - \frac{1}{f_\pi}\epsilon^{abc}\hat{\pi}^b\bar{N}\gamma^\mu\frac{\tau^c}{2}N + O(\pi^2)$$

$$\mathcal{A}_{\pi N}^{(3)a\mu} = -\frac{i\hat{c}_4}{2M}\bar{N}\sigma^{\mu\nu}[\xi^\dagger\tau^a\xi + \xi\tau^a\xi^\dagger, a_\nu]N - \frac{2\hat{c}_3}{M}\bar{N}N\text{Tr}[\xi^\dagger\tau^a\xi + \xi\tau^a\xi^\dagger, a_\mu] \quad (3.32)$$

$$= \frac{\hat{c}_4}{f_\pi M}\epsilon^{abc}\partial_\nu\pi^b\bar{N}\tau^c\sigma^{\mu\nu}N - \frac{2\hat{c}_3}{f_\pi M}\bar{N}N\partial^\mu\pi^a + O(\pi^2)$$

$$\mathcal{A}_{NN}^{(3)a\mu} = -D_1\bar{N}\gamma^\mu\gamma_5\tau^aN\bar{N}N \quad (3.33)$$

The notation used in the upper index denotes:  $(\nu_{\mathcal{L}})$  is the chiral order,  $a = 0, \pm 1$  is the isospin projection, and  $\mu = 0, \dots, 3$  is the Lorentz vector projection. The expansion is

used to construct the Feynman diagrams for the currents (see Appendix D).

### 3.5 Nuclear Currents Operators

Using the equations of the two previous sections, one constructs the Feynman rules. The rules derived from the Lagrangian are used to construct nuclear forces form  $\chi$ PT. Let us assume a case, in which the interaction Lagrangian is

$$\hat{\mathcal{L}} = -gS_\mu(\vec{x})\hat{\mathcal{J}}^\mu(\vec{x}), \quad (3.34)$$

where  $S_\mu$  is an outer source current, and  $\hat{\mathcal{J}}^\mu$  is the nuclear current. This Lagrangian is relevant for low-energy electro-weak interaction (cf. Eqs. (2.5,2.21)). The Feynman rules derived from the Nöther of the Lagrangian symmetry, are used to construct the nuclear currents.

An extensive description of the Feynman rules and the derivation of the nuclear currents appear in Appendix D. In view of the typical momentum of the processes in discussion, one can use a soft probe approximation and write the currents to first order in the momentum transfer. It is also clear that any recoil of nucleons is smaller, and thus the use of heavy baryon expansion is justified, expanding the nucleon spinors to leading order in  $\frac{1}{M_N}$  (see Appendix C)

The leading nuclear current operators are single nucleon operators, i.e. describing a coupling to only one nucleon within the nucleus, as if it was a free particle. The next contribution involves two nucleons, in which case the probe interacts via a contact term of two nucleons or a nucleon-pion vertex.

The resulting matrix elements are expressed in momentum space, and as they originate in EFT approach, they are valid up to a cutoff momentum  $\Lambda$ . The cutoff momentum is chosen such that  $\Lambda \gg Q$ , and lower than QCD scale. A proper choice is thus  $\Lambda = 400 - 800$  MeV, as in (Park et al., 2003; Ordóñez et al., 1994; Grdestig and Phillips, 2006). The renormalization group theory states that an observable does not depend on the cutoff momentum. Any cutoff dependence implies excitation of higher energy degrees of freedom. Thus, the cutoff dependence is a consistency check

for the theory. In the Lagrangians of the previous section, the only LEC with a connection to higher energy modes is  $\hat{d}_r$ , thus one should expect a rather steep cutoff dependence for this LEC, and its cutoff dependence is chosen in such manner that the triton half-life reproduces its experimental value.

The nuclear wave functions are written in configuration space, thus one should use a proper transform to move the operators to this basis. Fourier transform is of no help as it includes high momentum. Following Park et al. (2003), let us define the cutoff Fourier transform of an n-body current as

$$\begin{aligned} \hat{\mathcal{J}}_{12\dots n}^a(\vec{x}_1, \dots, \vec{x}_n; \vec{q}) &= \\ &= \left[ \prod_{i=1}^n \int \frac{d^3 k_i}{(2\pi)^3} e^{i\vec{k}_i \cdot \vec{x}_i} S_\Lambda(\vec{k}_i^2) \right] (2\pi)^3 \delta^{(3)}(\vec{q} + \vec{k}_1 + \vec{k}_2 + \dots + \vec{k}_n) \hat{\mathcal{J}}_{12\dots n}^a(\vec{k}_1, \dots, \vec{k}_n; \vec{q}). \end{aligned} \quad (3.35)$$

The cutoff function,  $S_\Lambda(k) = \exp(-\frac{k^2}{2\Lambda^2})$ , does not influence one body currents, due to the momentum conserving  $\delta$  function. For  $Q \lesssim \Lambda$  the cutoff function  $S_\Lambda(k)$  is unity, and it approaches zero for  $Q \gtrsim \Lambda$ . This choice of cutoff function is convenient both for numerical and analytical calculations. One should note that this cutoff function inserts an additional  $\frac{k^2}{\Lambda^2}$  dependence to the currents. This is, however, a minor, negligible effect.

For low energy reactions, where meson exchange currents (MEC) are a perturbative effect, one can use the long wavelength approximation  $q = 0$ . Thus, the Fourier transform of a MEC depends only on the relative coordinate  $\vec{x}_{12} = \vec{x}_1 - \vec{x}_2$ , and

$$\mathcal{A}_{12}^a(\vec{x}_{12}) = \int \frac{d^3 k}{(2\pi)^3} e^{-i\vec{k} \cdot \vec{x}_{12}} S_\Lambda^2(\vec{k}^2) \mathcal{A}_{12}^a(\vec{k}_1 = -\vec{k}, \vec{k}_2 = \vec{k}). \quad (3.36)$$

As the Fourier transform acts on pion propagator, the needed functions are,

$$\delta_\Lambda^{(3)}(\vec{r}) \equiv \int \frac{d^3 k}{(2\pi)^3} e^{i\vec{k} \cdot \vec{r}} S_\Lambda^2(\vec{k}^2), \quad (3.37)$$

$$y_{\Lambda 0}^\pi(r) \equiv \int \frac{d^3 k}{(2\pi)^3} e^{i\vec{k} \cdot \vec{r}} S_\Lambda^2(\vec{k}^2) \frac{1}{k^2 + m_\pi^2}, \quad (3.38)$$

$$y_{\Lambda_1}^\pi(r) \equiv -\frac{\partial}{\partial r} y_{\Lambda_0}^\pi(r), \quad (3.39)$$

$$y_{\Lambda_2}^\pi(r) \equiv \frac{1}{m_\pi^2} r \frac{\partial}{\partial r} \frac{1}{r} \frac{\partial}{\partial r} y_{\Lambda_0}^\pi(r). \quad (3.40)$$

One reproduces the usual Yukawa functions in the limit  $\Lambda \rightarrow \infty$ .

This process leads to operators acting on one nucleon in the case of single nucleon operator, or on a pair of nucleons in the case of MEC operator. To move  $A$  nucleons (or  $\frac{A(A-1)}{2}$  pairs of nucleons) to their coordinates in configuration space one uses first quantization. For the single nucleon operators,

$$\hat{\mathcal{J}}^{(1)\mu}(\vec{x}) = \sum_{i=1}^A \hat{\mathcal{J}}_1^\mu(\vec{r}_i) \delta^{(3)}(\vec{x} - \vec{r}_i), \quad (3.41)$$

and for the MEC operators,

$$\hat{\mathcal{J}}^{(12)\mu}(\vec{x}) = \sum_{i<j}^A \hat{\mathcal{J}}_{12}^\mu(\vec{r}_{ij}) \delta^{(3)}(\vec{x} - \vec{r}_{ij}). \quad (3.42)$$

This leads to the final form of the operators. The single nucleon operators, which are often called the impulse approximation (IA) are the same as those derived from standard nuclear physics approach:

$$\hat{\mathcal{V}}_i^{(1)0} = \delta^{(3)}(\vec{x} - \vec{r}_i) - \frac{1}{2} \frac{\vec{\nabla}}{2M_N} \cdot \left\{ \vec{\sigma}_i \times \frac{\vec{p}_i}{2M_N}, \delta^{(3)}(\vec{x} - \vec{r}_i) \right\} \quad (3.43)$$

$$\hat{\mathcal{A}}_i^{(1)0} = -g_A \left( \vec{\sigma}_i \cdot \left\{ \frac{\vec{p}_i}{2M_N}, \delta^{(3)}(\vec{x} - \vec{r}_i) \right\} - \frac{1}{2} \left\{ \left( \frac{p_i}{2M_N} \right)^2, \delta^{(3)}(\vec{x} - \vec{r}_i) \right\} \right) \quad (3.44)$$

$$\hat{\mathcal{V}}_i^{(1)} = \left\{ \frac{\vec{p}_i}{2M_N}, \delta^{(3)}(\vec{x} - \vec{r}_i) \right\} \quad (3.45)$$

$$\begin{aligned} \hat{\mathcal{A}}_i^{(1)} &= -g_A \left( \vec{\sigma}_i \delta^{(3)}(\vec{x} - \vec{r}_i) - \frac{\vec{\sigma}}{2} \left\{ \frac{\vec{p}_i}{2M_N}, \left\{ \frac{\vec{p}_i}{2M_N}, \delta^{(3)}(\vec{x} - \vec{r}_i) \right\} \right\} \right) \\ &+ \left\{ \frac{\vec{p}_i}{2M_N} \cdot \vec{\sigma}, \left\{ \frac{\vec{p}_i}{2M_N}, \delta^{(3)}(\vec{x} - \vec{r}_i) \right\} \right\} + \frac{\vec{\nabla} \times}{4M_N} \left\{ \frac{\vec{p}_i}{2M_N}, \delta^{(3)}(\vec{x} - \vec{r}_i) \right\} \end{aligned} \quad (3.46)$$

Due to the Siegert theorem (Sec. 2.2.1) for low energy reactions, the conservation of

vector currents implies that neither the vector current nor the vector MEC should be calculated explicitly, as they are included implicitly in the calculation of the single nucleon charge operator.

The axial charge MEC operator is:

$$\hat{\mathcal{A}}_{12}^{0,a}(r_{ij}) = -\frac{g_A m_\pi}{4f_\pi^2} (\vec{\tau}^{(1)} \times \vec{\tau}^{(2)})^a (\vec{\sigma}^{(1)} + \vec{\sigma}^{(2)}) \cdot \hat{r}_{ij} y_{1\Lambda}^\pi(r_{ij}), \quad (3.47)$$

and the axial MEC,

$$\begin{aligned} \hat{\mathcal{A}}_{12}^{i,a}(r_{ij}) = & \frac{g_A}{2Mf_\pi^2} \left\{ \mathcal{O}_P^{i,a} y_{1\Lambda}^\pi(r_{ij}) + \hat{c}_3 (\mathcal{T}_\oplus^{i,a} - \mathcal{T}_\ominus^{i,a}) m_\pi^2 y_{2\Lambda}^\pi(r_{ij}) - \right. \\ & - \hat{c}_3 (\mathcal{O}_\oplus^{i,a} - \mathcal{O}_\ominus^{i,a}) \left( \frac{1}{3} \delta_\Lambda^{(3)}(\vec{r}_{ij}) - \frac{1}{3} m_\pi^2 y_{0\Lambda}^\pi \right) - \\ & - \left( \hat{c}_4 + \frac{1}{4} \right) \mathcal{O}_\otimes^{i,a} m_\pi^2 y_{2\Lambda}^\pi(r_{ij}) - \\ & \left. - \left( \hat{c}_4 + \frac{1}{4} \right) \mathcal{O}_\otimes^{i,a} \left( \frac{2}{3} \delta_\Lambda^{(3)}(\vec{r}_{ij}) - \frac{2}{3} m_\pi^2 y_{0\Lambda}^\pi \right) \right\} + \\ & + \frac{D_1}{2} (\mathcal{O}_\oplus^{i,a} + \mathcal{O}_\ominus^{i,a}) \delta_\Lambda^{(3)}(\vec{r}_{ij}) \end{aligned} \quad (3.48)$$

where

$$\vec{\mathcal{O}}_P^a \equiv -\frac{m_\pi}{4} (\vec{\tau}^{(1)} \times \vec{\tau}^{(2)})^a (\vec{P}_1 \vec{\sigma}^{(2)} \cdot \hat{r}_{12} + \vec{P}_2 \vec{\sigma}^{(1)} \cdot \hat{r}_{12}) \quad (3.49)$$

$$\mathcal{O}_\odot^{i,a} \equiv (\vec{\tau}^{(1)} \odot \vec{\tau}^{(2)})^a (\vec{\sigma}^{(1)} \odot \vec{\sigma}^{(2)})^i, \quad (3.50)$$

$$\mathcal{T}_\odot^{i,a} \equiv \left( \hat{r}_{12}^i \hat{r}_{12}^j - \frac{\delta^{ij}}{3} \right) \mathcal{O}_\odot^{i,a}, \quad (3.51)$$

and  $\odot = \times, +, -$ .

It is important to notice that the contact parts of the current, i.e. terms proportional to  $\delta(r)$ , do not vanish only for pairs in a relative  $L = 0$  state. This implies  $S + T = 1$ , meaning either  $S = 0$  or  $T = 0$ . Consequently, when  $\mathcal{O}_\oplus$  acting on these states, it vanishes.

An additional simplification is achieved by noting that  $\mathcal{O}_\otimes$  and  $\mathcal{O}_\ominus$  are connected. The fermion statistics implies  $\Xi^\tau \Xi^\sigma \Xi^\tau = -1$ , where  $\Xi^\tau$  exchanges isospin of the two particles,  $\Xi^\sigma$  exchanges spin, and  $\Xi^\tau$  exchanges locations. A trivial identity for Pauli

matrices:  $\vec{\sigma}^1 \times \vec{\sigma}^2 = i(\vec{\sigma}^1 - \vec{\sigma}^2)\Xi^\sigma$ . Thus,  $\mathcal{O}_\otimes = -\mathcal{O}_\ominus\Xi^r$ , and as  $\Xi^r\delta(r) = 1$  the connection is clear (Park et al., 2003).

Thus, all the coefficients of  $\delta^{(3)}(\vec{r})$  are combined into a single dimensionless LEC<sup>1</sup>  $\hat{d}_r = \frac{2Mf_\pi^2}{g_A}D_1 + \frac{\hat{c}_3}{3} + \frac{2}{3}(\hat{c}_4 + \frac{1}{4})$ . The  $O(\Lambda^{-2})$  appearing in  $\delta_\Lambda^{(3)}(\vec{r})$  has minor effect, which cancels when renormalizing  $\hat{d}_r$ . The renormalization  $\hat{d}_r(\Lambda)$  for a range of cutoff momentum  $\Lambda = 400 - 800$  MeV, is calibrated to reproduce the triton half-life.

Bearing this in mind, the axial MEC are

$$\begin{aligned} \hat{\mathcal{A}}_{12}^{i,a}(\vec{r}_{ij}) &= \frac{g_A}{2Mf_\pi^2}\hat{d}_r\mathcal{O}_\ominus^{i,a}\delta_\Lambda^{(3)}(\vec{r}_{ij}) - \frac{g_A m_\pi^2}{2Mf_\pi^2}\mathcal{O}_P^{i,a}y_{1\Lambda}^\pi(r_{12}) - \\ &\quad - \frac{g_A m_\pi^2}{2Mf_\pi^2}\left[\frac{\hat{c}_3}{3}(\mathcal{O}_\oplus^{i,a} + \mathcal{O}_\ominus^{i,a}) + \frac{2}{3}(\hat{c}_4 + \frac{1}{4})\mathcal{O}_\otimes^{i,a}\right]y_{0\Lambda}^\pi(r_{ij}) - \\ &\quad - \frac{g_A m_\pi^2}{2Mf_\pi^2}\left[\hat{c}_3(\mathcal{T}_\oplus^{i,a} + \mathcal{T}_\ominus^{i,a}) - (\hat{c}_4 + \frac{1}{4})\mathcal{T}_\otimes^{i,a}\right]y_{2\Lambda}^\pi(r_{ij}) \end{aligned} \quad (3.52)$$

## 3.6 Standard Nuclear Physics and EFT

This chapter has shown the vast advantage in applying EFT approach for the nuclear problem. The theory provides a perturbative approach with its symmetries completely under control. This fact gives a predictive measure to the approach.

These advantages are missing in the standard nuclear physics approach (SNPA), which is phenomenological. However, SNPA approach has many successes, using Lagrangians that include Nucleon–Nucleon potentials and three nucleon forces one can describe the low lying spectrum of nuclei with  $A < 12$ . SNPA Lagrangians are used to calculate electro-weak and strong nuclear reactions, to good accuracy. The Lagrangians are built to reproduce hundreds nucleon–nucleon scattering processes with energies up to 500 MeV, with  $\chi^2$  per datum close to unity. For example, the binding energies of light nuclei are reproduced using these forces to accuracy of tens of keV.

In order to reach this level of accuracy with EFT based Lagrangians, one has to expand to at least next-to-next-to-next-to-leading order, which includes more than

---

<sup>1</sup>Different variations of EFT (e.g. (Park et al., 2003)) lead to different descriptions of the short range forces. These, however, renormalize to the same LEC.

20 parameters. This was done only lately, by Epelbaum et al. (2000); Entem and Machleidt (2003), and still has not arrived the level of  $\chi^2$  achieved in SNPA.

Lately, Rho *et al.* (Rho, 2006; Park et al., 2003) tried to combine the advantages of both approaches. The idea relies on the fact that albeit phenomenological, the SNPA approach holds correct long range behavior. Thus, one may use the nuclear wave functions predicted by SNPA, and calculate reactions using the nuclear currents derived in EFT. The typical accuracy for reactions is in the percentage level, hence it is sufficient to expand the forces up to next-to-leading order, with only one unknown LEC needed for renormalization.

This hybrid approach, named EFT\*, is of course not consistent, as the currents and forces are not derived from the same Lagrangian. Nevertheless, it has been used to calculate reactions of  $A = 2, 3, 4$  nuclei (Rho, 2006; Park et al., 2003). The minor response of the calculated cross-sections to changes in the cutoff momentum is an evidence for the power of the method. This method will be used in this work (Chap. 7) for the calculation of neutrino scattering on  $A = 3$  and  ${}^4\text{He}$  nuclei.

# 4 LORENTZ INTEGRAL TRANSFORM METHOD

The response of a system to excitations is a key ingredient in understanding its properties: stability, energy levels, structure, etc.

For an inclusive reaction with energy transfer  $\omega$ , described by an interference between two operators  $O_1(\vec{q})$  and  $O_2(\vec{q})$ , the response function is defined as:

$$\mathcal{R}_{\hat{O}_1\hat{O}_2}(\omega, \vec{q}) \equiv \sum_f \delta(E_f - E_i - \omega) \langle i | \hat{O}_1^\dagger(\vec{q}) | f \rangle \langle f | \hat{O}_2(\vec{q}) | i \rangle, \quad (4.1)$$

where  $|i/f\rangle$  and  $E_{i/f}$  denote the initial and final wave functions and energies, respectively. In order to calculate this observable, one has to consider every possible final state, including those which are in the continuum. For the light nuclei, which have few bound excited states, if any, the continuum must be taken into account if one wants to consider  $\omega \neq 0$ . This makes an explicit calculation of the cross-section for such nuclei a difficult task, not only as one has to keep track of all break-up channels, but also since a general continuum state wave function is out of reach already for  $A = 4$ .

However, the response function is an integral quantity, as it depends only on projections of the initial state. This has been the motivation for using integral transforms on the response functions, by which, as shown in the next Section, one can avoid an explicit calculation of final state.

One of these transforms is Lorentz Integral Transform (LIT) method. This method has been used in the calculation of various strong and electro-magnetic nuclear reactions (see for example (Efros et al., 1997b,c,a, 2000; Barnea et al., 2001a; Bacca et al., 2002, 2004)). In this thesis the LIT method is applied for weak reactions on nuclei (Gazit and Barnea, 2004, 2007b,a,c). Though used here for inclusive reactions, it has been applied for exclusive reactions as well (Quaglioni et al., 2004).

## 4.1 Integral Transformations

Using integral transform transforms the response function to a continuous function, which depends on a parameter  $\sigma$ , using an analytic kernel function  $K(\omega, \sigma)$ . The integral transform is a functional of the response function, defined as:

$$\mathcal{I}[\mathcal{R}(\omega, \vec{q})](\sigma, \vec{q}) = \int_{0^-}^{\infty} d\omega \mathcal{R}(\omega, \vec{q}) K(\omega, \sigma) \quad (4.2)$$

The integration starts from  $0^-$  to include every possible scattering, including elastic channels. Finite transform and its existence depends on the high energy (high  $\omega$ ) behavior of both the response function and the kernel, and should be checked for each case.

The advantage in using an integral transform is easily viewed when inserting the definition of the response function, Eq. (4.1), in Eq. (4.2). The integration over the energy conserving  $\delta$  function is trivial,

$$\mathcal{I}(\sigma, \vec{q}) = \sum_f \langle i | \hat{O}_1^\dagger(\vec{q}) | f \rangle \langle f | \hat{O}_2(\vec{q}) | i \rangle K(E_f - E_i, \sigma).$$

As  $K(E_f - E_i, \sigma)$  is a number, one can insert it to the matrix element. Using then the fact that the states  $|f\rangle$  are eigenstates of the Hamiltonian,  $\hat{\mathcal{H}}$ , namely  $\hat{\mathcal{H}}|f\rangle = E_f|f\rangle$ , yields the expression

$$\mathcal{I}(\sigma, \vec{q}) = \sum_f \langle i | \hat{O}_1^\dagger(\vec{q}) K(\hat{\mathcal{H}} - E_i, \sigma) | f \rangle \langle f | \hat{O}_2(\vec{q}) | i \rangle.$$

One notes that in this expression the final state appears only through the projection operator  $|f\rangle\langle f|$ . The hermiticity of the Hamiltonian implies closure:  $\sum_f |f\rangle\langle f| = 1$ . Thus,

$$\mathcal{I}(\sigma, \vec{q}) = \langle i | \hat{O}_1^\dagger(\vec{q}) K(\hat{\mathcal{H}} - E_i, \sigma) \hat{O}_2(\vec{q}) | i \rangle. \quad (4.3)$$

There is no doubt that the use of integral transforms simplifies the calculation, as it depends only on the ground state properties. However, this is merely a disguise as the kernel operator depends explicitly on the Hamiltonian  $\hat{\mathcal{H}}$ . The latter acts on

$\hat{O}_2(\vec{q})|i\rangle$ , which is not an eigenstate, hence depends on all basis states. An additional unresolved question is the inversion of the transform.

Obviously, an intelligent choice of the kernel can solve both these problems. Nevertheless, the solution can never be perfect. A choice of a broad kernel smears out narrower structures, which when inverting the transform results in numerical instability. Choosing narrow kernel leads back to the solution of the continuum state problem.

In the literature, different kernels have been proposed. Among which is the Laplace kernel  $K(\omega, \sigma) = e^{-\sigma\omega}$ . The calculation of the transform with this kernel is relatively easy, as it can be presented as propagation in imaginary time. This fact has made the Laplace kernel appropriate for Quantum Monte Carlo calculation (e.g. (Carlson and Schiavilla, 1994)). The disadvantage is the fact that an inversion of Laplace transformation demands an analytic continuation of the integral transform, which is usually unavailable.

In view of the needed narrowness of an optimal kernel, it is valuable to use a kernel which depends on an additional parameter  $\sigma_W$ , with the following properties:

- $K(\omega, \sigma; \sigma_W) = K(\omega - \sigma; \sigma_W)$ .
- $\lim_{\sigma_W \rightarrow 0} K(\omega - \sigma; \sigma_W) = \delta(\omega - \sigma)$ .

The advantages are clear.  $\sigma_W$  is chosen in view of the anticipated width of the reaction cross-section. Photodissociation and neutrino scattering reactions are dominated by giant resonance excitations, with a typical width of 10 – 30 MeV. Thus a reasonable choice is  $\sigma_W \approx 10$  MeV.

Possible examples for kernels which satisfy the aforementioned properties are the Lorentzian and the Gaussian. The Lorentzian turns to be simple to calculate, hence attractive.

## 4.2 Integral Transform with a Lorentzian Kernel

A Lorentzian kernel is defined as  $K(\omega, \sigma) = \frac{1}{(\omega - \sigma_R) + i\sigma_I}$ , where  $\sigma = -\sigma_R + i\sigma_I$  is a complex continuous parameter, with a real part indicating the transform variable and

its imaginary part indicates the Lorentzian width. The Lorentz Integral Transform (LIT) is defined as,

$$\mathcal{L}(\sigma, \vec{q}) = \int_{0^-}^{\infty} d\omega \frac{\mathcal{R}(\omega, \vec{q})}{(\omega - \sigma_R) + \sigma_I^2}. \quad (4.4)$$

Putting the LIT kernel definition in Eq. (4.3) yields:

$$\mathcal{L}(\sigma, \vec{q}) = \langle i | \hat{O}_1^\dagger(\vec{q}) \frac{1}{\hat{\mathcal{H}} - E_0 + \sigma^*} \frac{1}{\hat{\mathcal{H}} - E_0 + \sigma} \hat{O}_2(\vec{q}) | i \rangle, \quad (4.5)$$

which has the form of an internal product:

$$\mathcal{L}(\sigma, \vec{q}) = \langle \tilde{\Psi}_1 | \tilde{\Psi}_2 \rangle \quad (4.6)$$

with,

$$|\tilde{\Psi}_i\rangle \equiv \frac{1}{\hat{\mathcal{H}} - E_0 + \sigma} \hat{O}_i(\vec{q}) | i \rangle, \text{ for } i = 1, 2. \quad (4.7)$$

This important result implies that the evaluation of the LIT requires the solution of the following equation:

$$(\hat{\mathcal{H}} - E_0 + \sigma) |\tilde{\Psi}_i(\sigma)\rangle = \hat{O}_i | i \rangle. \quad (4.8)$$

These equations have several appealing properties:

**Uniqueness and existence of the solution** The hermiticity of the Hamiltonian implies real energies, hence  $E_f - E_0 - \sigma \neq 0$  for  $\sigma_I \neq 0$ . Thus the homogenous equation has only the trivial solution. As a result, there could only be a unique solution dictated by the source term in the right-hand-side of the equation, and the boundary conditions are dictated by it. The source term has a finite norm, i.e. the boundary conditions of a bound state problem. This means that the inner product of Eq. (4.6) is finite and thus the transform exists, and unique.

**LIT is Schrödinger-like problem** In view of the bound state boundary conditions, Eq. (4.8) is a Schrödinger equation with a source term, thus can be solved using the variety of methods available for such problems. One of these methods is the Effective Interaction in the Hyperspherical Harmonics (EIHH)

discussed in the following chapter.

**LIT is a Green–function–like matrix element** It is easy to rewrite Eq. (4.5) as,

$$\mathcal{L}(\sigma, \vec{q}) = \frac{1}{\sigma_I} \text{Im} \left\{ \langle i | \hat{O}_1^\dagger(\vec{q}) \frac{1}{\hat{\mathcal{H}} - E_0 + \sigma} \hat{O}_2(\vec{q}) | i \rangle \right\}. \quad (4.9)$$

Thus, a matrix element of a green–function. Several methods exist to calculate such a matrix–element, one numerically effective method is the Lanczos algorithm, described in the following subsection.

The Lorentz integral transform clearly simplifies calculation of response functions. The method avoids the difficulty of calculating continuum wave functions. Instead a bound–state like equation has to be solved, enabling the theoretical evaluation of previously unreachable reactions.

### 4.2.1 Calculation of LIT using the Lanczos Algorithm

In this subsection an efficient algorithm for the calculation of the LIT presentation of Eq. (4.9) is reviewed, based on the Lanczos Algorithm (Lanczos, 1950). First, let us focus on the  $\hat{O}_1(\vec{q}) = \hat{O}_2(\vec{q}) = \hat{O}$  case.

The Lanczos basis  $\{|\varphi_n\rangle; n \geq 0\}$  is an orthonormal set of states starting with a known state  $|\varphi_0\rangle$ . The rest of the basis can be defined recursively,

$$b_{n+1}|\varphi_{n+1}\rangle = \hat{\mathcal{H}}|\varphi_n\rangle - a_n|\varphi_n\rangle - b_n|\varphi_{n-1}\rangle, \text{ for } n \geq 1, \quad (4.10)$$

With the condition  $b_0 = 0$ . From Eq. (4.10) it is trivial that the Lanczos coefficients  $a_n$  and  $b_n$  are given by:

$$a_n = \langle \varphi_n | \hat{\mathcal{H}} | \varphi_n \rangle \text{ and } b_n = \langle \varphi_n | \hat{\mathcal{H}} | \varphi_{n-1} \rangle. \quad (4.11)$$

Choosing the Lanczos pivot as

$$|\varphi_0\rangle = \frac{\hat{O}|i\rangle}{\sqrt{\langle i | \hat{O}^\dagger \hat{O} | i \rangle}}, \quad (4.12)$$

allows to write the LIT as

$$\mathcal{L}(\sigma) = \frac{1}{\sigma_I} \langle i | \hat{O}^\dagger \hat{O} | i \rangle \text{Im}\{x_{00}(E_0 - \sigma)\}, \quad (4.13)$$

Where

$$x_{n0}(z) \equiv \langle \varphi_n | \frac{1}{\hat{\mathcal{H}} - z} | \varphi_0 \rangle. \quad (4.14)$$

In order to calculate this , one uses the identity  $(\hat{\mathcal{H}} - z)(\hat{\mathcal{H}} - z)^{-1} = I$ , which leads to linear set of equations,

$$\sum_n (\hat{\mathcal{H}} - z)_{mn} x_{n0}(z) = \delta_{m0}. \quad (4.15)$$

Applying Kramers rule, one can express  $x_{n0}(z)$  as continuous fractions, in particular

$$x_{00}(z) = \frac{1}{(z - a_0) - \frac{b_1^2}{(z - a_1) - \frac{b_2^2}{(z - a_2) - \frac{b_3^2}{(z - a_3) - \dots}}}}. \quad (4.16)$$

In typical examples a few hundreds of Lanczos coefficients are sufficient to reach convergence in the LIT.

After defining  $x_{n0}(z)$ , a formulation of a LIT calculation with  $\hat{O}_1(\vec{q}) \neq \hat{O}_2(\vec{q})$  is available. In this formulation, the Lanczos pivot defined as  $|\varphi_0\rangle = \frac{\hat{O}_2|i\rangle}{\sqrt{\langle i|\hat{O}_2^\dagger\hat{O}_2|i\rangle}}$ . One inserts an identity operator  $\sum_i |\varphi_i\rangle\langle\varphi_i|$  to get:

$$\mathcal{L}(\sigma, \vec{q}) = \frac{\sqrt{\langle i|\hat{O}_2^\dagger\hat{O}_2|i\rangle}}{\sigma_I} \text{Im} \sum_n \langle i|\hat{O}_1^\dagger(\vec{q})|\varphi_n\rangle x_{n0}(z). \quad (4.17)$$

### 4.3 Inversion of the LIT

The success of an integral transform highly relies on the existence of a stable inversion. An analytic inversion for the Lorentz transform does not exist.

One can observe the problem in inverting the LIT in the following reason. Let us

perform a Fourier transform on Eq. (4.4). The r.h.s of that equation is a convolution of lorentzian and the response function. Bearing in mind that the fourier transform of a lorentzian is exponential decay, one gets

$$\mathcal{F}[\mathcal{L}(\sigma, \vec{q})](k) = \frac{\pi}{\sigma_I} e^{-\sigma_I |k|} \mathcal{F}[\mathcal{R}(\omega, \vec{q})](k). \quad (4.18)$$

As a result, high energy (short wavelengths) are suppressed when performing the LIT. Clearly, this fact creates instability in the inversion, which enhances short wavelength oscillations.

However, a hope lies in the fact that mathematically the inversion is unique. Moreover, there are several numerical approaches for the inversion in the literature, which have provided stable and successful results. The method used in this scope is expanding the wanted inversion (i.e. the nuclear response function) in a set of functions  $f_n(\omega)$ ,

$$\mathcal{R}(\omega, \vec{q}) = \sum_{n=1}^N c_n(\vec{q}) f_n(\omega). \quad (4.19)$$

Since the transform is linear, it is obvious that the LIT of Eq. (4.19)  $\mathcal{L}(\sigma, \vec{q}) = \sum_{n=1}^N c_n(\vec{q}) \mathcal{L}_n(\sigma)$ , where  $\mathcal{L}_n(\sigma)$  is the known LIT of  $\{f_n(\omega)\}$ . One obtains the coefficients  $c_n$  by solving the minimal squares problem, on a grid  $\{\sigma_R^i, i = 1, \dots, K\}$ :

$$\sum_{k=1}^K \left| \mathcal{L}(\sigma^k, \vec{q}) - \sum_{n=1}^N c_n(\vec{q}) \mathcal{L}_n(\sigma^k) \right|^2 = \min \quad (4.20)$$

The problem of the inversion is hence reduced to the solution of a set of linear equations. It has been shown (Efros et al., 1999; Efros, 1999) that fitting on a grid such that  $K \gg N$  regularizes the inversion, thus solves the stability problem.

In order to increase both accuracy and control over the inversion, one can take some important measures:

**Physical considerations** Often there are physical considerations on the asymptotic and threshold of the response function. The choice of a physical shape for  $f_n$  can diminishes the number of needed expansion functions, while increasing the

stability and accuracy of the inversion. Such a set of functions is:

$$f_n(\omega) = \omega^{n_0} e^{-\frac{\omega}{n\Delta E}}. \quad (4.21)$$

This choice uses the fact that the threshold behavior is a power law, with  $n_0 \sim 1.5$ , and that the high energy tail decays exponentially with characteristic width  $\Delta E$ .

**Sum Rules** Integration over the entirety of the response with a specific weight function depends on ground state properties. Thus, the inversion can be checked for consistency. In Chap. 6 an extensive discussion on the subject of sum rules in photodissociation processes is given.

**Stability with respect to  $\sigma_I$**  The LIT can be calculated for various widths  $\sigma_I$ . A stability of the inversion with respect to  $\sigma_I$  shows that there are no hidden structures of width less than  $\sigma_I$ .

# 5 NUCLEAR WAVE FUNCTIONS

The nuclear problem regards the properties of an  $A$ -body quantum mechanical non-relativistic system subjected to strong correlations. As a result, the calculation of exact solutions to the problem is a difficult task, demanding elaborate theoretical and numerical methods. In order to solve the LIT equations, one needs a good knowledge of the ground state wave function, and the ability to calculate matrix elements.

In the non-relativistic approximation the nuclear Hamiltonian,

$$\mathcal{H} = \sum_{i=1}^A \frac{p_i^2}{2M_N} + \sum_{i<j=1}^A V^{(2)}(\vec{r}_{ij}) + \sum_{i<j<k=1}^A V^{(3)}(\vec{r}_i, \vec{r}_j, \vec{r}_k), \quad (5.1)$$

includes not only a nucleon-nucleon (NN) interaction  $V^{(2)}(\vec{r}_{ij})$ , which depends on the distance between the nucleons  $\vec{r}_{ij} \equiv \vec{r}_i - \vec{r}_j$ , but also three nucleon force (3NF)  $V^{(3)}(\vec{r}_i, \vec{r}_j, \vec{r}_k)$ . The need in 3NF is observed already in the trinuclei binding energies, where state of the art NN potentials lead to underbindings of about 10%.

In this chapter I will present the use of hyperspherical coordinates and functions for the evaluation of nuclear wave functions and matrix elements. The effective interaction in hyperspherical harmonics (EIH) approach is introduced at the end of the chapter.

## 5.1 Few-Body problems in terms of the Hyperspherical Harmonics

The most simple  $A$ -body problem is the 2-body problem. One of the conclusions from the solution of the 2-body problem is that a natural selection for representing the problem is to separate the center of mass movement and the relative motion among

the bodies. In the case of an isolated system the center of mass movement is trivial and does not affect the system. The center of mass coordinate, for a system of  $A$  equal masses is  $\vec{R}_{cm} = \frac{1}{A} \sum_{i=1}^A \vec{r}_i$ . The internal coordinates are defined as  $\vec{r}'_i = \vec{r}_i - \vec{R}_{cm}$ . This way, when working in the center of mass frame,  $\sum_i \vec{r}'_i = 0$ .

It is clear that a good choice of internal coordinates can help representing the nuclear problem. The Jacobi coordinates provide such a choice, as the logic of their construction is the separation of a subset of particles from the center of mass of the other particles.

For a one body operator, one chooses

$$\vec{\eta}_{k-1} = \sqrt{\frac{k-1}{k}} \left( \vec{r}_k - \frac{1}{k-1} \sum_{i=1}^{k-1} \vec{r}_i \right) ; k = 2, \dots, A. \quad (5.2)$$

In this set, the last Jacobi coordinate is proportional to the coordinate of the last particle,  $\vec{\eta}_{A-1} = \sqrt{\frac{A}{A-1}} \vec{r}'_A$ .

For a two-body operator, one chooses

$$\vec{\eta}_k = \sqrt{\frac{A-k}{A+1-k}} \left( \vec{r}_k - \frac{1}{A-k} \sum_{i=k+1}^A \vec{r}_i \right) ; k = 1, \dots, A-1. \quad (5.3)$$

In this set, the last Jacobi coordinate is proportional to the relative distance between the two last coordinates,  $\vec{\eta}_{A-1} = \sqrt{\frac{1}{2}} (\vec{r}_{A-1} - \vec{r}_A)$ .

As a result, the matrix element depends only on the last Jacobi coordinate. One can use the invariance of the matrix element to the other Jacobi coordinates by defining a generalization of the spherical coordinates, *the hyperspherical coordinates*.

### 5.1.1 Hyperspherical Coordinates

The hyper-radius of a  $k$ -body internal system is defined as (Efros, 1972),

$$\rho_k^2 = \sum_{i=1}^k \eta_i^2 = \frac{1}{k} \sum_{i<j}^{k+1} (\vec{r}_i - \vec{r}_j)^2. \quad (5.4)$$

From this definition it is clear that  $\rho_k^2 = \rho_{k-1}^2 + \eta_k^2$ , so that  $(\rho_{k-1}, \eta_k, \rho_k)$  is a pythagorean triplet, with a hyper-angle  $\varphi_k \in [0, \frac{\pi}{2}]$ :

$$\begin{aligned}\rho_{k-1} &= \rho_k \cos \varphi_k, \\ \eta_k &= \rho_k \sin \varphi_k.\end{aligned}\tag{5.5}$$

With this, the  $A - 1$  internal degrees of freedom are described by one hyper-radius  $\rho_{A-1}$ ,  $A - 2$  hyper-angles  $\varphi_{(A-2)} \equiv \{\varphi_2, \dots, \varphi_{A-1}\}$ , and  $2(A - 1)$  degrees of freedom related to the solid angles of the Jacobi coordinates  $\Omega_{(A-1)} \equiv \{\hat{\eta}_1, \dots, \hat{\eta}_{A-1}\}$ .

The volume element related to the internal  $A$ -body system is (Barnea, 1997)

$$\begin{aligned}dV_{3(A-1)} &= \rho_{A-1}^{3A-4} dS_{3A-4} \\ &= \rho_{A-1}^{3A-4} \sin^2(\varphi_{A-1}) \cos^{3A-7}(\varphi_{A-1}) d\varphi_{A-1} d\hat{\eta}_{A-1} dS_{3A-7},\end{aligned}\tag{5.6}$$

where  $dS_N$  is a hyper-sphere surface element in  $N$  dimensions.

One still has to write the kinetic energy operator using hyperspherical coordinates. It is again useful to start with an analogy to the 2-body problem, where the Laplace operator for one relative coordinate is

$$\Delta_{\vec{\eta}_1} = \Delta_{\eta_1} - \frac{\hat{l}_1^2}{\eta_1^2}\tag{5.7}$$

here the radial part is  $\Delta_{\eta_1} = \frac{1}{\eta_1^2} \frac{\partial}{\partial \eta_1} \left( \eta_1^2 \frac{\partial}{\partial \eta_1} \right)$ . For a set of  $A - 1$  Jacobi coordinates, the Laplace operator is a sum  $\Delta_{(A-1)} = \sum_{i=1}^{A-1} \Delta_{\vec{\eta}_i}$ . After a transformation to  $\rho_{A-1}, \varphi_A$ , one gets (Efros, 1972):

$$\Delta_{(A-1)} = \Delta_{\rho_{A-1}} - \frac{\hat{K}_{A-1}^2}{\rho_{A-1}^2}\tag{5.8}$$

with the hyper-radial part

$$\Delta_{\rho_{A-1}} = \frac{\partial^2}{\partial \rho_{A-1}^2} + \frac{3(A-1) - 1}{\rho_{A-1}} \frac{\partial}{\partial \rho_{A-1}}.\tag{5.9}$$

The grand-angular-momentum operator  $\hat{K}_{A-1}$  is built recursively, starting with  $\hat{K}_1 \equiv$

$\hat{l}_1$ . The construction is done by choosing two subsets of Jacobi coordinates, and using Eq. (5.5). If one chooses  $A - 2$  coordinates as a subset, the recurrence relation is  $\Delta_{(A-1)} = \Delta_{(A-2)} + \Delta_{\vec{r}_{A-1}}$ . Putting Eqs. (5.7,5.8) in this relation, one gets:

$$\begin{aligned} \hat{K}_{A-1} = & -\frac{\partial^2}{\partial\varphi_{A-1}^2} + \frac{3[(A-1)-2] - [3(A-1)-2]\cos 2\varphi_{A-1}}{\sin 2\varphi_{A-1}} \frac{\partial}{\partial\varphi_{A-1}} + \\ & + \frac{\hat{K}_{A-2}^2}{\cos^2 \varphi_{A-1}} + \frac{\hat{l}_{A-1}^2}{\sin^2 \varphi_{A-1}} \end{aligned} \quad (5.10)$$

If we define the internal angular momentum operator  $\hat{L}_{A-1} = \sum_{i=1}^{A-1} \hat{l}_i$ , it is clear that the operators  $\hat{K}_{A-1}$ ,  $\hat{l}_{A-1}$ ,  $\hat{K}_{A-2}$ ,  $\hat{L}_{A-1}^2$  and  $\hat{L}_{A-1}^Z$  are commutative. Thus, an eigenstate of the Laplacian can be labeled by the quantum numbers  $K_{A-1}, \dots, K_1, l_1, \dots, l_{A-1}, L_{A-1}, \dots, L_1$  and  $M_{A-1}$ .

### 5.1.2 The Hyperspherical Harmonics Functions

The hyperspherical harmonics functions are the eigen-functions of the Laplace operator. As explained in the previous section the operator is built recursively, a fact which reflects upon the construction of its eigen-functions.

In general, when treating the nuclear problem as  $A$  identical particles (i.e. when identifying protons and neutrons in the isospin symmetry) the internal wave functions belong to an irreducible representation (*irrep*) of the symmetric group  $\mathcal{S}_A$ . This simplifies the calculation of matrix elements, as for a generic  $N$ -body operator  $\hat{O}_{(N)} = \sum_{i_1 < i_2 < \dots < i_N=1}^A \hat{O}_{i_1, i_2, \dots, i_N}$  the problem reduces to a matrix element of an operator acting on one  $N$ -body subsystem  $\langle \Psi | \hat{O}_{(N)} | \Psi' \rangle = \binom{A}{N} \langle \Psi | \hat{O}_{A-N+1, \dots, A} | \Psi' \rangle$ . The relevant cases of one-, two-, and three-body operators are written explicitly as,

$$\begin{aligned} \langle \Psi | \hat{O}_{(1)} | \Psi' \rangle &= A \langle \Psi | \hat{O}_A | \Psi' \rangle \\ \langle \Psi | \hat{O}_{(2)} | \Psi' \rangle &= \frac{A(A-1)}{2} \langle \Psi | \hat{O}_{A, A-1} | \Psi' \rangle \\ \langle \Psi | \hat{O}_{(3)} | \Psi' \rangle &= \frac{A(A-1)(A-2)}{6} \langle \Psi | \hat{O}_{A, A-1, A-2} | \Psi' \rangle \end{aligned}$$

In order to construct a hyperspherical function with such a property, one starts in the 2–body problem. In this case there exists one Jacobi coordinate, and the hyper–spherical formalism coincides with the usual spherical formalism, thus the eigen–functions are the spherical harmonics,  $Y_{l_1 m_1}(\hat{\eta}_1)$ . The latter also belongs to a well defined *irrep* of the symmetry group  $\mathcal{S}_2$ . Adding an additional particle is done by the usual coupling of angular momenta,

$\Phi_{L_2, M_2; l_1, l_2}(\Omega_{(2)}) = \sum_{m_1, m_2} (l_1 m_1 l_2 m_2 | L_2, M_2) Y_{l_1 m_1}(\hat{\eta}_1) Y_{l_2 m_2}(\hat{\eta}_2)$ . This does not exhaust the eigen–function of the 3–body grand–angular momentum  $\hat{K}_2$ , as there is an additional dependence on the hyper–angle coordinate  $\varphi_2$ . The resulting differential equation is separable, bringing to the hyperspherical function for three particles,

$$\mathcal{Y}_{K_2, L_2, M_2, l_1, l_2}(\Omega_{(2)}, \varphi_2) = \Psi_{K_2; l_1 l_2}(\varphi_2) \Phi_{L_2, M_2; l_1, l_2}. \quad (5.11)$$

By a linear combination of these functions with common  $K_2, L_2, M_2$  one can construct basis functions that belong to well defined *irreps* of the orthogonal group  $\mathcal{O}(2)$ . Consequently, the hyperspherical function depends on the Gel’fand–Zetlin (GZ) symbol  $\Lambda_2$ , and a multiplicity label  $\alpha_2$ . So the hyperspherical function is labeled by five good quantum numbers,  $\mathcal{Y}_{[K_2]}(\Omega_{(2)}, \varphi_2)$ , with  $[K_2] \equiv K_2, L_2, M_2, \Lambda_2, \alpha_2$ .

As mentioned, the construction of the hyper–spherical function for the  $A$ –body,  $A-1$  Jacobi coordinates, problem is done recursively. Let us assume the construction led to  $\mathcal{Y}_{[K_{A-2}]}(\Omega_{(A-2)}, \varphi_{(A-2)})$  with  $[K_{A-2}] \equiv K_{A-2}, L_{A-2}, M_{A-2}, K_{A-3}, L_{A-3}, l_{A-2}, \Lambda_{A-3}, \alpha_{A-3}$ . By coupling this to  $Y_{l_{A-1} m_{A-1}}(\hat{\eta}_{A-1})$  one gets

$$\begin{aligned} \Phi_{L_2, M_2; l_1, l_2}(\Omega_{(2)}) &= \quad (5.12) \\ &= \sum_{M_{A-2}, m_{A-1}} (L_{A-2} M_{A-2} l_{A-1} m_{A-1} | L_{A-1}, M_{A-1}) \mathcal{Y}_{[K_{A-2}]}(\Omega_{(A-2)}, \varphi_{(A-2)}) Y_{l_{A-1} m_{A-1}}(\hat{\eta}_{A-1}). \end{aligned}$$

Next, one constructs the orthonormalized eigen–functions of the grand angular momentum operator  $\hat{K}_{A-1}^2$  (Efros, 1972):

$$\begin{aligned} \Psi_{K_{A-1}; l_{A-1} K_{A-2}}(\varphi_{A-1}) &= \quad (5.13) \\ \mathcal{N}_{A-1}(K_{A-1}; l_{A-1} K_{A-2}) (\sin \varphi_{A-1})^{l_{A-1}} (\cos \varphi_{A-1})^{K_{A-2}} P_{n_{A-1}}^{(l_{A-1} + \frac{1}{2}, K_{A-2} + \frac{3A-8}{2})}(\cos 2\varphi_{A-1}), \end{aligned}$$

where  $P_n^{(\alpha,\beta)}$  are the Jacobi polynomials,  $n_{A-1} = \frac{K_{A-1} - K_{A-2} - l_{A-1}}{2}$ , and the normalization factor is (Efros, 1972):

$$\mathcal{N}_{A-1}(K_{A-1}; l_{A-1} K_{A-2}) = \sqrt{\frac{(2K_{A-1} + 3A - 5)n_{A-1}! \Gamma(n_{A-1} + K_{A-2} + l_{A-1} + \frac{3A-5}{2})}{\Gamma(n_{A-1} + l_{A-1} + \frac{3}{2}) \Gamma(n_{A-1} + K_{A-2} + \frac{3A-6}{2})}}. \quad (5.14)$$

The function  $\Psi$  is an eigen-function of  $\hat{K}_{A-1}^2$  with an eigen-value  $K_{A-1}(K_{A-1} + 3A - 5)$ . By construction,  $K_{A-1} - (K_{A-2} + l_{A-1}) \geq 0$ , and even. As a result  $n_{A-1}$  is a non-negative integer.

The result of the complete separation between hyper-angular coordinate and the Jacobi coordinates, means that one can construct the hyper-spherical function

$$\mathcal{Y}_{[K_{A-1}]}(\Omega_{(A-1)}, \varphi_{(A-1)}) = \Psi_{K_{A-1}; l_{A-1} K_{A-2}}(\varphi_{A-1}) \Phi_{L_{A-1}, M_{A-1}; [K_{A-2}] l_{A-1}}(\Omega_{(A-2)} \varphi_{(A-2)}) \quad (5.15)$$

where  $[K_{A-1}]$  stands for  $K_{A-1}, L_{A-1}, M_{A-1}, K_{A-2}, L_{A-2}, l_{A-1}, \Lambda_{A-2}, \alpha_{A-2}$ . These functions are a complete set, orthonormal in each of the quantum numbers.

However, using this construction, the hyperspherical harmonics functions still do not possess the symmetry property for quantum symmetry, i.e. they do not belong to an *irrep* of the symmetry group  $\mathcal{S}_A$ . For this purpose we use an algorithm developed by Barnea and Novoselsky (1997), which uses an extension of the Novoselsky, Katriel, Gilmore (NKG) algorithm (Novoselsky et al., 1988), and yields an  $A$  particle state belonging to well defined *irreps* of both the orthogonal and the symmetry groups.

The process starts with a part overlooked in the previous explanation, the recursive construction of the hyperspherical functions as an *irrep* of  $\mathcal{O}(A-1)$ . This step is done by understanding that the GZ states can be expressed recursively  $\Lambda_N = [\boldsymbol{\lambda}_N \Lambda_{N-1}]$ , where  $\boldsymbol{\lambda}_N$  is an *irrep* of  $\mathcal{O}(N)$  containing the *irreps* represented by the GZ state  $\Lambda_{N-1}$ . Using this relation, one gets

$$\begin{aligned} |K_N L_N M_N \Lambda_N \alpha_N\rangle &= \quad (5.16) \\ &= \sum_{K_{N-1} L_{N-1} \alpha_{N-1} l_N} [(K_{N-1} L_{N-1} \boldsymbol{\lambda}_{N-1} \alpha_{N-1}; l_N) K_N L_N] |K_N L_N \boldsymbol{\lambda}_{N-1} \alpha_{N-1}\rangle \times \\ &\quad \times |(K_{N-1} L_{N-1} \Lambda_{N-1} \alpha_{N-1}; l_N) K_N L_N\rangle K_N L_N M_N \rangle. \end{aligned}$$

The transformation coefficients connect  $N - 1$  coordinates with the  $N^{\text{th}}$  coordinate, thus called the hyperspherical orthogonal coefficients of fractional parentage (hsocfps). in Barnea and Novoselsky (1997) it is shown that the hsocfps depend only on the  $\mathcal{O}(N)$  and  $\mathcal{O}(N - 1)$  *irreps*, and are independent of  $M_N$ .

The next step is the reduction of the kinematical symmetry to the permutation symmetry, i.e.  $\mathcal{O}(A - 1) \rightarrow \mathcal{S}_A$  in the case of  $A$  identical particles. The NKG algorithm is based on the recursive construction of a state of an *irrep* of  $\mathcal{S}_N$  from a state of an *irrep* of  $\mathcal{S}_{N-1}$ . The algorithm uses the transposition representation of a permutation, by which any contained permutation is represented as a subset of the transpositions. By construction, a state with  $N$  particles is characterized by the symmetric group *irrep* that correspond to the group-subgroup chain  $\mathcal{S}_1 \subset \mathcal{S}_2 \subset \dots \subset \mathcal{S}_N$ , represented by Young diagrams  $\Gamma_1, \dots, \Gamma_N$ . For short, one uses the Yamanouchi symbol  $Y_N = [\Gamma_N \Gamma_{N-1} \dots \Gamma_1] = [\Gamma_N Y_{N-1}]$ . The symmetry adaptation of the  $\mathcal{O}_{N-1}$  symmetry to include the permutation symmetry has its price, letting go of the kinematical symmetry chain of group-subgroup  $\Lambda_{N-1}$  and holding only the  $\mathcal{O}_{N-1}$  representation invariant, i.e.  $\lambda_{N-1}$ . Also, a possibility of degeneracy of the permutation states in the kinematical group, suggests an additional label  $\beta_N$ . This is a kind of parentage transformation, thus its coefficients are called orthogonal coefficients of fractional parentage (ocfps).

Summing this up, we have the recursive relation:

$$\begin{aligned}
& |K_{A-1} L_{A-1} M_{A-1} \lambda_{A-1} \alpha_{A-1} \Gamma_A Y_{A-1} \beta_A \rangle = & (5.17) \\
& = \sum_{\lambda_{A-2} \beta_{A-1}} [(\lambda_{A-2} \Gamma_{A-1} \beta_{A-1}) \lambda_{A-1}] \lambda_{A-1} \Gamma_A \beta_A \times \\
& \times \sum_{K_{A-2} L_{A-2} \alpha_{A-2} l_{A-1}} [(K_{A-2} L_{A-2} \lambda_{A-2} \alpha_{A-2}; l_{A-1}) K_{A-1} L_{A-1}] \lambda_{A-1} \alpha_{A-1} \times \\
& \times |(K_{A-2} L_{A-2} \lambda_{A-2} \alpha_{A-2} \Gamma_{A-1} Y_{A-2} \beta_{A-1}; l_{A-1}) K_{A-1} L_{A-1} M_{A-1} \lambda_{A-1} \rangle.
\end{aligned}$$

Where of course,

$$\langle \Omega | K_{A-1} L_{A-1} M_{A-1} \lambda_{A-1} \alpha_{A-1} \Gamma_A Y_{A-1} \beta_A \rangle = \mathcal{Y}_{K_{A-1} L_{A-1} M_{A-1} \lambda_{A-1} \Gamma_A Y_{A-1} \alpha_A^K}(\Omega), \quad (5.18)$$

with  $\Omega = (\Omega_{(A-1)}, \varphi_{(A-1)})$  for the angular coordinates, and  $\alpha_A^K = (\alpha_{A-1}, \beta_A)$  is the multiplicity label.

### 5.1.3 The Hyperspherical Formalism with Internal Degrees of Freedom

Pauli principle suggests that a set of identical particles would have good symmetry properties with respect not only to the configurational exchange of two particles, but to all the degrees of freedom of the particle. In the case of nucleons, this means that the wave function of the  $A$ -body nucleus can be written as,

$$\Phi(\vec{\eta}_1 \dots \vec{\eta}_N, s_1 \dots s_A, t_1 \dots t_A) = \sum_{[K]\nu} R_{[K];\nu}(\rho) H_{[K]}(\Omega, s_1 \dots s_A, t_1 \dots t_A). \quad (5.19)$$

$R_{[K];\nu}(\rho)$  are solutions to the hyper-radial equation, with quantum number  $\nu$ , and  $[K] \equiv J_A, J_A^z, [K_A], S_A, T_A, T_A^z, \alpha_A^{ST}$ . The function  $H_{[K]}(\Omega; s_1 \dots s_A; t_1 \dots t_A)$  possesses the correct symmetry property for a set of fermions, i.e. antisymmetric in any exchange of particles. The nuclear states are described by total isospin,  $T$ , and total angular momentum  $J$ . The latter is the sum of the total spin  $S$  and orbital angular momentum  $L$ .

It is clear that in order to couple the hyperspherical harmonics to a spin-isospin state, one needs to create the latter as a representation of the permutation group.

This is done, once again, by means of the NKG algorithm. One uses spin-isospin coefficients of fractional parentage (stcfps), to build the state

$$\begin{aligned} \chi_{S_A S_A^z T_A T_A^z \Gamma_A Y_{A-1} \alpha_A^{ST}}(s_1, \dots, s_A; t_1, \dots, t_A) = & \sum_{S_{A-1} T_{A-1} \alpha_{A-1}^{TS}} \quad (5.20) \\ & [(S_{A-1}; s_A) S_A(T_{A-1}; t_A) T_A \Gamma_{A-1} \alpha_{A-1}^{TS} | \} S_A T_A \Gamma_A \alpha_A^{ST}] \times \\ & [\chi_{S_{A-1} T_{A-1} \Gamma_{A-1} Y_{A-2} \alpha_{A-1}^{ST}} \otimes s_A t_A]^{S_A S_A^z T_A T_A^z}, \end{aligned}$$

where  $S_A$  ( $T_A$ ) is the total spin (isospin), with projection  $S_A^z$  ( $T_A^z$ ), and the label  $\alpha_A^{ST}$  is needed to remove the degeneracy.

Consequently, the function  $H_{[K]}(\Omega; s_1, \dots, s_A; t_1, \dots, t_A) = \langle \Omega, s_1 \dots s_A, t_1 \dots t_A | [K] \rangle$  is just,

$$H_{[K]}(\Omega; s_1, \dots, s_A; t_1, \dots, t_A) = \sum_{Y_{A-1}} \frac{\Lambda_{\Gamma_A, Y_{A-1}}}{\sqrt{|\Gamma_A|}} \times \quad (5.21)$$

$$\times \left[ \mathcal{Y}_{K_{A-1} L_{A-1} \lambda_{A-1} \Gamma_A Y_{A-1} \alpha_N^K}(\Omega) \otimes \chi_{S_A T_A T_A^z \tilde{\Gamma}_A \tilde{Y}_{A-1} \alpha_A^{ST}}(s_1, \dots, s_A; t_1, \dots, t_A) \right]_{J_A}^{J_A},$$

where  $\Lambda_{\Gamma_A, Y_{A-1}}$  are phase factors, which in the case of fermionic system are positive (negative) when the number of boxes in the diagram  $\Gamma_A$  below the row of the  $A^{\text{th}}$  particle is odd (even).  $|\Gamma_A|$  is the dimension of the young diagram. This function couples the total spin and orbital angular momentum to angular momentum  $J_A$ , with projection  $J_A^z$ , i.e. an  $LS$  scheme. However, in microscopic problems, where the forces are not necessarily central, a  $JJ$  coupling scheme is usually preferred.

In the  $JJ$  coupling scheme, one first couples the spin and angular momentum of the last particle  $s_A = \frac{1}{2}$  and  $l_A$  to  $j_A$ , which is then coupled to the total angular momentum  $J_{A-1}$  of the residual  $A - 1$  particles, given by the coupling of  $S_{A-1}$  and  $L_{A-2}$ . Finally, the hyperspherical spin-isospin basis state is written as

$$[[K]]_{(1)} = \sum_{Y_{A-1}} \frac{\Lambda_{\Gamma_A, Y_{A-1}}}{\sqrt{|\Gamma_A|}} \sum_{\lambda_{A-2} \beta_{A-1}^\lambda} [(\lambda_{A-2} \Gamma_{A-1} \beta_{A-1}^\lambda) \lambda_{A-1} | \lambda_{A-1} \Gamma_A \beta_A^\lambda] \times$$

$$\sum_{K_{A-2} L_{A-2} \beta_{N-1}^K l_{A-1}} [(K_{A-2} L_{A-2} \lambda_{A-2} \beta_{A-2}^K; l_{A-1}) K_{A-1} L_{A-1} | K_{A-1} L_{A-1} \lambda_{A-1} \beta_{A-1}^K] \times$$

$$\sum_{S_{A-1} T_{A-1} \alpha_{A-1}^{ST}} [(S_{A-1}; s_A) S_A(T_{A-1}; t_A) T_A \Gamma_{A-1} \alpha_{A-1}^{ST} | S_A T_A \Gamma_A \alpha_A^{ST}] \times \quad (5.22)$$

$$\sum_{j_A J_{A-1}} \sqrt{(2S_A + 1)(2L_{A-1} + 1)(2j_A + 1)(2J_{A-1} + 1)} \left\{ \begin{array}{ccc} S_{A-1} & s_A & S_A \\ L_{A-2} & l_{A-1} & L_{A-1} \\ J_{A-1} & j_A & J_A \end{array} \right\} \times$$

$$|(T_{A-1}, t_A) T_A T_A^z \rangle \times$$

$$|((S_{A-1}; K_{A-2} L_{A-2} \lambda_{A-2} \beta_{A-2}^K \Gamma_{A-1} Y_{A-2} \beta_{A-1}^\lambda) J_{A-1}; (s_A; l_{A-1}) j_A) J_A J_A^z \rangle$$

This is relevant mainly when the choice of Jacobi coordinates is according to Eq. (5.2),

in which the last coordinate is proportional to the last particle coordinate.

A different  $JJ$  coupling scheme is used when the choice of Jacobi coordinates is according to Eq. (5.3), i.e. the last coordinate is proportional to the relative coordinate of the last two particles. In this scheme, one couples the last two particles total spin  $\hat{s} = \hat{s}_A + \hat{s}_{A-1}$  and orbital angular momentum  $\hat{l} = \hat{l}_A + \hat{l}_{A-1}$  to a total angular momentum  $\hat{j}$ . The latter is then coupled to the total angular momentum of the residual  $A - 2$  particle system, which is the coupling of its spin  $S_{A-2}$  and orbital angular momentum  $L_{A-3}$ . This leads to the following representation of the basis state,

$$\begin{aligned}
|[K]\rangle_{(2)} = & \sum_{Y_{A-1}Y_{A-2}} \frac{\Lambda_{\Gamma_A, Y_{A-1}}}{\sqrt{|\Gamma_A|}} \frac{\Lambda_{\Gamma_{A-1}, Y_{A-2}}}{\sqrt{|\Gamma_{A-1}|}} \sum_{\lambda_{A-2}\beta_{A-1}^\lambda} [(\lambda_{A-2}\Gamma_{A-1}\beta_{A-1}^\lambda)\lambda_{A-1}] \lambda_{A-1} \Gamma_A \beta_A^\lambda \times \\
& \sum_{K_{A-2}L_{A-2}\beta_{A-2}^K} [(K_{A-2}L_{A-2}\lambda_{A-2}\beta_{A-2}^K; l)K_{A-1}L_{A-1}] K_{A-1}L_{A-1} \lambda_{A-1} \beta_{A-1}^K \times \\
& \sum_{S_{A-1}T_{A-1}\alpha_{A-1}^{ST}} [(S_{A-1}; s_A)S_A(T_{A-1}; t_A)T_A \Gamma_{A-1} \alpha_{A-1}^{ST}] S_A T_A \Gamma_A \alpha_A^{ST} \times \\
& \sum_{S_{A-2}T_{A-2}\alpha_{A-2}^{ST}} [(S_{A-2}; s)S_{A-1}(T_{A-2}; t)T_{A-1} \Gamma_{A-2} \alpha_{A-2}^{ST}] S_{A-2} T_{A-2} \Gamma_{A-2} \alpha_{A-2}^{ST} \times \quad (5.23) \\
& \sum_{jstJ_{A-2}} (-)^{S_{A-2}+S_A} \sqrt{(2S_{A-1}+1)(2s+1)} \begin{Bmatrix} S_{A-2} & \frac{1}{2} & S_{A-1} \\ \frac{1}{2} & S_A & s \end{Bmatrix} \times \\
& (-)^{T_{A-2}+T_A} \sqrt{(2T_{A-1}+1)(2t+1)} \begin{Bmatrix} T_{A-2} & \frac{1}{2} & T_{A-1} \\ \frac{1}{2} & T_A & t \end{Bmatrix} \times \\
& \sqrt{(2S_A+1)(2L_{A-1}+1)(2j_A+1)(2J_{A-1}+1)} \begin{Bmatrix} S_{A-2} & s & S_A \\ L_{A-2} & l & L_{A-1} \\ J_{A-2} & j & J_A \end{Bmatrix} \times \\
& |(T_{A-2}, t)T_A T_A^z\rangle \times \\
& |((S_{A-2}; K_{A-2}L_{A-2}\lambda_{A-2}\beta_{A-2}^K \Gamma_{A-1} Y_{A-2} \beta_{A-1}^\lambda) J_{A-2}; (s; l)j) J_A J_A^z\rangle
\end{aligned}$$

With these results, one can now proceed to the calculation of matrix elements.

### 5.1.4 Matrix Elements within the Hyperspherical Formalism

In nuclear problems one has to consider matrix elements of operators of pure isospin  $\mathcal{T}$ , and its projection  $\mathcal{T}_z$ , and spin-orbital coupling to a total angular momentum  $\mathcal{J}$  with projection  $\mathcal{M}$ . This operator can act either on a single nucleon, or more. In the general case of an operator acting on  $N$  nucleons, one considers the following operator:

$$\hat{\mathcal{O}}_{(N)}^{\mathcal{J}\mathcal{M};\mathcal{T}\mathcal{T}_z} = \sum_{i_1 < i_2 < \dots < i_N = 1}^A \hat{\mathcal{O}}^{\mathcal{J}\mathcal{M}}(\vec{r}_{i_1}, \dots, \vec{r}_{i_N}; s_{i_1}, \dots, s_{i_N}) \hat{\mathcal{O}}^{\mathcal{T}\mathcal{T}_z}(t_{i_1}, \dots, t_{i_N}) \quad (5.24)$$

In the case of  $N = 1$  or  $2$ , i.e. one and two body matrix elements, one can use hyperspherical wave functions of Eqs. (5.22, 5.23), which lead to explicit dependence on one Jacobi coordinate. The advantage is that usually one can separate the hyper-radial part from the hyper angular part, i.e.

$$\hat{\mathcal{O}}^{\mathcal{J}\mathcal{M}} = \mathcal{R}^{\mathcal{J}}(L\eta_{A-1}) \hat{\mathcal{O}}^{\mathcal{J}\mathcal{M}}(\eta_{A-1}, spins) \quad (5.25)$$

where  $L = \sqrt{2}$  for two-body operator, and  $L = \sqrt{\frac{A}{A-1}}$  for one-body operator. The matrix element of the scalar operator  $\mathcal{R}^{\mathcal{J}}(L\eta_{A-1})$  includes two integrations. The first integration is over the hyper-angle,

$$\begin{aligned} \mathcal{M}^{\mathcal{J}}(\rho) &= \langle K_{A-2}l; K_{A-1} | \mathcal{R}^{\mathcal{J}}(L\rho \sin \varphi_A) | K_{A-2}l'; K'_{A-1} \rangle = \\ &\mathcal{N}(K_{A-1}; lK_{A-2}) \mathcal{N}(K'_{A-1}; l'K_{A-2}) \times \\ &\times \int_0^{\frac{\pi}{2}} d\varphi (\sin \varphi)^{\alpha+\alpha'} (\cos \varphi)^{\beta-1} P_n^{(\alpha,\beta)}(\cos 2\varphi) \mathcal{R}^{\mathcal{J}}(L\rho \sin \varphi_A) P_n^{(\alpha',\beta)}(\cos 2\varphi) \end{aligned} \quad (5.26)$$

where  $\alpha = l + \frac{1}{2}$ ,  $\alpha' = l' + \frac{1}{2}$ , and  $\beta = K_{A-2} + \frac{3A-8}{2}$  (see Eq. (5.13) for the other notations). This integration can be performed analytically by expanding the interaction to power series (Barnea, 1997). Due to the orthonormality of the Jacobi polynomials, this integration includes a finite number of elements.

One now integrates over the hyperradius, by expanding the hyperradial part of

the wave function (cf. Eq. (5.19)) as,

$$R_{[K];\nu}(\rho) = \sum C_{n_\rho}^{[K];\nu} \phi_{n_\rho}^{(a,b)} \left( \frac{\rho}{b} \right). \quad (5.27)$$

Here,  $\phi_{n_\rho}^{(a,b)}(x)$  are the ortho-normalized generalized Laguerre polynomials of order  $n_\rho$  and parameters  $a, b$ . The parameter  $b$  is a length scale for the integration. Explicitly, we take

$$\phi_n^{(a,b)}(x) = \sqrt{\frac{n!}{(n+a)!}} b^{-\frac{3(A-1)}{2}} x^{\frac{a-(3A-4)}{2}} L_n^a(x) e^{-\frac{x}{2}} \quad (5.28)$$

As a result, the hyperradial matrix element is written as

$$\langle R_{[K];\nu}(\rho) | \mathcal{M}^{\mathcal{J}}(\rho) | R_{[K]';\nu'}(\rho) \rangle = \sum C_{n'_\rho}^{[K]';\nu'} C_{n_\rho}^{[K];\nu} \int_0^\infty d\rho \rho^{3A-4} \phi_n^{(a,b)} \left( \frac{\rho}{b} \right) \mathcal{M}^{\mathcal{J}}(\rho) \phi_{n'}^{(a',b)} \left( \frac{\rho}{b} \right) \quad (5.29)$$

This integration is done numerically, using Gauss–Laguerre quadrature.

In the current work, we confront also three-body matrix elements, which include the coupling of two Jacobi coordinates (Barnea et al., 2004).

## 5.2 Effective Interaction with the Hyperspherical Harmonics

The Hyperspherical Harmonics expansion has the correct asymptotic behavior, thus provides a promising channel to the solution of the nuclear problem defined by the Hamiltonian in Eq. (5.1). Two of the advantages in using this expansion are the removal of the center of mass coordinate; and the localization of the quantum description, provided by the explicit dependence in the hyperradius, which holds within information regarding the entire nucleus.

Alas, in order to reach convergence in the expansion of the nuclear wave function one has to expand up to very high grand angular momentum  $K$ . In order to cope with this disadvantage it was proposed to replace the bare potential with an effective interaction, which truncates the model space. The concept of effective interaction has been used traditionally in the framework of harmonic oscillator basis. However, lately

(Barnea et al., 2000, 2001b, 2004) it was extended to the hyperspherical harmonics basis. This method, the Effective Interaction with the Hyperspherical Harmonics (EIHH), has been shown to give excellent results both in comparison to other few-body methods, and in confronting previously unreachable nuclear reactions. In this section I will present a brief overview of the method, as used for the calculations shown in the following chapters.

### 5.2.1 Lee–Suzuki Approach for Effective Interactions

The effective interactions are projections of the bare interactions to a subspace of the entire model space. Defining  $P$  as the projection operator onto the model space, then  $Q = 1 - P$  is the projection operator onto the complementary space. By definition, the effective interaction leaves unchanged the low lying eigen-energies.

The first step in the construction of the effective interaction is choosing the model space. It is helpful to note that the hyper-radius, by definition, limits the inter-nucleon distance. This fact makes it possible to choose the model space as the product of the entire hyper-radial space and the set of HH basis functions with  $K \leq K_{max}$ . It is clear that  $V_{eff} \rightarrow V$  as  $K_{max} \rightarrow \infty$ , and the same follows for the eigen-energies and states of the Hamiltonian.

In order to continue, one method is to use the Lee-Suzuki procedure (Suzuki and Lee, 1980, 1982, 1983), in which one uses a similarity transformation  $X$ . The effective Hamiltonian is given by

$$\mathcal{H}_{eff} = PX^{-1}\mathcal{H}XP. \quad (5.30)$$

The effective interaction acts only in the  $P$ -space. The operator  $X = e^\omega$  re-projects the information contained in the  $Q$ -space back to the model space, i.e.  $\omega = Q\omega P$  (which also leads to  $\omega^2 = \omega^3 = \dots = 0$ , and thus  $X = 1 + \omega$ , and  $X^{-1} = 1 - \omega$ ). One can summarize this method in the following way (we use the notation  $O_{AB} \equiv AOB$ )

(Bacca, 2004):

$$\mathcal{H} = \left( \begin{array}{c|c} \mathcal{H}_{PP} & \mathcal{H}_{QP} \\ \hline \mathcal{H}_{PQ} & \mathcal{H}_{QQ} \end{array} \right) \longrightarrow \tilde{\mathcal{H}} = X^{-1}\mathcal{H}X = \left( \begin{array}{c|c} \tilde{\mathcal{H}}_{PP} & 0 \\ \hline \tilde{\mathcal{H}}_{PQ} & \tilde{\mathcal{H}}_{QQ} \end{array} \right) \longrightarrow \mathcal{H}_{eff} = \tilde{\mathcal{H}}_{PP}. \quad (5.31)$$

The implicit condition that  $\omega$  has to fulfill  $\tilde{\mathcal{H}}_{QP} = 0$  can be rearranged to the equation:

$$Q(\mathcal{H} + [\mathcal{H}, \omega] - \omega\mathcal{H}\omega)P = 0. \quad (5.32)$$

The strength of the effective interaction approach is that the low energy solutions to the original problem can be exhausted from the eigen-vectors of the effective Hamiltonian,  $\mathcal{H}_{eff}$ , which by construction are in the  $P$  space. The theorem states: let  $\tilde{\epsilon}_P$  be the eigen-vectors of this subspace, then  $\epsilon_P \equiv X\tilde{\epsilon}_P$  are eigen-vectors of the true Hamiltonian with the same eigen-value.

In order to prove this theorem, let  $|\tilde{\Psi}_\mu\rangle \in \tilde{\epsilon}_P$ , i.e.,  $\mathcal{H}_{eff}|\tilde{\Psi}_\mu\rangle = \epsilon_\mu|\tilde{\Psi}_\mu\rangle$  and  $P|\tilde{\Psi}_\mu\rangle = |\tilde{\Psi}_\mu\rangle$ . Then  $\mathcal{H}|\Psi_\mu\rangle = \mathcal{H}X|\tilde{\Psi}_\mu\rangle = XX^{-1}\mathcal{H}X|\tilde{\Psi}_\mu\rangle = X\mathcal{H}_{eff}|\tilde{\Psi}_\mu\rangle = \epsilon_\mu X|\tilde{\Psi}_\mu\rangle = \epsilon_\mu|\Psi_\mu\rangle$ , which concludes the proof.

The subspace  $\epsilon_P$  contains information regarding both the  $P$  and the  $Q$  spaces. Furthermore, the similarity transformation depends only on this space. Let  $|\alpha\rangle$  ( $|\beta\rangle$ ) be a basis for the  $P$  ( $Q$ ) space, and  $(A)_{\alpha\mu} = \langle\alpha|\Psi_\mu\rangle$ ,  $(B)_{\beta\mu} = \langle\beta|\tilde{\Psi}_\mu\rangle$ . Then, it is easily proven that a solution to Eq. (5.32) is

$$\omega = A \cdot (B)^{-1}. \quad (5.33)$$

This similarity transformation is not hermitian, however an equivalent effective interaction can be written as,

$$\mathcal{H}_{eff} = \frac{P + \omega}{\sqrt{P(1 + \omega^\dagger\omega)P}} \mathcal{H} \frac{P + \omega}{\sqrt{P(1 + \omega^\dagger\omega)P}}. \quad (5.34)$$

It is clear that the effective interaction stores information regarding correlations in the  $Q$ -space, while solving only in the  $P$  space. Alas, this procedure produces, in general,  $A$ -body interactions, which solution is as difficult as finding the full space

solutions. To cope with this problem, one approximates the effective interaction, while keeping the property of converging to the bare interaction as  $P \rightarrow 1$ .

A good approximation is used in the “No Core Shell Mode” (NCSM) approach (Navrátil and Barrett, 1996, 1998, 1999). The approximation is to include in the effective potential only two-body effective interactions:

$$V_{eff} = PX^{-1} \left[ \sum_{i<j=1}^A V_{ij} \right] XP \longrightarrow V_{eff}^{app} = \sum_{i<j=1}^A V_{eff,ij}^{(2)}. \quad (5.35)$$

The two-body effective potential is the non-trivial part of the two-body effective Hamiltonian, i.e. one decomposes  $\mathcal{H}^{(2)} = H_0 + \sum_{i<j=1}^A V_{ij}^{(2)}$  with  $[H_0, P] = [H_0, Q] = 0$  and  $QH_0P = PH_0Q = 0$ . Then the two-body effective Hamiltonian is built using a Lee-Suzuki transformation:

$$\mathcal{H}_{eff}^{(2)} = \frac{P_2 + \omega_2}{\sqrt{P_2(1 + \omega_2^\dagger \omega_2)P_2}} \mathcal{H}^{(2)} \frac{P_2 + \omega_2}{\sqrt{P_2(1 + \omega_2^\dagger \omega_2)P_2}}, \quad (5.36)$$

thus,

$$\sum_{i<j=1}^A V_{eff,ij}^{(2)} = \mathcal{H}_{eff}^{(2)} - PH_0P. \quad (5.37)$$

### 5.2.2 EIHH method

In the EIHH method, one solves the hyper-radial part of the Hamiltonian. Then, for each hyper-radius  $\rho$ , the two-body hamiltonian is clearly

$$\mathcal{H}^{(2)} = \frac{1}{2M_N} \frac{\hat{K}^2}{\rho^2} + V_{A,A-1}. \quad (5.38)$$

Let us note that:

- This Hamiltonian includes the total hyper-angular kinetic energy.
- The only interacting particles are the “last” two.
- The residual  $A - 2$  system acts as a mean-field force, entering only through the

collective hyper-radius. The hyper-radius enters not only in the kinetic energy, but also in the potential matrix element, as the relative distance between the last two particles is  $\vec{r}_{A,A-1} = \sqrt{2}\vec{\eta}_{A-1} = (\sqrt{2}\rho \sin \varphi_A, \hat{\eta}_{A-1})$ .

- The calculation includes only one-dimensional integration.

Choosing the model space within the HH formalism is quite natural, as the two-body Hamiltonian of Eq. (5.38) is diagonal in the quantum numbers of the  $A - 2$  residual system. Thus, the  $P_2$ -space is chosen as  $P_2 = \{[K] : K \leq K_{max}, [K_{A-2}] \text{ fixed}\}$ . It is clear that  $Q_2 = \{[K] : K > K_{max}, [K_{A-2}] \text{ fixed}\}$ . A numerical calculation of the  $Q_2$  space includes a numerical cutoff  $K_{MAX}$  which assures convergence. This depends on the orbitals of the potential, and was checked to be  $K_{MAX} \sim 60$  for  $S$ -wave interaction and  $K_{MAX} \sim 180$  for  $P$ -wave interaction. The construction of  $\epsilon_P$  space is now trivial, using Eq. (5.33).

By construction, the effective interaction is “state dependent”. This means that for every fixed value of  $K_{A-2}$  one has to calculate a similarity transformation. In Mintkevich and Barnea (2004) it was demonstrated that the “no-core” approach is equivalent to the bare Hamiltonian (through a unitary transformation), in the limit  $P \rightarrow 1$ . It was also shown that any effective two body operators constructed through the Lee-Suzuki similarity transformation of Eq. (5.36) can be regarded accurate to second order in the limit  $P \rightarrow 1$ .

The EHH method accelerates the convergence of the HH expansion, and has been shown to do so in the calculation of nuclear bound states and reactions of nuclei in the mass range  $3 \leq A \leq 7$  (for example (Barnea et al., 2000, 2001b,a; Bacca et al., 2004, 2002; Gazit and Barnea, 2004; Gazit et al., 2006a; Gazit and Barnea, 2007c)).

# 6 PHOTOABSORPTION ON ${}^4\text{He}$ WITH A REALISTIC NUCLEAR FORCE

---

In previous chapters I outlined a detailed description of the theoretical background for *ab-initio* calculation of few-body nuclear structure and reactions. In the first section of this chapter, the application of these methods to the  ${}^4\text{He}$  total photoabsorption cross section is presented with the realistic nucleon-nucleon (NN) potential Argonne  $v_{18}$  and the three-nucleon force (3NF) Urbana IX, as published in Gazit et al. (2006a). In the second part of the chapter, based on (Gazit et al., 2006b), sum-rules of this cross-section are investigated, emphasizing relations to ground state properties.

## 6.1 Photoabsorption Calculation

### 6.1.1 The Unretarded Dipole Approximation

For low energy reactions, below the pion production threshold, a good approximation for the photoabsorption cross-section,  $\sigma_\gamma$ , is using only the leading electric dipole ( $E1$ ) in its non-relativistic long wavelength approximation. In addition, since the Siegert theorem (Sec. 2.3) applies for the conserved electro-magnetic current, the dipole operator is proportional to the Coulomb multipole. Thus, the effects of MEC are implicitly included.

As a result, the total photoabsorption cross section is given by

$$\sigma_\gamma(\omega) = \frac{4\pi^2\alpha}{2J_0 + 1} \omega R(\omega), \quad (6.1)$$

where  $\alpha$  is the fine structure constant,  $J_0$  denoting the nucleus total angular momentum, and

$$R(\omega) = \sum_f \left| \langle \Psi_f | \hat{D}_z | \Psi_0 \rangle \right|^2 \delta(E_f - E_0 - \omega) \quad (6.2)$$

is the response function in the unretarded dipole approximation with  $\hat{D}_z = \sum_{i=1}^A \frac{\tau_i^3 z'_i}{2}$ .

The wave functions of the ground and final states are denoted by  $|\Psi_{0/f}\rangle$  and the energies by  $E_{0/f}$ , respectively. The operators  $\tau_i^3$  and  $z'_i$  are the third components of the  $i$ -th nucleon isospin and center of mass frame position.

We refer back to Sec. 2.3 and recall the Siegert theorem, which ensures that the dominant part of the exchange current contribution is included. In the classical few-body nuclei this has proven to be an excellent approximation (Golak et al., 2002; Arenhövel and Sanzone, 1991), particularly for photon energies below 50 MeV.

For triton,  $\sigma_\gamma({}^3\text{H})$  (Golak et al., 2002) the contributions of retardation and other multipoles lead to an enhancement of  $\sigma_\gamma$  by less than 1% for  $\omega \leq 40$  MeV. The contribution grows with energy transfer. This result is rather insensitive to the nuclear force model. When calculating with AV18 NN potential only, the contribution is 5% for  $\omega = 60$  MeV, 16% for  $\omega = 100$  MeV, and 26% at pion threshold ( $\omega = 140$  MeV). When including UIX 3NF the numbers change to 5%, 18%, and 33% at  $\omega = 60$ , 100, and 140 MeV, respectively. If one bears in mind that the cross-section is almost exhausted in the giant dipole resonance (GDR), below 40 MeV, the approximation is appropriate for the photoabsorption process below pion-threshold.

### 6.1.2 Calculation of The Response Function

In order to find the Response function, the LIT method is used, calculated with the Lanczos algorithm (see Chap. 4).

The EIH expansion of the ground state  $|\Psi_0\rangle$  and the LIT vector  $|\tilde{\Psi}\rangle$  are performed with the full HH set up to maximal values of the HH grand-angular momentum quantum number  $K$  ( $K \leq K_m^0$  for  $\Psi_0$ ,  $K \leq K_m$  for  $\tilde{\Psi}$ ).

The ground state properties of  ${}^4\text{He}$  calculated using the EIH approach are shown in Tab. 6.1. The convergence of the binding energy,  $E_b$ , and matter radius are presented as a function of  $K_m^0$ . Since the EIH method is not variational the asymptotic  $E_b$  value can be reached from below or above, in fact both cases are realized in Tab. 6.1. Both convergence patterns are not sufficiently regular to allow safe extrapolations to asymptotic values. The calculated ground state properties of  ${}^4\text{He}$  agree quite well

Table 6.1: Convergence of HH expansion for the  ${}^4\text{He}$  binding energy  $E_b$  [MeV] and root mean square matter radius  $\langle r^2 \rangle^{\frac{1}{2}}$  [fm] with the AV18 and AV18+UIX potentials. Also presented are results of other methods (see text).

$K_m^0$	AV18		AV18+UIX	
	$E_b$	$\langle r^2 \rangle^{\frac{1}{2}}$	$E_b$	$\langle r^2 \rangle^{\frac{1}{2}}$
6	25.312	1.506	26.23	1.456
8	25.000	1.509	27.63	1.428
10	24.443	1.520	27.861	1.428
12	24.492	1.518	28.261	1.427
14	24.350	1.518	28.324	1.428
16	24.315	1.518	28.397	1.430
18	24.273	1.518	28.396	1.431
20	24.268	1.518	28.418	1.432
FY1	24.25	-	28.50	-
FY2	24.22	1.516	-	-
HH	24.21	1.512	28.46	1.428
GFMC	-	-	28.34	1.44

with those of other methods, presented in Tab. 6.1. The other calculations are done with the FY equations (in Nogga et al. (2002); Lazauskas and Carbonell (2004)), the HH expansion (in Viviani et al. (2005)) and the GFMC method (Wiringa et al., 2000), and appear in this order in Tab. 6.1. One should compare the binding energies to the experimental value of 28.296 MeV.

The EIIH convergence of the transform  $\mathcal{L}(\sigma)$  is excellent for the AV18 potential. Here we discuss in detail only the case AV18+UIX, where the convergence is quite good, but not at such an excellent level. The reason is that in our present EIIH calculation an effective interaction is constructed only for the NN potential, while the 3NF is taken into account as bare interaction.

In Fig. 6.1 we show results for the transform  $\mathcal{L}$  obtained with various  $K_m$  and  $K_m^0$  values. Since we take  $K_m^0 = K_m - 1$ , the corresponding transform can be denoted by  $\mathcal{L}_{K_m}$ . One sees that there is a very good convergence beyond the peak, that the peak height is very well established, but that the peak position is not yet fully converged

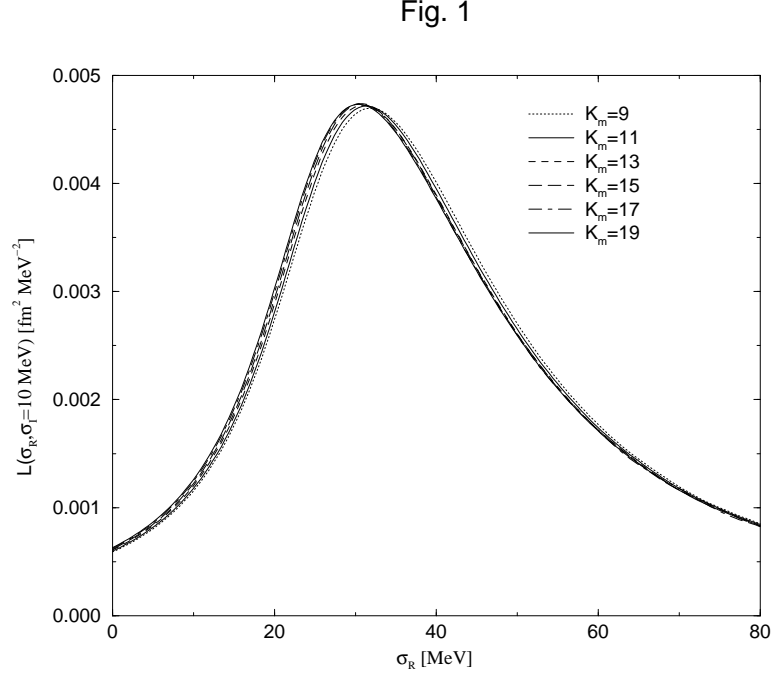


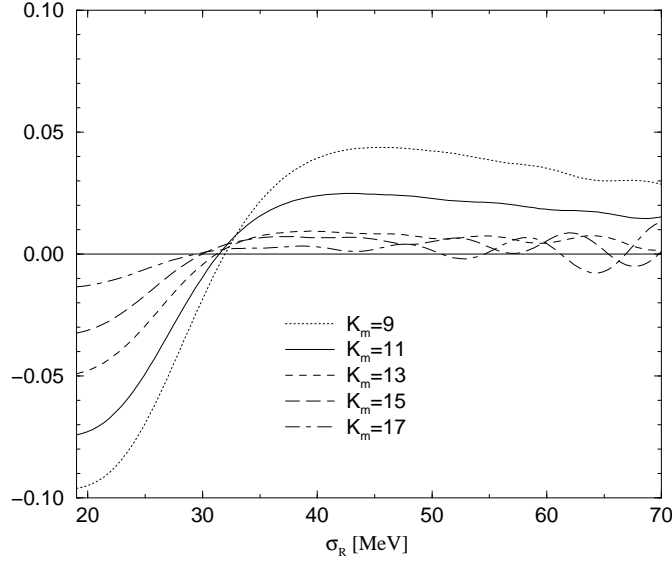
Figure 6.1: Convergence of  $\mathcal{L}_{K_m}$  with  $\sigma_I = 10$  MeV (AV18+UIX).

in view of the fact that we aim for a percentage level accuracy. In fact with increasing  $K_m$  the peak is slightly shifted towards lower  $\sigma_R$ .

By observing the relative error of the transform,  $\Delta_{K_m} = \mathcal{L}_{K_m,19}/\mathcal{L}_{19}$  with  $\mathcal{L}_{\alpha,\beta} = \mathcal{L}_\alpha - \mathcal{L}_\beta$ , this point is illustrated better, see Fig. 6.2 (the chosen  $\sigma_R$ -range starts at the  ${}^4\text{He}(\gamma)$  break-up threshold). One again notes the very good convergence for  $\sigma_R > 30$  MeV with almost identical results from  $\mathcal{L}_{13}$  to  $\mathcal{L}_{19}$ . Altogether we consider our result for  $\sigma_R > 30$  MeV as completely sufficient. However, it is obvious that convergence is not entirely reached for lower  $\sigma_R$ .

A trivial solution for this is an additional increase in  $K_m$ . However,  $\mathcal{L}_{19}$  includes already 364000 states in the HH expansion. Thus, a further increase is beyond our present computational capabilities. Fortunately a closer inspection of Fig. 6.2 shows that the convergence proceeds with a rather regular pattern: (i)  $\mathcal{L}_{13,11} \simeq \mathcal{L}_{11,9}$  and  $\mathcal{L}_{17,15} \simeq \mathcal{L}_{15,13}$  and (ii)  $\mathcal{L}_{19,17} \simeq \mathcal{L}_{17,15}/1.5 \simeq \mathcal{L}_{13,11}/(1.5)^2$ . Therefore it is possible to obtain an extrapolated asymptotic result.

Fig. 2


 Figure 6.2: Convergence of  $\Delta_{K_m} = (\mathcal{L}_{K_m} - \mathcal{L}_{19})/\mathcal{L}_{19}$  (AV18+UIX).

The extrapolation used is a Padé approximation (Fabian and Arenhövel, 1976; Basdevant, 1972)

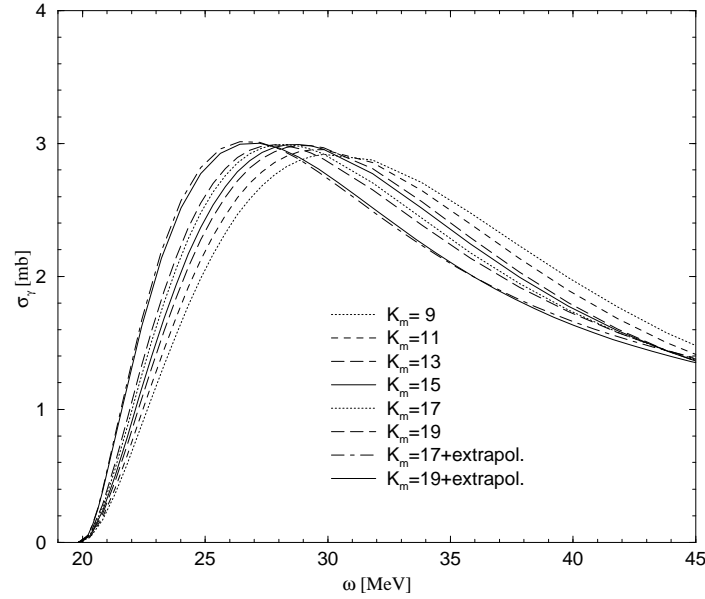
$$\mathcal{L}_{K_m}^\infty = \mathcal{L}_{K_m-8} + \mathcal{L}_{K_m-4, K_m-8} / \left(1 - \frac{\mathcal{L}_{K_m, K_m-4}}{\mathcal{L}_{K_m-4, K_m-8}}\right). \quad (6.3)$$

### 6.1.3 Results and Discussion

In Fig. 6.3 the results for  $\sigma_{\gamma, K_m}$  obtained from the inversions of the transforms  $\mathcal{L}_{K_m}$  are presented. Due to the Lorentz kernel the  $\sigma_\gamma$  presents the same features as  $\mathcal{L}$  itself: stable peak height with a value very close to 3 mb, and not yet completely converged peak position.

In Fig. 6.3 the asymptotic Padé approximations are given, where  $\sigma_{\gamma, 17}^\infty$  and  $\sigma_{\gamma, 19}^\infty$  result from the inversions of  $\mathcal{L}_{17}^\infty$  and  $\mathcal{L}_{19}^\infty$ . Unquestionably, the extrapolated  $\mathcal{L}_{K_m}^\infty$  have a lower numerical quality than the calculated  $\mathcal{L}_{K_m}$  and consequently the stability for the corresponding inversions worsens. Therefore, an additional constraint in the inversion is imposed by fixing the peak cross section to the already converged value of

Fig. 3


 Figure 6.3: Convergence of  $\sigma_{\gamma, K_m}$  (AV18+UIX), also shown  $\sigma_{\gamma, 17}^{\infty}$  and  $\sigma_{\gamma, 19}^{\infty}$ .

3 mb. In Fig. 6.3 it is evident that  $\sigma_{\gamma, 17}^{\infty}$  and  $\sigma_{\gamma, 19}^{\infty}$  are very similar, hence establishing a very good approximation for the asymptotic  $\sigma_{\gamma}$ . One also notices that compared to  $\sigma_{\gamma, 19}$  they show a shift of the peak position by about 1 MeV towards lower energy.

The final results for the cross-section are presented in Fig. 6.4a. Due to the 3NF one observes a reduction of the peak height by about 6% and a shift of the peak position by about 1 MeV towards higher energy. Very large effects of the 3NF are found above 50 MeV with an enhancement of  $\sigma_{\gamma}$  by e.g. 18, 25, and 35% at  $\omega = 60$ , 100, and 140 MeV, respectively. The discussion in the previous section indicates that the 3NF effect could change somewhat if all multipole contributions are considered.

It is very interesting to compare the 3NF effects on  $\sigma_{\gamma}({}^4\text{He})$  to those found for  $\sigma_{\gamma}({}^3\text{H}/{}^3\text{He})$  (Efros et al., 2000; Golak et al., 2002). Surprisingly, the reduction of the peak height is smaller for  ${}^4\text{He}$ . For  ${}^3\text{H}/{}^3\text{He}$  the size of the reduction is similar to the increase of  $E_b$  (10%), whereas for  ${}^4\text{He}$  the 3NF increases  $E_b$  by 17%, but reduces the peak by only 6% and thus cannot be interpreted as a simple binding effect.

Fig. 4

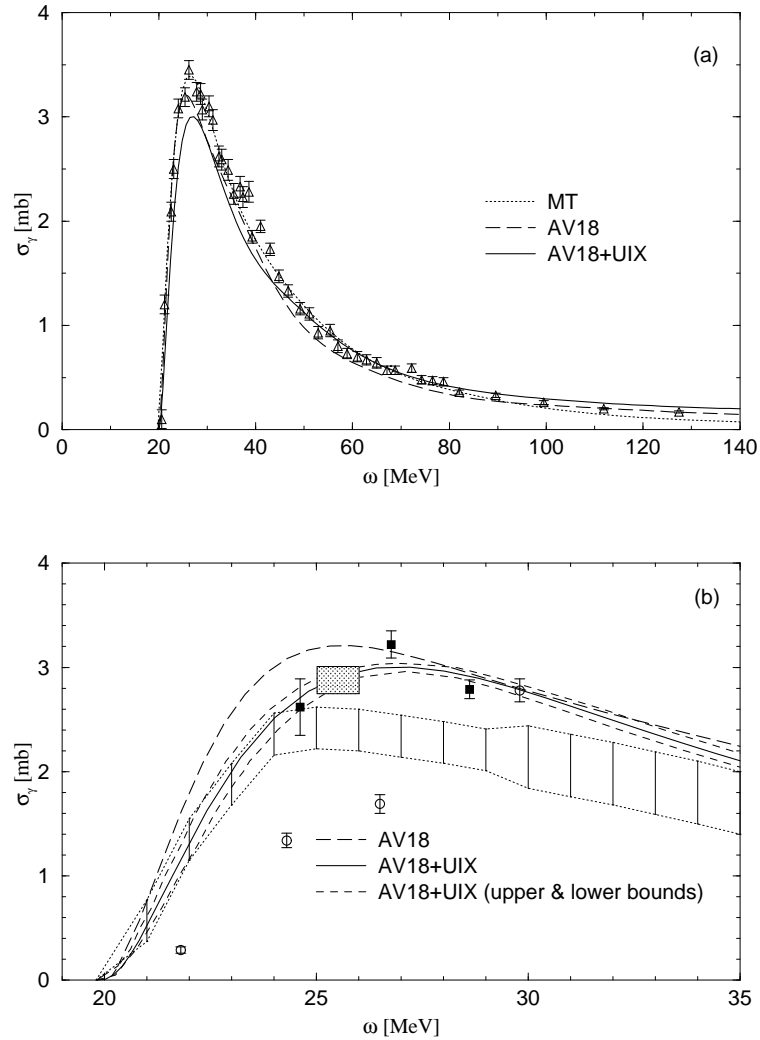


Figure 6.4: Total  ${}^4\text{He}$  photoabsorption cross section: (a)  $\sigma_\gamma$  (MT,AV18) and  $\sigma_{\gamma,19}^\infty$  (AV18+UIX); experimental data from (Arkatov et al., 1979). (b) as (a) but also included upper/lower bounds and various experimental data (see text), area between dotted lines (Berman et al., 1980; Feldman et al., 1990), dotted box (Wells et al., 1992), squares (Nilsson et al., 2005), and circles (Shima et al., 2005).

One can find additional differences at higher energy-transfer. The enhancement of  $\sigma_\gamma({}^4\text{He})$  due to the 3NF is significantly stronger, namely about two times larger than for the three-body case. Interestingly this reflects the above mentioned different ratios between triplets and pairs in three- and four-body systems. An integration of  $\sigma_\gamma$  up to pion threshold yields 93.0 (AV18) and 97.4 MeVmb (AV18+UIX) thus showing a rather small difference. If one considers also contributions beyond pion threshold the difference becomes more pronounced, in fact integrating up to 300 MeV one finds 103 (AV18) and 114 MeVmb (AV18+UIX). The latter values correspond to enhancements of 72 % (AV18) and 91 % of the classical Thomas-Reiche-Kuhn sum rule. Different sum-rules will be discussed in the next section.

In Fig. 6.4a we compare the cross-section with the one achieved using the semi-realistic Malfliet-Tjon (MT) NN potential (Efros et al., 1997b; Barnea et al., 2001a). Similar to  $\sigma_\gamma({}^3\text{H}/{}^3\text{He})$  (Efros et al., 2000) one finds a rather realistic result in the giant resonance region (overestimation of the peak by about 10-15%) and quite a correct result for the the peak position; however, at higher energy  $\sigma_\gamma$  is strongly underestimated for  ${}^4\text{He}$ , by a factor of three at pion threshold. Also shown are data from Arkatov et al. (1979), the only measurement of  $\sigma_\gamma({}^4\text{He})$  in the whole energy range up to pion threshold. In the peak region the data agree best with the MT potential, while for the high-energy tail one finds the best agreement with the AV18 potential.

A comparison of the low-energy results to further data is presented in Fig. 6.4b. For the AV18+UIX case upper/lower bounds are included to account for possible errors in the extrapolation, Eq. (6.3). As bounds we take  $\pm(\sigma_{\gamma,19}^\infty - \sigma_{\gamma,19})/2$ ; we believe that this is a rather safe error estimate.

For a better understanding of the data in Fig. 6.4b a few comments are needed:

1. In Wells et al. (1992) the peak cross section is determined from Compton scattering via dispersion relations.
2. The dashed curve corresponds to the sum of cross sections for  $(\gamma, n)$  from Berman et al. (1980) and  $(\gamma, p){}^3\text{H}$  from Feldman et al. (1990) as already shown in Efros et al. (1997b).

3. The data from the above mentioned recent  $(\gamma, n)$  experiment (Nilsson et al., 2005) are included only up to about the three-body break-up threshold, where one can rather safely assume that  $\sigma_\gamma \simeq 2\sigma(\gamma, n)$  (see also Quaglioni et al. (2004)).
4. In Shima et al. (2005) all open channels are considered. One sees that the various experimental  $\sigma_\gamma$  are quite different, exhibiting maximal deviations of about a factor of two.

The theoretical  $\sigma_\gamma$  agrees quite well with the low-energy data of (Berman et al., 1980; Feldman et al., 1990). In the peak region, however, the situation is very unclear. There is a rather good agreement between the theoretical  $\sigma_\gamma$  and the combined data of (Nilsson et al., 2005) and (Wells et al., 1992), while those of (Berman et al., 1980; Feldman et al., 1990) are quite a bit lower. Very large discrepancies are found in comparison to the recent data of Shima et al. (2005). It is evident that the experimental situation is rather unsatisfactory and further improvement is urgently needed.

## 6.2 Photonuclear Sum Rules and the Tetrahedral Configuration of ${}^4\text{He}$

Sum rules (SR) are related to moments of different order of the photonuclear cross section and reflect important electromagnetic properties of nuclei. In fact they can often be expressed in terms of simple ground state properties in a model independent or quasi model independent way. Well known examples are the Thomas-Reiche-Kuhn (TRK) sum rule (Landerburg and Reiche, 1923; Kuhn, 1923; Thomas, 1925), which gives information about the importance of exchange effects in nuclear dynamics via the so-called TRK enhancement factor  $\kappa^{\text{TRK}}$ , the bremsstrahlung sum rule (BSR) (Levinger and Bethe, 1950; Brink, 1957; Foldy, 1957; Dellafiore and Brink, 1977), which is connected to the nuclear charge radius and to the mean distance between protons (Dellafiore and Lipparini, 1982), and the polarizability sum rule (PSR) (Friar, 1975), related to the electric nuclear polarizability, which is proportional to the shift in energy levels due to external electric field.

These SR assume that the dominant contribution to the cross section comes from unretarded electric dipole (E1UR) transitions. Two- and three-body studies (Arenhövel and Sanzone, 1991; Golak et al., 2002) indeed confirm that other contributions are much smaller. Much discussed is also the Gerasimov-Drell-Hearn (GDH) sum rule (Drell and Hearn, 1966; Gerasimov, 1965), which is related to the nuclear anomalous magnetic moment.

In this chapter, the TRK, BSR and PSR of  ${}^4\text{He}$  are considered within a realistic nuclear potential model consisting of two- and three-body forces (AV18 and UIX (Wiringa et al., 1995; Pudliner et al., 1997)). The GDH sum rule is trivial for  ${}^4\text{He}$ : it vanishes, since the  ${}^4\text{He}$  total angular momentum is equal to zero. Also investigated are the related moments by integrating explicitly the properly weighted total photoabsorption cross section calculated in the previous section.

The aim of this study is to show that in some cases sum rules can allow an experimental access to two-body properties of the nuclear ground state, like the proton-proton, neutron-neutron and proton-neutron distances. In the case of  ${}^4\text{He}$  this allows to test the validity of the configuration tetrahedral symmetry of this nucleus and at the same time to “measure” the amount of symmetry breaking.

This section aims also at providing a guideline for experiments, for which a direct test of SR is difficult, as only lower bounds for the SR can be determined, as well as at giving an idea of the reliability of the SR approach to heavier systems, where the direct theoretical determination of the cross section, and therefore its integration, is presently out of reach. The advantage to perform this kind of study in  ${}^4\text{He}$ , compared to analogous ones in the two- (Arenhövel and Fabian, 1977) and three-body systems (Efros et al., 1997a), is that  ${}^4\text{He}$  is a rather dense and compact nucleus, resembling heavier systems more closely. Only now that realistic theoretical results for the photonuclear cross section are available such a study is possible and one can put the extrapolation of the results to heavier systems on safer grounds.

### 6.2.1 SR and the Nucleus Ground State

We start by recalling the formalism of the photonuclear SR. The various moments of the photonuclear cross section are defined as

$$m_n(\bar{\omega}) \equiv \int_{\omega_{th}}^{\bar{\omega}} d\omega \omega^n \sigma_\gamma^{\text{E1UR}}(\omega), \quad (6.4)$$

where  $\omega$  is the photon energy and  $\omega_{th}$  and  $\bar{\omega}$  indicate threshold energy and upper integration limit, respectively. Where  $\sigma_\gamma^{\text{E1UR}}(\omega)$  is the unretarded dipole cross section, which can be written as

$$\sigma_\gamma^{\text{E1UR}}(\omega) = \mathcal{G} \omega R(\omega), \quad (6.5)$$

where  $\mathcal{G} = 4\pi^2\alpha/(3(2J_0 + 1))$ .  $R(\omega)$  is the nuclear response function to excitations of the operator  $\vec{D}$  is the unretarded dipole operator:

$$\vec{D} = \sum_{i=1}^A \vec{r}_i \tau_i^3 / 2, \quad (6.6)$$

where  $A$  is the number of nucleons and  $\tau_i^3$  and  $\vec{r}_i$  are the third component of the isospin operator and the coordinate of the  $i$ th particle in the center of mass frame, respectively. For  $n = 0$  the SR is the TRK SR,  $n = -1$  is the BSR, and  $n = -2$  the PSR.

Assuming that  $\sigma_\gamma^{\text{E1UR}}(\omega)$  converges to zero faster than  $\omega^{-n-1}$  and applying the closure property of the eigenstates of the hamiltonian  $H$ , it is straight forward to get the following identities for SR with  $n = 0, -1, -2$ :

$$\Sigma^{\text{TRK}} \equiv m_0(\infty) = \frac{\mathcal{G}}{2} \langle 0 | [\vec{D}, [H, \vec{D}]] | 0 \rangle \quad (6.7)$$

$$\Sigma^{\text{BSR}} \equiv m_{-1}(\infty) = \mathcal{G} \langle 0 | \vec{D} \cdot \vec{D} | 0 \rangle \quad (6.8)$$

$$\Sigma^{\text{PSR}} \equiv m_{-2}(\infty) = \mathcal{G} \sum_n (E_n - E_0)^{-1} |\langle n | \vec{D} | 0 \rangle|^2, \quad (6.9)$$

Working out the expressions in Eqs. (6.7 - 6.9), one finds that those moments are related to interesting properties of the system under consideration. In fact the

TRK sum rule is also given by the well known relation (Landerburg and Reiche, 1923; Kuhn, 1923; Thomas, 1925)

$$\Sigma^{\text{TRK}} = \mathcal{G} \frac{3NZ}{2mA} (1 + \kappa^{\text{TRK}}), \quad (6.10)$$

where  $N$  and  $Z$  are the neutron and proton numbers, respectively,  $m$  is the nucleon mass and  $\kappa^{\text{TRK}}$  is the so-called TRK enhancement factor defined as

$$\kappa^{\text{TRK}} \equiv \frac{mA}{3NZ} \langle 0 | [\vec{D}, [V, \vec{D}]] | 0 \rangle. \quad (6.11)$$

From this expression it is evident that  $\kappa^{\text{TRK}}$  embodies the exchange effects of the nuclear potential  $V$ , since the double commutator in (6.11) vanishes for systems like atoms, where no exchange effects are present.

In the literature one finds a few interesting equivalences for the bremsstrahlung sum rule. Rewriting the dipole operator as  $\vec{D} = (NZ/A)\vec{R}_{PN}$ , where  $\vec{R}_{PN}$  denotes the distance between the proton and neutron centers of mass, one has (Brink, 1957)

$$\Sigma^{\text{BSR}} = \mathcal{G} \left( \frac{NZ}{A} \right)^2 \langle 0 | R_{PN}^2 | 0 \rangle. \quad (6.12)$$

Foldy (1957) demonstrated that

$$\Sigma^{\text{BSR}} = \mathcal{G} \frac{NZ}{A-1} \langle r_p^2 \rangle, \quad (6.13)$$

where  $\langle r_p^2 \rangle$  is the mean square (m.s.) point proton radius

$$\langle r_p^2 \rangle \equiv \frac{1}{Z} \langle 0 | \sum_{i=1}^Z r_i^2 | 0 \rangle. \quad (6.14)$$

However, this relation is valid only under the assumption that the ground state wave function is symmetric in the space coordinates of the nucleons.

Dellafore and Brink (1977) have found that, in the framework of the oscillator

shell model, one has

$$\Sigma^{\text{BSR}} = \mathcal{G} \left( Z^2 \langle r_p^2 \rangle - Z \langle r_p'^2 \rangle \right), \quad (6.15)$$

where  $\langle r_p'^2 \rangle$  is the m.s. distance of protons with respect to the proton center of mass  $\vec{R}_P$

$$\langle r_p'^2 \rangle \equiv \frac{1}{Z} \langle 0 | \sum_{i=1}^Z (\vec{r}_i - \vec{R}_P)^2 | 0 \rangle. \quad (6.16)$$

Later, in Dellafore and Lipparini (1982), it was shown that the validity of Eq. (6.15) is not limited to the oscillator shell model, but it is a model independent relation, which can also be written as

$$\Sigma^{\text{BSR}} = \mathcal{G} \left( Z^2 \langle r_p^2 \rangle - \frac{Z(Z-1)}{2} \langle r_{pp}^2 \rangle \right), \quad (6.17)$$

where  $\langle r_{pp}^2 \rangle$  is the m.s. proton-proton distance

$$\langle r_{pp}^2 \rangle \equiv \frac{1}{Z(Z-1)} \langle 0 | \sum_{i,j=1}^Z (\vec{r}_i - \vec{r}_j)^2 | 0 \rangle. \quad (6.18)$$

For the BSR two additional relations exist, which are easy to prove, but, to our knowledge, have not been considered in the literature, viz

$$\Sigma^{\text{BSR}} = \mathcal{G} \left( N^2 \langle r_n^2 \rangle - \frac{N(N-1)}{2} \langle r_{nn}^2 \rangle \right) \quad (6.19)$$

and

$$\Sigma^{\text{BSR}} = \mathcal{G} \frac{NZ}{2} (\langle r_{pn}^2 \rangle - \langle r_p^2 \rangle - \langle r_n^2 \rangle), \quad (6.20)$$

where  $\langle r_n^2 \rangle$  is the m.s. point neutron radius and  $\langle r_{\alpha\beta}^2 \rangle$  are the m.s. nucleon-nucleon (NN) distances, i.e.

$$\langle r_{nn}^2 \rangle \equiv \frac{1}{N(N-1)} \langle 0 | \sum_{i,j=1}^N (\vec{r}_i - \vec{r}_j)^2 | 0 \rangle, \quad (6.21)$$

$$\langle r_{pn}^2 \rangle \equiv \frac{1}{NZ} \langle 0 | \sum_{i=1}^Z \sum_{j=1}^N (\vec{r}_i - \vec{r}_j)^2 | 0 \rangle. \quad (6.22)$$

It is interesting to note that Eqs. (6.17), (6.19) and (6.20) express  $\Sigma^{\text{BSR}}$  via a one-body ( $\langle r_\alpha^2 \rangle$ ) as well as a two-body quantity ( $\langle r_{\alpha\beta}^2 \rangle$ ).

Finally, regarding the polarizability sum rule, one has

$$\Sigma^{PSR} = 2\pi^2 \alpha_D, \quad (6.23)$$

where  $\alpha_D$  denotes the nuclear polarizability in the E1UR approximation.

## 6.2.2 Calculation of SR using the LIT method

There are various approaches for the calculation of moments and sum rules. The obvious one is to obtain the moments by integrating the  ${}^4\text{He}$  total photoabsorption cross section of Sec. 6.1. However, a more direct approach to obtain the SR exist, as explained in the following.

One way to evaluate the LIT is by using the Lanczos technique described in Subsec. 4.2.1. We recall that the LIT can be re-expressed as

$$\mathcal{L}(\sigma_R, \sigma_I) = \frac{1}{\sigma_I} \langle 0 | \vec{D} \cdot \vec{D} | 0 \rangle \text{Im } x_{00}(z) \quad (6.24)$$

with  $z = E_0 + \sigma_R + i\sigma_I$  and

$$|\phi_0\rangle = \frac{\vec{D}|0\rangle}{\sqrt{\langle 0 | \vec{D} \cdot \vec{D} | 0 \rangle}}. \quad (6.25)$$

$x_{00}(z)$  can be expressed (cf. Eq. (4.16)) as a continued fraction containing the Lanczos coefficients  $a_i$  and  $b_i$ , defined in Eq. (4.10).

Therefore, the implementation of the Lanczos algorithm leads to  $\mathcal{L}(\sigma_R, \sigma_I)$ . While the inversion of the LIT (Efros et al., 1999) gives access to  $R(\omega)$ , and thus to the moments of Eq. (6.4), the normalization of the Lanczos "pivot"  $|LP\rangle = \vec{D}|0\rangle$  and the

Lanczos coefficients allow to obtain the SR of Eqs. (6.7-6.9). In fact one has:

$$\Sigma^{\text{PSR}} = \mathcal{G} x_{00}(E_0), \quad (6.26)$$

$$\Sigma^{\text{BSR}} = \mathcal{G} \langle LP|LP \rangle, \quad (6.27)$$

$$\Sigma^{\text{TRK}} = (a_0 - E_0) \Sigma^{\text{BSR}}. \quad (6.28)$$

### 6.2.3 Results and Discussion

We use a HH basis, therefore the ground state  $|0\rangle$ , the Lanczos "pivot"  $|LP\rangle$  and the Lanczos coefficients  $a_n$  are given in terms of HH expansions. While for the ground state the expansion is characterized by an even hyperspherical grand-angular quantum number  $K$  and total isospin  $T=0$ ,  $|LP\rangle$  has to be expanded on  $\{K' = K + 1, T = 1\}$  states (we neglect the AV18 isospin mixing, which is very small, as shown for the  ${}^4\text{He}$  ground state in Nogga et al. (2002); Viviani et al. (2005)). The rate of convergence of the various SR results from Eqs.(6.26-6.28) is given in Tab. 6.2 as a function of the hyperspherical grand-angular quantum number  $K$ . One observes sufficiently good convergence patterns for  $\Sigma^{\text{TRK}}$  and  $\Sigma^{\text{BSR}}$ . For the latter an additional test of the convergence is performed, calculating  $\Sigma^{\text{BSR}}$  directly as mean value of the operator  $\vec{D} \cdot \vec{D}$  on the ground state (Eq. (6.8)). In this way the expansion of  $|LP\rangle$  on  $\{K' = K + 1, T = 1\}$  states is avoided. We obtain practically identical results.

From Tab. 6.2 one sees that the convergence of  $\Sigma^{\text{PSR}}$  is slower when the three-nucleon force (3NF) is included. This is not a surprise, in view of the problem found for the cross section itself in the previous section. In fact it has been shown that the peak of the giant dipole resonance is slightly shifting towards lower energies with increasing  $K$ . The sum rule  $\Sigma^{\text{PSR}}$ , which has the strongest inverse energy weighting, is more sensitive to this shift than the other two SR.

We have used  $\sigma_\gamma^\infty$  extrapolated in the previous section, to determine from Eq. (6.4) the various moments for  $\bar{\omega} = 300$  and 135 MeV. These results are also listed in Table 6.2.

For  $\Sigma^{\text{TRK}}$  one sees that the SR is not yet exhausted at 300 MeV. In fact more than 20% of the strength is still missing. At pion threshold, one has only about 2/3

	AV18+UIX		
K	$\Sigma^{\text{PSR}}$ $10^{-2}[\text{mb MeV}^{-1}]$	$\Sigma^{\text{BSR}}$ [mb]	$\Sigma^{\text{TRK}}$ $10^2[\text{mb MeV}]$
8	6.230	2.398	1.430
10	6.277	2.396	1.448
12	6.331	2.394	1.451
14	6.382	2.401	1.458
16	6.434	2.406	1.460
18	6.473	2.410	1.462
	AV18		
	7.681	2.696	1.383
	AV18+UIX		
$\bar{\omega}$ [MeV]	$m_{-2}(\bar{\omega})$	$m_{-1}(\bar{\omega})$	$m_0(\bar{\omega})$
135	6.55	2.27	.944
300	6.55	2.37	1.14

Table 6.2: Convergence in K of the SR for AV18+UIX potentials. The converged AV18 results are also shown. The last two lines of the table show the convergence in  $\bar{\omega}$  of the various moments.

of  $\Sigma^{\text{TRK}}$ . As was already discussed in (Efros et al., 2000) for the triton case, the rather strong contribution from higher energies seems to be connected to the strong short range repulsion of the AV18 potential. As to the TRK enhancement factor the present calculation gives  $\kappa^{\text{TRK}} = 1.31$  for AV18 and 1.44 for AV18+UIX. These numbers are somewhat larger than older results obtained either with a variational wave function and AV14+UVII potential ( $\kappa^{\text{TRK}} = 1.29$  (Schiavilla et al., 1987)) or with more approximated wave functions and various soft and hard core NN potentials ( $\kappa^{\text{TRK}} = 0.9 - 1.30$  (Weng et al., 1973; Heinze et al., 1978; Gari et al., 1978)).

For  $\Sigma^{\text{BSR}}$ , as expected, the contribution at high energy is much smaller than for  $\Sigma^{\text{TRK}}$ , in fact at  $\bar{\omega} = 300$  MeV the missing sum rule strength is less than 2%. For  $\Sigma^{\text{PSR}}$  the strength beyond 300 MeV is even more negligible. Actually in this case the explicit integration leads to an even higher result than the sum rule evaluation of Eq. (6.27). The seeming contradiction is explained by the already discussed fact that  $\Sigma^{\text{PSR}}$  is not yet convergent, while for the explicit integration an extrapolated

cross section is used. Indeed, integrating the  $K=18$  cross section we obtain a value of 6.46 mb, which is consistent with the corresponding sum rule result of 6.47 mb, within the numerical error of the calculation. For the AV18+UIX force the value of the polarizability  $\alpha_D$  that we deduce from the extrapolated  $\Sigma^{\text{PSR}}$  is  $0.0655 \text{ fm}^3$ . The AV18 result, which already shows a good convergence for  $K = 16$ , is  $0.0768 \text{ fm}^3$ . This means that the 3NF reduces the polarizability by 15%. It would be very interesting to measure this nuclear polarizability by Compton scattering, as a test of the importance of the three-body force on such a classical low-energy observable. We find that  $\Sigma^{\text{PSR}}$  is the SR that is affected most by the 3NF. In fact  $\Sigma^{\text{BSR}}$  is reduced by only 10% and one has an opposite effect on  $\Sigma^{\text{TRK}}$  with a 5% increase. The quenching or enhancement of SR due to the 3NF is the reflection of its effects on the cross section i.e a decrease of the peak and an increase of the tail.

This work allows a few conclusions regarding a very old question, already discussed in Levinger and Bethe (1950), of the “existence” of the SR (finiteness of  $m_n(\bar{\omega})$  for  $\bar{\omega} \rightarrow \infty$ ), which is connected to the high-energy fall-off of the E1UR cross section. Since there is a rather good consistency between the SR and the moment values, it can be stated with a rather high degree of confidence that  $\Sigma^{\text{TRK}}$  (and consequently the other two SR) “exist”. Therefore one can try to extract some information about the high energy behavior of the cross section and hence about the “existence” of SR with higher  $n$ . With an  $\omega^{-p}$  ansatz for the fall-off of the cross section above pion threshold, and requiring that  $\Sigma^{\text{TRK}}$  is 146 mb MeV (see Table 6.2), one gets a rather weak energy fall-off, i.e.  $p \simeq 1.5$ . This value is also consistent with  $\Sigma^{\text{BSR}}$ . In fact, adding such a tail contribution to  $m_{-1}(135)$  one gets  $\Sigma^{\text{BSR}} = 2.39 \text{ mb}$ , to be compared with 2.41 mb in Table 6.2. The value of  $p$  might be somewhat different for other potentials, but probably it will not change much. An additional, rather safe, conclusion is that higher order SR do not exist for realistic nuclear potential models.

A very interesting aspect can be viewed by observing the BSR. As already mentioned  $\Sigma^{\text{BSR}}$  contains information about one- and two-body densities via  $\langle r_\alpha^2 \rangle$  and  $\langle r_{\alpha\beta}^2 \rangle$ , respectively. This means that a measurement of  $\Sigma^{\text{BSR}}$  and the knowledge of the experimental m.s. radius allow to determine  $\langle r_{\alpha\beta}^2 \rangle$  via Eqs. (6.17),(6.19) and (6.20). In this way one gets information about the internal configuration of  ${}^4\text{He}$  as it is

explained in the following.

In his derivation of Eq. (6.13), Foldy assumed a totally symmetric  ${}^4\text{He}$  spatial wave function, which corresponds to a configuration where the four nucleons are located at the four vertexes of a tetrahedron. For such a configuration one has  $\langle r_p^2 \rangle = \langle r_n^2 \rangle = \langle r^2 \rangle$  and  $\langle r_{pp}^2 \rangle = \langle r_{nn}^2 \rangle = \langle r_{np}^2 \rangle$  with  $Q_T \equiv \langle r_{\alpha\beta}^2 \rangle / \langle r^2 \rangle = 8/3$ . Foldy's assumption is a very good approximation for  ${}^4\text{He}$ , but other spatial symmetries (mixed symmetry, antisymmetric) are also possible.

*What can be learned from  $\Sigma^{\text{BSR}}$  with respect to this question?*

For  ${}^4\text{He}$ , which is a  $T=0$  system one can safely assume that  $\langle r_p^2 \rangle = \langle r^2 \rangle = \langle r_n^2 \rangle$  (isospin mixing is tiny (Viviani et al., 2005; Nogga et al., 2002)). Using in Eqs. (6.17), (6.19) and (6.20) the AV18+UIX value of  $\langle r^2 \rangle = 2.04 \text{ fm}^2$  from Sec. 6.1 (which coincides with the experimental one (Borie and Rinker, 1978), corrected for the proton charge radius) and  $\Sigma^{\text{BSR}}$  from Table 6.2, one obtains  $\langle r_{pp}^2 \rangle = \langle r_{nn}^2 \rangle = 5.67 \text{ fm}^2$  and  $\langle r_{pn}^2 \rangle = 5.34 \text{ fm}^2$ , i.e. two values which differ by about 6%.

The ratios  $Q_{pp(nn)} \equiv \langle r_{pp(nn)}^2 \rangle / \langle r^2 \rangle$  and  $Q_{np} \equiv \langle r_{np}^2 \rangle / \langle r^2 \rangle$  are not much different from the correspondent value  $Q_T$  of a classical tetrahedral configuration. We obtain  $Q_{pp} = 2.78$  and  $Q_{np} = 2.62$  instead of  $Q_T = 2.67$ . One notices that  $Q_{pp(nn)} - Q_T \simeq 2(Q_{np} - Q_T)$ . This reflects the different numbers of proton-proton and neutron-neutron pairs (2) with respect to proton-neutron pairs (4). Using Eq. (6.12) one can also derive the distance between the proton and neutron centers of mass. One has  $R_{pn} = 1.58 \text{ fm}$  instead of 1.65 fm for the tetrahedral configuration.

Notice that with  $\langle r^2 \rangle = 2.04 \text{ fm}^2$  the "tetrahedral" BSR would be 2.62 mb, the same value that one obtains using Eq. (6.13). This value is 9% larger than our result. The distortions that I find from the 9% smaller BSR are the consequence of the different effects of the potential on isospin triplet and isospin singlet pairs.

A rather intriguing conclusion arises: when considered in its body frame  ${}^4\text{He}$  should look like a slightly *deformed* tetrahedron. Of course this statement has to be interpreted in a quantum mechanical sense, regarding the mean square values of the nucleon-nucleon distances on the two-body density. It is clear that one cannot measure this *deformation* "directly", since it is not a deformation of the one-body charge density (the  ${}^4\text{He}$  charge density has only a monopole). On the other hand such

a *deformation* is accessible experimentally in an indirect way via the measurements of the charge radius and of  $\Sigma^{\text{BSR}}$ .

This leads to the question how exactly  $\Sigma^{\text{BSR}}$  can be measured in a photonuclear experiment. Two points have to be addressed: i) the contributions of E1 retardation and higher multipoles, which are not contained in  $\Sigma^{\text{BSR}}$ , but which will contribute to the experimental cross section and ii) the contribution of the high energy tail.

Regarding point i), additional effects of the E1 retardation and higher multipoles have been calculated in Ref. (Golak et al., 2002) for the AV18+UIX potentials in a Faddeev calculation. Using those results one finds that E1 retardation and higher multipoles increase  $m_{-1}(135)$  by about 1% only. In fact according to Gerasimov(Gerasimov, 1964) there is a large cancelation of E1 retardation and other multipoles. There is no reason for a larger effect in  ${}^4\text{He}$ . On the contrary, since the leading isovector magnetic dipole (M1) transition is suppressed in this nucleus (it is zero for an S-wave) one can expect an even smaller contribution. As to point ii), considering the fall-off of the triton E1UR cross section around pion threshold from Ref. (Golak et al., 2002) one obtains a result very similar to our  ${}^4\text{He}$  case, namely  $p \simeq 1.5$ . However, including the other multipole contributions one gets a considerably smaller value, namely  $p \simeq 1.1$ . This is no contradiction with the small increase of 1% for  $\Sigma^{\text{BSR}}$ , since the inverse energy weighted cross section integrated from 100 to 135 MeV gives only a rather small contribution to the sum rule. On the other hand one would overestimate  $\Sigma^{\text{BSR}}$  taking the full cross section. Thus it is suggested that the tail contribution to an experimental BSR should be estimated using the theoretically established fall-off  $\omega^{-p}$  with  $p \simeq 1.5$ .



# NEUTRINO SCATTERING ON LIGHT NUCLEI IN SUPERNOVAE

---

The inelastic scattering of neutrino off  $A = 3$  nuclei and  ${}^4\text{He}$  is calculated microscopically at energies typical for core collapse supernova environment. The calculation is carried out with the Argonne  $v_{18}$  nucleon–nucleon potential and the Urbana IX three nucleon force. Full final state interaction is included via the Lorentz integral transform (LIT) method. The contribution of axial meson exchange currents to the cross sections is taken into account from effective field theory of nucleons and pions to order  $\mathcal{O}(Q^3)$ . The main results of the chapter are based on a series of papers published in Gazit and Barnea (2004, 2007b,a,c); O’Connor et al. (2007).

The chapter starts with an overview on core collapse supernovae, emphasizing the abundances and role of  ${}^4\text{He}$  and  $A=3$  nuclei in the processes taking place in the SN environment. The cross-sections are then presented and discussed. Finally, neutrino mean-free-paths in the neutrinosphere region are evaluated.

## 7.1 Core-collapse Supernovae

A massive star, above about 10 solar masses, evolves over millions of years, to create an onion–like structure of layers, with lighter elements in the atmosphere and heavier in the center, where the gravitational pressure is highest. The cycle of fusion stops when the core burns Si nuclei to iron. Further burning can not be a source of energy, as the binding energy per nucleon is peaked in iron. Consequently, the evolution of the star comes to an end. Observations have shown that this death is not peaceful, it is followed by an enormous explosion, shining in a magnitude of a galaxy, believed to occur in the following chain of events.

When the core reaches the Chandrasekhar mass it cannot support its own gravity and collapses. The collapse halts only when the core reaches nuclear density, in which

short-range nuclear forces dominate the dynamics. This initiates an outgoing shock wave. As the shock travels through the outer layers of the core it loses energy due to thermal neutrino radiation, and dissociation of iron nuclei (bound by about 8 MeV/nucleon) to  $\alpha$  particles and free nucleons.

The fate of this shock is a matter of debate. In the “prompt shock” mechanism, the shock has enough initial energy to burst through the core and cause an explosion. However, in modern calculations, about 100 milliseconds after bounce the shock stalls at about 200 km from the center and becomes an accretion shock, with matter from the outer layers of the star falling through it. During this period the newly born proto-neutron star in the center of the star cools by neutrino emission. This huge burst of neutrinos, in total energy of almost  $10^{53}$  ergs, is believed to deposit enough energy in the matter below the shock to revive the shock. This so called “delayed shock” mechanism has not been quantitatively proved in numerical calculations, but received a qualitative proof in the observation of SN 1987A. Comparing the energy of the neutrino-burst to the gravitational well of the star, it is easy to realize that one needs only 1% of neutrino energy to be transferred to matter. This turns to be a highly delicate problem, in which the accuracy of the microscopic input is a crucial factor. The heating is achieved through elastic scattering on nucleons and electrons. Haxton (1988) has suggested that inelastic scattering on nuclei can increase neutrino-matter coupling. The higher energy of the heavy flavored neutrinos<sup>1</sup> favors neutral scattering on nuclei as an energy transfer method. Thus, neutrino interaction with nuclei, which exist below the shock, is believed to have an important part in the explosion process. This will be discussed thoroughly in Subsec. 7.1.1.

Another outcome of the huge neutrino flux is changing the chemical evolution of the star, mainly by break-up of nuclei into fragments of nuclei which act as seeds for different nucleosynthesis processes.  $^4\text{He}$  break-up by neutrinos has a role in this process, which will be reviewed in Subsec. 7.1.2.

---

<sup>1</sup>The characteristic temperatures of the emitted neutrinos are about 6 – 10 MeV for  $\nu_{\mu,\tau}$  ( $\bar{\nu}_{\mu,\tau}$ ), 5 – 8 MeV for  $\bar{\nu}_e$ , and 3 – 5 MeV for  $\nu_e$

### 7.1.1 Shock revival and Light Nuclei

In order to estimate how significant is neutrino interaction with light nuclei in the shocked region, one needs to know not only the neutrino luminosity but also the mean-free-paths of neutrinos in the region. Thus one needs the composition of the shocked regions and the cross-sections for neutrino scattering on light nuclei. In Fig. 7.1 one can view the density profile of an  $11M_{\odot}$  progenitor, 120 milliseconds after bounce (Livne, 2007). The calculation is 1D simulation, with full neutrino-transport, and using the equation of state developed by Shen et al. (1998). The red line in the Figure is the  $\alpha$  mass-fraction, which is the most abundant nuclei in the shocked region by this calculation. The rest of the composition are nuclei and free electrons. One can see that in this simulation the amount of  ${}^4\text{He}$  is about 1% up to 100 km off center and rises to around 10–20% just below the shock. Thus neutrino scattering off  ${}^4\text{He}$  could play a role in the revival of the shock, as first indicated by Haxton (1988). Moreover, the energy transfer due to elastic scattering is low,  $\omega \sim T^2/m$ , therefore inelastic scattering could be as important as elastic scattering on nucleons. One has to keep in mind that with every inelastic scattering there is a substantial release of energy – larger than the break-up energy of 20 MeV. A complete study on the role of  ${}^4\text{He}$  excitation on the shock revival was not done, and is called for. However, a first study was carried out by (Ohnishi et al., 2006), and showed a small effect on accretion shock instabilities.

Nuclear statistical equilibrium (NSE) models, like those used by Shen et al. (1998), predict abundances based on binding energies and the quantum numbers of nuclei. However, NSE models only treat approximately (or neglect) strong interactions between nuclei, and consequently break down as the density increases. Recently a description of low-density nuclear matter (composed of neutrons, protons and alpha particles) in thermal equilibrium based on the virial expansion was developed (Horowitz and Schwenk, 2006a,b). The virial equation of state (EoS) systematically takes into account contributions from bound nuclei and the scattering continuum, and thus provides a framework to include strong-interaction corrections to NSE models. This formalism makes model-independent predictions for the conditions near the neutrinosphere, i.e. for densities of  $\rho \sim 10^{11-12} \text{ g/cm}^3$  and high

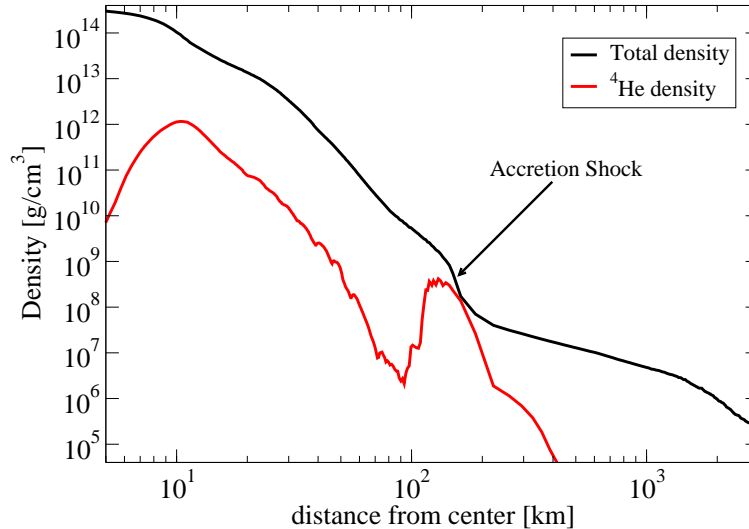


Figure 7.1: Density profile of  $11M_{\odot}$  star, 120 milliseconds after bounce. The black line is the total density, and the red line is the  $\alpha$  mass fraction. One can view the accretion shock at about 200 km off center.

temperatures  $T \sim 4$  MeV (Costantini et al., 2004; Lunardini and Smirnov, 2004). In particular, the resulting alpha particle concentration differs from all equations of state currently used in SN simulations, and the existence of trinuclei in this area is expected. For example, in Fig. 7.1 the region of about 10 – 30 km off center is characterized by this density range. Thus, the calculation substantially underestimates the abundances of  $A = 3, 4$  nuclei in this region.

To determine the abundance of  $A = 3$  nuclei near the neutrinosphere in supernovae, we presented in O’Connor et al. (2007) an extension of the virial approach to the EoS to explicitly include neutrons, protons,  $\alpha$  particles,  ${}^3\text{H}$  and  ${}^3\text{He}$  nuclei; deuterons are included as a bound state contribution to the proton-neutron virial coefficient.

The resulting mass fractions  $x_i = A_i n_i / n_b$  ( $n_i$  is the density of the  $i$  element of mass  $A_i$ , and  $n_b$  is the baryon density), are shown in Fig. 7.2 for neutrinosphere densities and temperatures, and various proton fractions  $Y_p = (n_p + 2n_{\alpha} + 2n_{{}^3\text{He}} + n_{{}^3\text{H}}) / n_b$ , i.e. the ratio of proton number to baryon number.

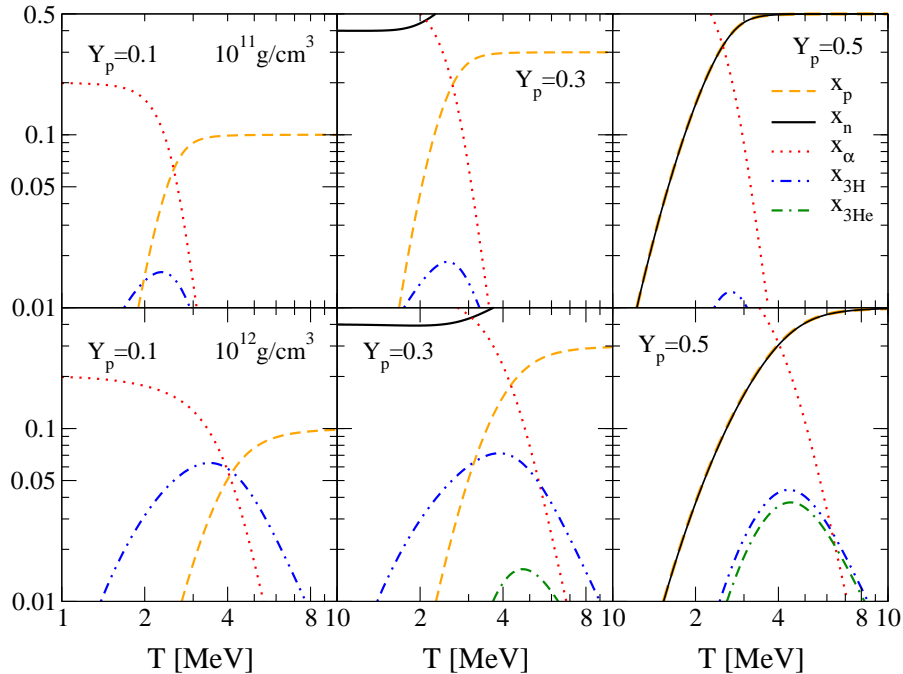


Figure 7.2: Mass fractions of nucleons and  $A = 3, 4$  nuclei in chemical equilibrium as a function of temperature  $T$ . The top and bottom rows correspond to a density of  $10^{11} \text{ g/cm}^3$  and  $10^{12} \text{ g/cm}^3$  respectively, and from left to right the proton fractions are  $Y_p = 0.1, 0.3$  and  $0.5$ .

The main result of this EoS is the model-independent prediction that the mass-three fraction can be significant (up to 10%) near the neutrinosphere. Thus, we present in Sec. 7.3.4 predictions for the neutral-current inclusive inelastic cross-sections on mass-three nuclei, based on microscopic two- and three-nucleon interactions and meson-exchange currents, including full final-state interactions via the Lorentz integral transform (LIT) method.

### 7.1.2 Nucleosynthesis and $\nu - \alpha$ Interaction

Due to the high temperature of  $\mu$  and  $\tau$  neutrinos (and anti-neutrinos), a substantial amount of them carry more than 20 MeV, and may dissociate the  ${}^4\text{He}$  nucleus through inelastic neutral current reactions. This creates the seed to light element

nucleosynthesis in the surrounding stellar envelope (Woosley et al., 1990). As a part of this explosive nucleosynthesis, or “ $\nu$ -nucleosynthesis”, a knock out of a nucleon from a  ${}^4\text{He}$  nucleus in the helium rich layer, followed by a fusion of the remaining trinucleus with another  $\alpha$  particle, will result in a 7-body nucleus. This process is an important source of  ${}^7\text{Li}$ , and of  ${}^{11}\text{B}$  and  ${}^{19}\text{F}$  through additional  $\alpha$  capture reactions. In fact the production of  ${}^{11}\text{B}$  in supernovae (also due to neutrino interaction on  ${}^{12}\text{C}$ ) can be calibrated by measuring ratio of  ${}^{11}\text{B}$  to  ${}^{10}\text{B}$  in meteorites. Woosley and Weaver (1995) have suggested that the calculated abundance is too large. Yoshida et al. (2005) have shown that the Li and B production depends highly on the neutrino temperature, and mainly on the spectrum character of the high energy tail (due to the high dissociation energy of  $\alpha$ ). They used this observation to fit the neutrino temperature to reproduce the measured abundance. However, a correct description of the process must contain an exact, energy dependent cross-section for the neutral inelastic  $\alpha - \nu$  reaction, which initiates the process.

The relatively low temperature of  $\nu_e$  and  $\bar{\nu}_e$  emitted from the core suppress the probability for inelastic reactions of these neutrinos with  ${}^4\text{He}$  in the supernova scenario. However, the mixing of the first and the third neutrino mass eigen-states is enhanced, due to matter effects, in the Oxygen/Carbon layers, just below the He layer. This significantly changes the spectrum of electron (anti-)neutrinos reaching the He layer, and yields a secondary source of energetic electron neutrinos. As indicated by Yoshida et al. (2006), the resulting charge current inelastic reactions on  ${}^4\text{He}$  could double the aforementioned yields. In this reference, they speculate that a test for neutrino oscillation properties could be observing the ratio of  ${}^7\text{Li}$  to  ${}^{11}\text{B}$  in stars. Yet again, this could lead to quantitative conclusions only if neutrino- ${}^4\text{He}$  cross-sections are available and accurate.

Elements heavier than iron are produced mainly by a different nucleosynthesis process – neutron capture. The so called  $r$ -process, in which this capture is rapid, is still missing a neutron-source in nature. Epstein et al. (1988) have suggested that neutrons produced by neutrino spallation of  ${}^4\text{He}$  in the helium rich layer could be such a source.

However, the most probable source of  $r$ -process neutrons is the neutrino-driven

wind blowing from the surface of a newly born proto-neutron star (PNS). This is a high entropy region, thus all protons combine with neutrons to form  ${}^4\text{He}$ , with excess neutrons left over. This makes the  $r$ -process picture puzzling, as the free neutrons that initially accompany the  ${}^4\text{He}$ , are then converted to protons by charge current reactions, which then form more  ${}^4\text{He}$  (Woosley and Hoffman, 1992). Thus it is very hard to maintain a neutron excess (necessary for the  $r$ -process) in the wind. Neutrino cross sections for  ${}^4\text{He}$  breakup are part of the detailed balance that determines what residual neutron abundance will remain in a neutrino-driven wind.

## 7.2 Weak Interaction Observable – Beta Decay Rate

In order to give parameter free *predictions* of weak processes, one needs the LECs of the EFT. There is only one unknown LEC, which is calibrated to fit a weak interaction observable.

A most researched weak interaction observable is the  $\beta$  decay. In this decay, a neutron (which can be free or bound in a nucleus) spontaneously transforms into a proton, accompanied by electron and anti-neutrino emission. This instability could be found in many elements, transforming one element to another. The lightest elements undergoing this decay are:  $n \rightarrow p + e^- + \bar{\nu}_e$ ,  ${}^3\text{H} \rightarrow {}^3\text{He} + e^- + \bar{\nu}_e$  and  ${}^6\text{He} \rightarrow {}^6\text{Li} + e^- + \bar{\nu}_e$ .

The  $\beta$  decay rate provides a direct test for the weak interaction model and the axial currents in the nucleus. This aspect is even more appealing as the  $\beta$  transitions are between bound-states of nuclei, and usually include small momentum transfer. Thus, the decay is governed by the Gamow–Teller and Fermi operators, which are proportional to the low momentum transfer approximation of  $E_1^A$  and  $C_0^V$  operators. In fact, to leading order the  $\beta$  decay rate is simply given by (see for example (Schiavilla and Wiringa, 2002))

$$\Gamma_{fi}^\beta = f_t \frac{G^{(+)}{}^2 m_e^5}{2\pi^3} (|F|^2 + g_A^2 |GT|^2) \quad (7.1)$$

where the Gamow Teller and Fermi reduced matrix elements:

$$F \equiv \langle f \parallel \sum_{i=1}^A \tau_{i,+} \parallel i \rangle \quad (7.2)$$

$$GT \equiv \langle f \parallel \sum_{i=1}^A \tau_{i,+} \vec{\sigma}_i \parallel i \rangle, \quad (7.3)$$

$f_t$  includes the entirety of the kinematics:

$$f_t \equiv \int_1^{\overline{m}_i - \overline{m}_f} d\epsilon \epsilon \sqrt{\epsilon^2 - 1} (\overline{m}_i - \overline{m}_f - \epsilon)^2 F^{(+)}(Z_f, \epsilon) \quad (7.4)$$

here  $\epsilon$  is electron energy in units of electron mass,  $\overline{m}$  are masses in the same units, with subscript  $i(f)$  indicating initial (final) state, respectively. Since isospin mixing is usually small for light nuclei, the Fermi operator can be evaluated accurately. Thus, by using this formula, one can deduce the experimental GT to very good accuracy (Chou et al., 1993):

$$GT(n \rightarrow p + e^- + \bar{\nu}_e) = \sqrt{3} \cdot (1 \pm 0.003) \quad (7.5)$$

$$GT(^3\text{H} \rightarrow ^3\text{He} + e^- + \bar{\nu}_e) = \sqrt{3} \cdot (0.961 \pm 0.005) \quad (7.6)$$

The axial coupling constant,  $g_A = 1.2670 \pm 0.0004$ , is calibrated using the neutron life-time, where the matrix element is analytic. For the triton, axial MEC in the nuclei influence the half-life. Thus, the triton GT is used to calibrate unknown constants in the MEC model. In the case of MEC based on the EFT introduced in Chap. 3, the only unknown is the renormalization LEC  $\hat{d}_r$ .

Keeping the philosophy of the EFT\* approach, the AV18/UIX Hamiltonian is used as the nuclear interaction for the calculation of the trinuclei wave functions. One then calculates the GT ( $E_A^1$ ) using the EFT based MEC, and calibrates  $\hat{d}_r$  to reproduce the half life. This procedure follows (Park et al., 2003). One could use their result for  $\hat{d}_r(\Lambda)$ . However, as a test for both the nuclear wave functions and the numerics.

When reproducing, there are additional benchmarks one should note. First, the

Method	Binding Energy [MeV]	
	${}^3\text{H}$	${}^3\text{He}$
EIHH	8.471(2)	7.738(2)
CHH	8.474	7.742
FY	8.470	7.738
Experimental	8.482	7.718

Table 7.1: Binding energies of  ${}^3\text{H}$  and  ${}^3\text{He}$  calculated using AV18/UIX Hamiltonian model compared to the same calculation done by using FY equations and expansion on correlated hyperspherical harmonics (CHH) basis (Nogga et al., 2003). For the EIHH calculation, the number in parenthesis indicates the numerical error. Also shown are the experimental values.

calculation can be checked by comparing binding energies of the trinuclei to those achieved by the FY and the correlated hyperspherical harmonics methods (Nogga et al., 2003), with the same potential model. This appears in Table 7.1. One can see a very good comparison between the calculations.

An additional benchmark is a calculation of the single operator contribution to the GT amplitude of  ${}^3\text{H}$  half life (which will be denoted by  $\text{GT}_{1B}$ ) (Schiavilla et al., 1998) with the same potential model, using the CHH method. This comparison reads:  $\text{GT}_{1B}(\text{CHH}) = 1.596 \Leftrightarrow \text{GT}_{1B}(\text{EIHH}) = 1.598(1)$ .

Finally, I reproduce the  $\hat{d}_r(\Lambda)$  of (Park et al., 2003). My results are:

$$\begin{aligned}
 \hat{d}_r &= 1.02 \pm 0.02 \pm 0.08 \quad \text{for } \Lambda = 500 \text{ MeV} \\
 \hat{d}_r &= 1.78 \pm 0.03 \pm 0.08 \quad \text{for } \Lambda = 600 \text{ MeV} \\
 \hat{d}_r &= 3.8 \pm 0.06 \pm 0.12 \quad \text{for } \Lambda = 800 \text{ MeV}
 \end{aligned}
 \tag{7.7}$$

Where the first error is numerical, i.e. convergence of the calculation, and the second correspond to the experimental uncertainty in the triton GT strength. This is to be

compared with (Park et al., 2003),

$$\hat{d}_r = 1.00 \pm 0.07 \text{ for } \Lambda = 500 \text{ MeV}$$

$$\hat{d}_r = 1.78 \pm 0.08 \text{ for } \Lambda = 600 \text{ MeV}$$

$$\hat{d}_r = 3.9 \pm 0.10 \text{ for } \Lambda = 800 \text{ MeV}.$$

The minor differences are of the order of those encountered in other observables. The differences in the error-bars are probably due to differences in the experimental source.

Summing up, the results of this section give us the needed information to carry on *parameter free predictions* of weak processes. As a side benefit, I get a verification of the numerical methods used, and the derived weak currents.

### 7.3 Neutrino Scattering Cross-sections Calculation

The calculation of the neutral-current inclusive inelastic cross-sections follows the procedure used to calculate the photoabsorption process. We solve the bound state problem based on the Argonne  $v_{18}$  nucleon-nucleon potential (Wiringa et al., 1995) and the Urbana IX three-nucleon interaction (Pudliner et al., 1997). The bound state binding energies of the trinuclei are given in the previous section, and those of  ${}^4\text{He}$  in Table 6.1.

Neutrino scattering on  $A = 3$  and  ${}^4\text{He}$  nuclei only induces transitions to continuum states, since the nuclei have no bound excited states. The correct description of the process is achieved via the LIT method. The resulting Schrödinger-like equations are solved using the effective interaction hyperspherical harmonics (EIH) approach of Chap. 5.

We use chiral EFT meson-exchange currents (MEC) as presented in Chap. 3. The EFT approach is an appropriate approximation, as  $Q \lesssim 60 \text{ MeV}$  is the typical energy in our processes of interest, and the cutoff  $\Lambda$  is of the order of the EFT breakdown scale  $\Lambda = 400 - 800 \text{ MeV}$ . In configuration space, the MEC are obtained from a Fourier transform of propagators with a cutoff  $\Lambda$  (cf. Eq. (3.36)). This leads to a

cutoff dependence, which is renormalized by the cutoff-dependent counterterm  $\hat{d}_r(\Lambda)$ , given in Eq. (7.7).

### 7.3.1 Leading Multipole Contributions

In the supernova scenario one has to consider neutrinos with up to about 60 MeV. The main result of this is that it is sufficient to retain contributions up to  $O(q^2)$  in the multipole expansion. This conclusion is checked on  ${}^4\text{He}$ , and is accurate to the percentage level. This is consistent with the discussion of Sec. 2.3. The leading contributions to the inelastic cross-section are due to the axial vector operators  $E_1^A$ ,  $E_2^A$ ,  $M_1^A$ ,  $L_2^A$ ,  $L_0^A$  and the vector operators  $C_1^V$ ,  $E_1^V$ ,  $L_1^V$ . As explained in the previous chapter, the leading vector operators are all proportional to each other due to the Siegert theorem, valid in this energy range (see discussion in Sec. 2.3). The axial charge operator  $C_0^A$  and the magnetic  $M_1^V$  operator are both proportional to the inverse of the nucleon mass – thus have no substantial contribution, exactly as relativistic corrections. In fact, for a percentage level accuracy, the following long wavelength approximation can be used (Donnelly and Walecka, 1976), for the impulse approximation the spin-orbital parts of the operators are

$$\begin{aligned}
 C_0^V(q) &= \frac{1}{\sqrt{4\pi}} \\
 C_0^A(q) &= \frac{i}{\sqrt{4\pi}} \vec{\sigma} \cdot \vec{\nabla} \\
 L_0^A(q) &= ig_A \frac{qr}{3} [\vec{\sigma} \otimes Y_1(\hat{r})]^{(0)} \\
 E_{1M}^A(q) &= -ig_A \sqrt{\frac{2}{3}} [\vec{\sigma} \otimes Y_0(\hat{r})]_M^{(1)} \\
 C_{1M}^V(q) &= \frac{qr}{3} Y_{1M}(\hat{r}) \\
 E_{1M}^V(q) &= -\sqrt{2} \frac{\omega}{q} C_{1M}^V(q) \\
 L_{1M}^V(q) &= -\frac{\omega}{q} C_{1M}^V(q) \\
 M_{1M}^V(q) &= -\frac{i}{\sqrt{6\pi}} \frac{q}{2M_N} l_M
 \end{aligned}$$

$$\begin{aligned}
 M_{1M}^A(q) &= -g_A \frac{qr}{3} [\vec{\sigma} \otimes Y_1(\hat{r})]_M^{(1)} \\
 E_{2M}^A(q) &= i \sqrt{\frac{3}{5}} g_A \frac{q}{3} [\vec{\sigma} \otimes Y_1(\hat{r})]_M^{(2)} \\
 L_{2M}^A(q) &= \sqrt{\frac{2}{3}} E_{2M}^A(q)
 \end{aligned}$$

The axial MEC operator, given in Eq. (3.48), is invariant to an exchange between the particles. Thus, it does not influence multipoles of opposite symmetry. The MEC will have a substantial influence only on the GT ( $E_A^1$ ) operator, as it will be discussed in the following subsections.

### 7.3.2 Inelastic Cross-sections and Energy-transfer

The result of the current calculation gives an energy and angle dependent inclusive cross-section. In order to present the cross-sections, we use the fact that the neutrino spectra are approximately thermal. Thus, the calculated cross sections are averaged over energy and angle, assuming a Fermi-Dirac distribution for the neutrinos with zero chemical potential, temperature  $T_\nu$ , and neutrino momentum  $k$ ,

$$f(T_\nu, k) = \frac{N}{T_\nu^3} \frac{k^2}{e^{k/T_\nu} + 1}, \quad (7.8)$$

where  $N^{-1} = 2 \sum_{n=1}^{\infty} (-1)^{n+1} / n^3$  is a normalization factor. The quantities of interest are the cross-sections and energy transfer cross-sections averaged over neutrino spectra of temperature  $T_\nu$ ,

$$\langle \sigma \rangle_{T_\nu} = \int_{\omega_{\text{th}}}^{\infty} d\omega \int dk_i f(T_\nu, k_i) \frac{d\sigma}{dk_f}, \quad (7.9)$$

$$\langle \omega \sigma \rangle_{T_\nu} = \int_{\omega_{\text{th}}}^{\infty} d\omega \int dk_i f(T_\nu, k_i) \omega \frac{d\sigma}{dk_f}, \quad (7.10)$$

where  $k_{i,f}$  are the initial and final neutrino energy,  $\omega = k_i - k_f$  is the energy transfer, and  $\omega_{\text{th}}$  denotes the threshold energy of the breakup reaction. For  ${}^4\text{He}$ ,  ${}^3\text{He}$  and  ${}^3\text{H}$  the threshold energies are  $\omega_{\text{th}} = 19.95, 6.23, 5.5$  MeV respectively.

It is well known that realistic 2-body NN potentials lead to an under-binding of about 0.5–1 MeV for the  ${}^3\text{He}$  and the triton nuclei and an under-binding of about 3–4 MeV for  ${}^4\text{He}$ . The AV18 threshold energies are 16.66 MeV, 5.37 MeV and 4.67 MeV for  ${}^4\text{He}$ ,  ${}^3\text{He}$  and triton breakup reaction, respectively. Thus the AV18 model has a discrepancy,  $\Delta \approx 3.3$  MeV for the threshold energy of the  ${}^4\text{He}$ ,  $\Delta \approx 0.83$  MeV for  ${}^3\text{He}$  break-up, and  $\Delta \approx 0.86$  MeV for  ${}^3\text{H}$ , with respect to the experimental inelastic reaction threshold.

Thermal averaging is highly influenced by the threshold energy, thus very sensitive to this discrepancy. In order to correct for this difference the response function is shifted to the true threshold, i.e.  $R(\omega) \rightarrow R(\omega - \Delta)$ , when only NN potentials are used.

### 7.3.3 Neutrino scattering on ${}^4\text{He}$ nucleus

In terms of “many-body” nuclear physics,  ${}^4\text{He}$  is a closed shell nucleus, i.e. its total angular momentum is zero and its spin structure is governed by an  $S$ -wave. Some of the leading operators are strongly suppressed due to the special structure of the ground state.

In fact, the Gamow-Teller operator contributes only due to the small  $P$ - and  $D$ -wave components of the ground state wave function. This reflects on the axial MEC contribution to the cross-section. In magnitude, the Gamow-Teller strength is less than 0.25% of the total cross-section, for all considered nuclear potentials: AV18, AV8', and AV18/UIX. Due to MEC, the strength grows to  $1\% \pm 0.5\%$ . The error is due to the  $\Lambda$  dependence. In this case, the part of the error which correspond to the triton half-life is of no importance. The MEC contribution is calculated only for the AV18/UIX potential model, and  $\hat{d}_r$  is taken from Eq. (7.7).

The special internal structure of the nucleus affects also the  $M_1^V$  operator, which vanishes for  ${}^4\text{He}$ . In addition,  ${}^4\text{He}$  is an almost pure zero-isospin state (Nogga et al., 2002), hence the Fermi operator vanishes.

As a result, the leading contributions to the inelastic cross-section are due to the axial vector operators  $E_2^A, M_1^A, L_2^A, L_0^A$  and the vector operators  $C_1^V, E_1^V, L_1^V$ , which

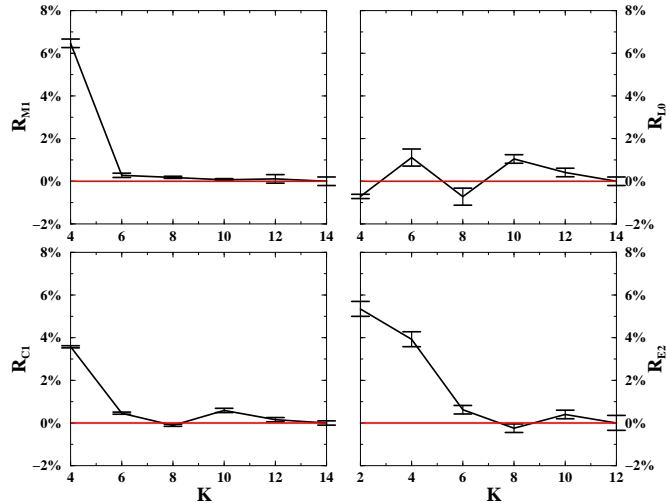


Figure 7.3: Relative error in the sum-rule of the leading response functions with respect to the hyper-angular momentum quantum number  $K$  (for  ${}^4\text{He}$ ). Calculated using the AV8' NN potential model. The error bars reflect the uncertainty in inverting the LIT.

are all proportional to the momentum transfer  $q$ .

The combination of the EIHH and LIT methods brings to a rapid convergence in the Response functions. In Fig. 7.3, one can see the relative error in the sum-rule of the main response functions when calculated with NN potential (in this case Argonne  $v'_8$ , but the conclusions hold for AV18 as well), with respect to the hyper-angular momentum quantum number  $K$ . It can be seen that upon convergence the relative error is well below 1%. The error bars presented reflect the error in inverting the LIT. This convergence pattern holds also for the AV18 potential model. Bearing in mind that the cross-section, up to kinematical factors, is the sum of the response functions, this is a measure of the accuracy in the calculated cross-section.

The convergence rate is outstanding even when including the 3NF. In Fig. 7.4 we present for the leading multipoles the convergence of the LIT as a function of  $K$ . It can be seen that the EIHH method results in a rapid convergence of the LIT calculation to a sub-percentage numerical accuracy. We conclude that the 3NF does not affect the convergence rate of these operators.

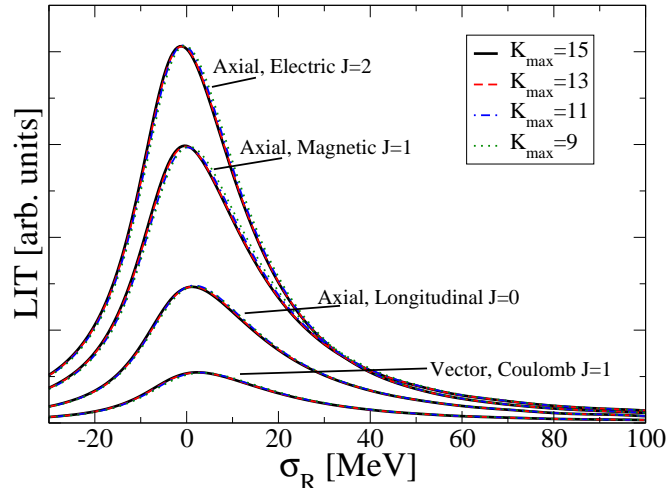


Figure 7.4: Convergence of  $\mathcal{L}_{\hat{\sigma}_1\hat{\sigma}_2}/q$  for the leading operators, as a function of the HH grand angular momenta  $K$  (for  ${}^4\text{He}$ ).

The general form of the cross-section is shown in Fig. 7.5.

In Table 7.2 we present the temperature averaged total neutral current inelastic cross-section as a function of the neutrino temperature for the AV8', AV18, and the AV18+UIX nuclear Hamiltonians and for the AV18+UIX Hamiltonian adding the axial MEC. From the table it can be seen that the low-energy cross-section is rather sensitive to details of the nuclear force model. This sensitivity is visible already when comparing the AV8' and AV18 results, where an effect of about 10% is discovered.

The 3NF have a bigger influence of about 25%. Similar tendency was also observed for the *hep* process (Marcucci et al., 2000). The effect reduces with neutrino temperature, from 35% for  $T_\nu = 2$  MeV, to 23% for  $T_\nu = 12$  MeV.

The results are of the same order of magnitude as previous estimates (Woosley et al., 1990), also appearing in the Table, though the differences can reach 25%. The current work predicts a stronger temperature dependence, with substantial increment at high temperatures. This indicates a different structure of the predicted resonances.

The cross-section is dominated by the axial  $E_2$  and  $M_1$  multipoles, which for example exhaust about 90% of the cross-section at  $T_\nu = 10$  MeV.

T	$\langle \sigma_x^0 \rangle_T = \frac{1}{2} \frac{1}{A} \langle \sigma_{\nu_x}^0 + \sigma_{\bar{\nu}_x}^0 \rangle_T [10^{-42} \text{cm}^2]$				
[MeV]	AV8'	AV18	AV18+UIX	AV18+UIX+MEC	Woosley (1990)
4	$2.09 \times 10^{-3}$	$2.31 \times 10^{-3}$	$1.63 \times 10^{-3}$	$1.66 \times 10^{-3}$	—
6	$3.84 \times 10^{-2}$	$4.30 \times 10^{-2}$	$3.17 \times 10^{-2}$	$3.20 \times 10^{-2}$	$3.87 \times 10^{-2}$
8	$2.25 \times 10^{-1}$	$2.52 \times 10^{-1}$	$1.91 \times 10^{-1}$	$1.92 \times 10^{-1}$	$2.14 \times 10^{-1}$
10	$7.85 \times 10^{-1}$	$8.81 \times 10^{-1}$	$6.77 \times 10^{-1}$	$6.82 \times 10^{-1}$	$6.87 \times 10^{-1}$
12	2.05	2.29	1.79	1.80	1.63
14	4.45	4.53	3.91	3.93	—

Table 7.2: Temperature averaged neutral current inclusive inelastic cross-section per nucleon as a function of neutrino temperature. The last column is the calculation in Woosley et al. (1990).

T	$\langle \sigma \rangle_T [10^{-42} \text{cm}^2]$			
[MeV]	$(\nu_x, \nu'_x)$	$(\bar{\nu}_x, \bar{\nu}'_x)$	$(\nu_e, e^-)$	$(\bar{\nu}_e, e^+)$
2	$1.47 \times 10^{-6}$	$1.36 \times 10^{-6}$	$7.40 \times 10^{-6}$	$5.98 \times 10^{-6}$
4	$1.73 \times 10^{-3}$	$1.59 \times 10^{-3}$	$8.60 \times 10^{-3}$	$6.84 \times 10^{-3}$
6	$3.34 \times 10^{-2}$	$3.07 \times 10^{-2}$	$1.63 \times 10^{-1}$	$1.30 \times 10^{-1}$
8	$2.00 \times 10^{-1}$	$1.84 \times 10^{-1}$	$9.61 \times 10^{-1}$	$7.68 \times 10^{-1}$
10	$7.09 \times 10^{-1}$	$6.54 \times 10^{-1}$	3.36	2.71
T	$\langle \sigma \omega \rangle_T [10^{-42} \text{MeVcm}^2]$			
[MeV]	$(\nu_x, \nu'_x)$	$(\bar{\nu}_x, \bar{\nu}'_x)$	$(\nu_e, e^-)$	$(\bar{\nu}_e, e^+)$
2	$3.49 \times 10^{-5}$	$3.23 \times 10^{-5}$	$1.76 \times 10^{-4}$	$1.42 \times 10^{-4}$
4	$4.50 \times 10^{-2}$	$4.15 \times 10^{-2}$	$2.27 \times 10^{-1}$	$1.80 \times 10^{-1}$
6	$9.26 \times 10^{-1}$	$8.56 \times 10^{-1}$	4.56	3.70
8	5.85	5.43	28.4	22.9
10	21.7	20.2	103.8	84.4

Table 7.3: Temperature averaged inclusive inelastic cross-section (upper part) and energy transfer cross-section (lower part) per nucleon as a function of temperature.

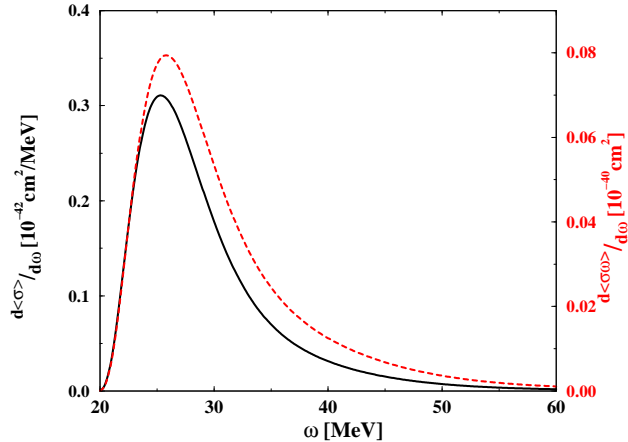


Figure 7.5: Temperature averaged inelastic cross-sections at temperature  $T = 10$  MeV for  ${}^4\text{He}$ . The solid line is the differential cross-section,  $\langle \frac{d\sigma}{d\omega} \rangle_T = \frac{1}{2} \frac{1}{A} \langle \frac{d\sigma_\nu}{d\omega} + \frac{d\sigma_{\bar{\nu}}}{d\omega} \rangle_T$ , (left scale). The dashed line is the differential energy transfer cross-section,  $\langle \omega \frac{d\sigma}{d\omega} \rangle_T = \frac{1}{2} \frac{1}{A} \langle \omega \frac{d\sigma_\nu}{d\omega} + \omega \frac{d\sigma_{\bar{\nu}}}{d\omega} \rangle_T$ , (right scale).

In Table 7.3 we present (for AV18+UIX+MEC) the temperature averaged cross-section and energy transfer as a function of the neutrino temperature for the various processes. In both tables it can be seen that the charged current process is roughly a factor of five more efficient than the neutral current process.

### 7.3.4 Neutrino scattering on $A = 3$ nuclei

Contrary to  ${}^4\text{He}$ , the GT is not suppressed for the trinuclei, which have  $J = \frac{1}{2}$  total angular momentum. At low-momentum transfer, the Gamow-Teller operator dominates for the cross section. It contributes about 60% of the cross-section at a temperature of 1 MeV. At higher-momentum transfer, higher-order multipoles (mainly the axial  $E_2$  and  $M_1$ ) start to play an important role, thus the GT part of the cross-section decreases to about 20% at  $T_\nu = 5$  MeV, and to about 10% at neutrino temperature of 10 MeV.

As a consequence of the descending importance of GT, the MEC contribution also decreases with temperature. In Fig. 7.6, one can view the relative contribution

$T_\nu$ [MeV]	${}^3\text{H}$		${}^3\text{He}$	
1	$1.97 \times 10^{-6}$	$1.68 \times 10^{-5}$	$3.49 \times 10^{-6}$	$2.76 \times 10^{-5}$
2	$4.62 \times 10^{-4}$	$4.73 \times 10^{-3}$	$6.15 \times 10^{-4}$	$5.94 \times 10^{-3}$
3	$5.53 \times 10^{-3}$	$6.38 \times 10^{-2}$	$6.77 \times 10^{-3}$	$7.41 \times 10^{-2}$
4	$2.68 \times 10^{-2}$	$3.37 \times 10^{-1}$	$3.14 \times 10^{-2}$	$3.77 \times 10^{-1}$
5	$8.48 \times 10^{-2}$	1.14	$9.70 \times 10^{-2}$	1.25
6	$2.09 \times 10^{-1}$	2.99	$2.35 \times 10^{-1}$	3.21
7	$4.38 \times 10^{-1}$	6.61	$4.87 \times 10^{-1}$	7.03
8	$8.20 \times 10^{-1}$	13.0	$9.03 \times 10^{-1}$	13.7
9	1.41	23.4	1.54	24.6
10	2.27	39.3	2.47	41.2

Table 7.4: Averaged neutrino- and anti-neutrino- ${}^3\text{H}$  and  ${}^3\text{He}$  neutral-current inclusive inelastic cross-sections per nucleon ( $A=3$ ),  $\langle \sigma \rangle_{T_\nu} = \frac{1}{2A} \langle \sigma_\nu + \sigma_{\bar{\nu}} \rangle_{T_\nu}$  (left columns), and energy transfer cross-sections,  $\langle \omega \sigma \rangle_{T_\nu} = \frac{1}{2A} \langle \omega \sigma_\nu + \omega \sigma_{\bar{\nu}} \rangle_{T_\nu}$  (right columns), as a function of neutrino temperature  $T_\nu$ , in units of  $10^{-42} \text{ cm}^2$  and  $10^{-42} \text{ MeV cm}^2$  respectively.

of MEC to the energy transfer,  $\frac{\langle \omega \sigma \rangle_{T_\nu}^{MEC} - \langle \omega \sigma \rangle_{T_\nu}^{No MEC}}{\langle \omega \sigma \rangle_{T_\nu}^{No MEC}}$ . The width of the line indicates the error in the theoretical estimate, due to the cutoff dependence. The cutoff dependence of both cross-sections is  $\sim 2\%$  for 1 MeV and  $< 1\%$  for higher temperatures. This is a rather strict validation of the calculation. The numerical convergence is very good for the trinuclei  $\sim 1\%$ .

The 3NF affect the cross-sections by about 15%, which is less than the their effect in  ${}^4\text{He}$ , however still substantial.

While not directly important for the shock revival, the asymmetry between the scattering of neutrinos and anti-neutrinos increases with temperature: the difference in the energy transfer grows gradually from 3% for a neutrino temperature of 3 MeV to  $> 50\%$  for 10 MeV temperatures.

### 7.3.5 Neutrino energy loss due to inelastic scattering

We can combine the energy transfer cross-sections with the  $A = 3, 4$  mass fractions of Fig. 7.2 to calculate the neutrino energy loss due to inelastic excitations of  $A = 3, 4$

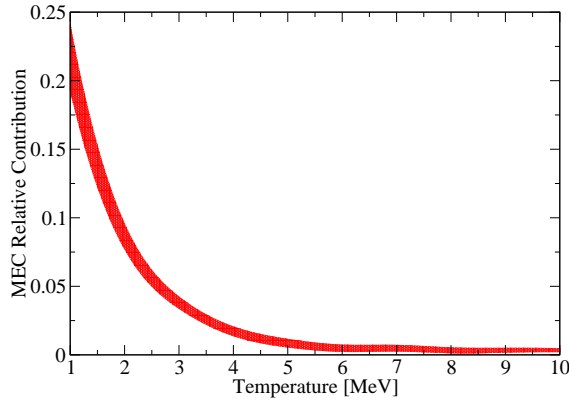


Figure 7.6: Relative contribution of MEC to the energy transfer, i.e.  $\frac{\langle \omega \sigma \rangle_{T_\nu}^{MEC} - \langle \omega \sigma \rangle_{T_\nu}^{No\ MEC}}{\langle \omega \sigma \rangle_{T_\nu}^{No\ MEC}}$ . The width of the line indicates the error in the theoretical estimate, due to the cutoff dependence.

nuclei. In Fig. 7.7 we compare the total energy transfer cross-sections for  ${}^3\text{H}$ ,  ${}^3\text{He}$  and  ${}^4\text{He}$ . The comparison clearly shows the huge difference between the cross-sections, originating in the “open-shell” character of the trinuclei.

The neutrino of energy  $E_\nu$  will decrease due to inelastic excitations, and heat the matter, at a rate  $dE_\nu/dx$  given by

$$\frac{dE_\nu}{dx} = n_b \sum_{i={}^3\text{H}, {}^3\text{He}, {}^4\text{He}} x_i \langle \omega \sigma \rangle_{i, T_\nu}. \quad (7.11)$$

For simplicity, we neglect the energy transfer from nuclei to neutrinos required by detailed balance. This is strictly correct only in the limit  $T \ll T_\nu$ .

In Fig. 7.8, the neutrino energy loss due to inelastic scattering is shown for a density of  $10^{12} \text{ g/cm}^3$  and neutrino temperature  $T_\nu = 6 \text{ MeV}$ , as a function of the matter temperature for various proton fractions. For  $T \gtrsim 4 \text{ MeV}$ , the energy loss is dominated by the contributions from  ${}^3\text{H}$  nuclei. The total abundance of  $A = 3$  nuclei depends only weakly on the proton fraction (see Fig. 7.2), which is reflected in the weak dependence of the neutrino energy loss as a function of proton fraction. Finally, for lower densities, mass-three nuclei are less abundant (see Fig. 7.2), and therefore also their contributions to the neutrino energy loss.

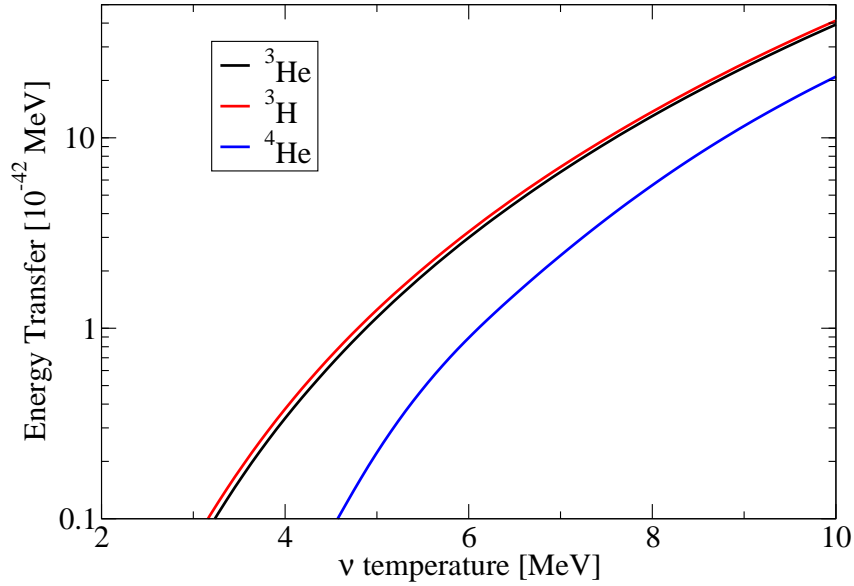


Figure 7.7: Neutrino total energy transfer cross-section a function of the neutrino temperature  $T_\nu$  for  $A = 3, 4$  nuclei.

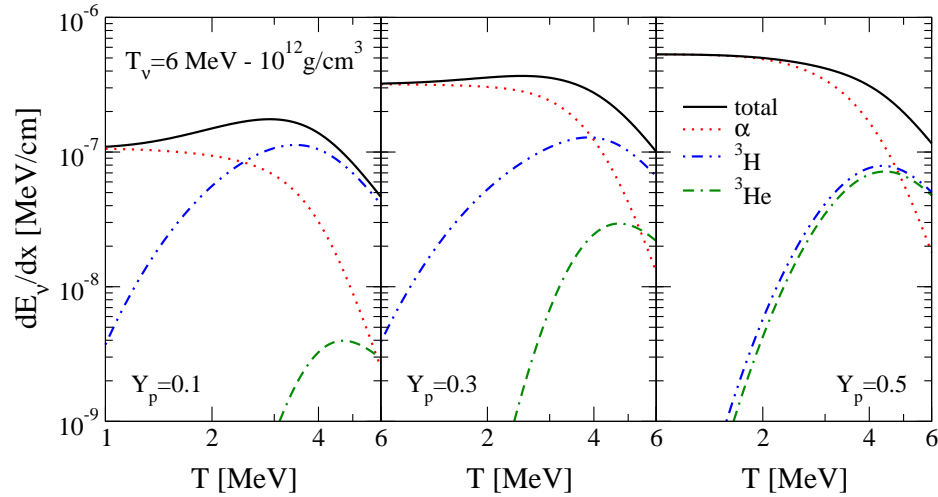


Figure 7.8: Neutrino energy loss  $dE_\nu/dx$  for inelastic excitations of  $A = 3, 4$  nuclei as a function of the matter temperature  $T$  at a density of  $10^{12} \text{ g/cm}^3$ . We assume that the neutrino energies are characterized by a Fermi-Dirac distribution with a temperature  $T_\nu = 6 \text{ MeV}$ . The contributions from  ${}^3\text{H}$ ,  ${}^3\text{He}$  and  ${}^4\text{He}$  nuclei, and the total neutrino energy loss are shown for proton fractions  $Y_p = 0.1, 0.3$  and  $0.5$ .

# 8 CONCLUSIONS

---

In this thesis I have presented the methods and the results of *ab-initio* calculations of electro-weak reactions on light nuclei. The reactions are calculated using realistic NN potential, Argonne  $v_{18}$ , and includes the Urbana IX 3NF. The full interaction is taken into account not only for the ground state, but also for the continuum states via the LIT method. For the solutions of the differential equations I use expansions in hyperspherical harmonics via the EIHH approach.

In the next two sections I will briefly summarize the main results and implications of the work.

## 8.1 Photoabsorption on $^4\text{He}$

I have presented the first complete calculation of the  $^4\text{He}$  total photoabsorption cross section using a realistic nuclear force (AV18 NN potential and the UIX-3NF). The results show a rather pronounced giant dipole peak typical to many body nuclei. This microscopic calculation of a complex nucleus settles the long living debate regarding the character of the peak.

The effect of the 3NF reduces the peak height by only 6%, less than expected considering its large effect of almost 20% on the  $^4\text{He}$  binding energy and its different role in the three-nucleon system. Beyond the giant dipole resonance 3NF effects become much larger. With growing energy transfer their importance increases and at pion threshold one finds a cross-section enhancement of 35%, about twice the effect discovered in  $^3\text{H}/^3\text{He}$  photoabsorption.

The calculated cross-section was integrated with energy-transfer weights to investigate sum-rules for  ${}^4\text{He}$ , which can be connected to important ground state properties. Three well known photonuclear sum rules for  ${}^4\text{He}$  are studied, viz the Thomas-Reiche-Kuhn, the bremsstrahlung and the polarizability SR. Two new equivalences for the BSR have allowed deduction of information about two-body properties of the nuclear ground state, like the proton-proton, neutron-neutron and proton-neutron distances.

A result with some beauty is tying the SR to the configuration symmetry of the nucleus. In particular, the configuration tetrahedral symmetry of  ${}^4\text{He}$  was tested, and found this symmetry to be slightly broken. An experimental way to access this symmetry breaking is proposed, via a measurement of the BSR which could be performed in one of the existing or planned low-intermediate energy photonuclear facility.

The calculated cross-section can be compared to numerous experiments estimating the reaction. Close to threshold the theoretical cross section agrees quite well with experimental data. In the giant resonance region, where there is no established experimental cross section, the results are in good agreement with the data of Nilsson et al. (2005) and Wells et al. (1992), while a strong disagreement is found when compared with the data of Shima et al. (2005). In order to understand whether a nuclear force model, which is constructed in the two- and three-nucleon systems, is sufficient to explain the four-nucleon photodisintegration, further experimental investigations are mandatory.

## 8.2 Neutrino Interaction with ${}^4\text{He}$ and $A=3$ nuclei in Supernova

The inelastic scatterings of neutrino off  ${}^4\text{He}$ ,  ${}^3\text{H}$  and  ${}^3\text{He}$  are calculated microscopically at energies typical for core collapse supernova environment. These are the first microscopic estimates of the processes, carried out with realistic nucleon forces. All breakup channels and full final-state interactions were included via the LIT method.

The contribution of axial meson exchange currents to the cross sections is taken into account from effective field theory of nucleons and pions to order  $\mathcal{O}(Q^3)$ , which reproduce the triton half-life.

I estimate the overall accuracy of the calculation to be of the order of 5%. This error is mainly due to the strong sensitivity of the cross-section to the nuclear model, in particular to the 3NF. The numerical accuracy of our calculations is of the order of 1%. The contribution of the axial MEC for  ${}^4\text{He}$  is small, in the percentage level. However, for the trinuclei the MEC contribution could be up to 30% for low temperature. The cutoff dependence for both  $A = 3, 4$  nuclei, which is indicative to the validity of the hybrid EFT approach, is negligible, less than a percent for neutrino temperature above 2 MeV.

Using the virial abundances and the microscopic energy transfer cross-sections, it is found that mass-three nuclei contribute significantly to the neutrino energy loss due to inelastic excitations for  $T \gtrsim 4$  MeV, conditions typical to the neutrinosphere. The predicted energy transfer cross-sections on mass-three nuclei in this area are approximately one order of magnitude larger compared to inelastic excitations of  ${}^4\text{He}$  nuclei.

To fully assess the role of neutrino breakup of  ${}^4\text{He}$  in core-collapse, the cross-sections should be included in SN simulations. The  $\nu - \alpha$  interaction is of central importance also for correct evaluation of the  $\nu$ - and  $r$ - nucleosynthesis processes.

With the present work, I have made an important step in the path towards a more robust and reliable description of neutrino-nuclei interaction role in core-collapse supernovae.

# A WEAK CURRENTS IN THE STANDARD MODEL

In this appendix, the general structure of the weak currents in nuclei are deduced from the standard model.

In the case of neutral neutrino scattering off a point proton, making use of the Feynman diagrams, with the  $Z^0$  boson propagator approximated as  $g_{\mu\nu}/M_Z^2$  one gets:

$$\begin{aligned}
 T_{fi} &= -M_Z^{-2} \cdot \bar{u}(k_f) \left[ \frac{-ig}{4\cos\theta_W} \gamma^\mu (1 - \gamma_5) \right] u(k_i) \cdot \\
 &\quad \cdot \bar{u}(P_f) \left[ \frac{-ig}{4\cos\theta_W} \gamma_\mu \left( (1 - 4\sin^2\theta_W) - \gamma_5 \right) \right] u(p_i) = \\
 &= \frac{G}{\sqrt{2}} [\bar{u}(k_2) \gamma^\mu (1 - \gamma_5) u(k_1)] \cdot \left[ \bar{u}(p_2) \gamma_\mu \left( \frac{1}{2}(1 - \gamma_5) - 2\sin^2\theta_W \right) u(p_1) \right]
 \end{aligned} \tag{A.1}$$

Where  $G \equiv \frac{\sqrt{2}g^2}{8M_Z^2\cos^2\theta_W}$  is the Fermi constant. A similar calculation for neutrino neutral scattering on neutron yields a different result:

$$T_{fi} = \frac{G}{\sqrt{2}} [\bar{u}(k_2) \gamma^\mu (1 - \gamma_5) u(k_1)] \cdot \left[ \bar{u}(p_2) \gamma_\mu \left( -\frac{1}{2}(1 - \gamma_5) \right) u(p_1) \right] \tag{A.2}$$

One can combine the results of equations A.2 and A.1, using the isospin symmetry to get for the nucleon current:

$$J^\mu = \bar{u}(p_2) \left[ \frac{\tau_0}{2} \gamma^\mu (1 - \gamma_5) - 2\sin^2\theta_W \gamma^\mu \frac{1}{2}(1 + \tau_0) \right] u(p_1) \tag{A.3}$$

For a complex nucleon, one keeps the symmetries of this current to write

$$\begin{aligned}
 \mathcal{J}_\mu^{(0)} &= (1 - 2 \cdot \sin^2\theta_W) \frac{\tau_0}{2} J_\mu^V + \frac{\tau_0}{2} J_\mu^A - 2 \cdot \sin^2\theta_W \frac{1}{2} J_\mu^V \\
 &= \frac{\tau_0}{2} (J_\mu^V + J_\mu^A) - 2 \cdot \sin^2\theta_W J_\mu^{em}
 \end{aligned} \tag{A.4}$$

Where  $J_\mu^V$  and  $J_\mu^A$  have vector and axial symmetry, respectively. The second equality takes advantage of the conserved vector current hypothesis, by which the weak-vector current is an isospin rotation of the electro-magnetic current.

A similar calculation for the charged current yields:

$$\mathcal{J}_\mu^{(\pm)} = \frac{\tau_\pm}{2} (J_\mu^V + J_\mu^A) \quad (\text{A.5})$$

# B LEPTON CURRENT

---

In this appendix the calculation of the lepton current matrix element is demonstrated. I will show this for the case of a neutrino scattering, as calculation of this matrix element for  $\beta$  decay or electron capture follow the same line.

The leptonic current is,

$$j_\mu(\vec{x}) = \bar{\psi}_\nu(\vec{x})\gamma_\mu(1 + \gamma_5)\psi_{\nu'}(\vec{x}) = l_\mu e^{-i\vec{q}\cdot\vec{x}} \quad (\text{B.1})$$

Where, for lepton reaction

$$l_\mu = \bar{u}(\nu)\gamma_\mu(1 + \gamma_5)u(\nu') \quad (\text{B.2})$$

Here, we keep the incoming particle is always a massless neutrino, while the outgoing can be either a neutrino or a massive lepton. For anti-lepton reaction,

$$l_\mu = \bar{v}(-\nu')\gamma_\mu(1 + \gamma_5)v(-\nu) \quad (\text{B.3})$$

For completeness, the needed matrix element for  $\beta^-$  decay is:

$$l_\mu = \bar{u}(e)\gamma_\mu(1 + \gamma_5)v(-\nu) \quad (\text{B.4})$$

The calculation of the cross-section include the expressions  $l_\lambda l_\nu^*$ . For the evaluation

of this expression, the following facts concerning the  $\gamma$  matrices are helpful,

$$\begin{aligned}
\{\gamma^\mu, \gamma^\nu\} &= 2g^{\mu\nu} \\
\{\gamma_5, \gamma^\mu\} &= 0 \\
(1 + \gamma_5)^2 &= 2(1 + \gamma_5) \\
\gamma_0 \gamma_\nu^\dagger \gamma_0 &= \gamma_\nu \\
tr\{\gamma_\lambda \gamma_\mu \gamma_\nu \gamma_{\mu'}\} &= 4(g_{\lambda\mu} g_{\nu\mu'} - g_{\lambda\nu} g_{\mu\mu'} + g_{\lambda\mu'} g_{\mu\nu}) \\
tr\{\gamma_\lambda \gamma_5 \gamma_\mu \gamma_\nu \gamma_{\mu'}\} &= -4i\epsilon_{\lambda\mu\nu\mu'}
\end{aligned}$$

where the metric tensor  $g^{\mu\nu} = \begin{pmatrix} 1 & 0 & 0 & 0 \\ 0 & -1 & 0 & 0 \\ 0 & 0 & -1 & 0 \\ 0 & 0 & 0 & -1 \end{pmatrix}$ .

For any two spinors  $\psi_1$  and  $\psi_2$  and any  $4 \times 4$  matrix  $\Gamma$ ,

$$(\bar{\psi}_1 \Gamma \psi_2)^* = \bar{\psi}_2 \gamma_0 \Gamma \gamma_0 \psi_1$$

thus, for lepton reaction,

$$l_\lambda l_\nu^* = \bar{u}^{(\alpha_2)}(k_2) \gamma_\mu (1 + \gamma_5) u^{(\alpha_1)}(k_1) \bar{u}^{(\alpha_1)}(k_1) (1 - \gamma_5) \gamma_\nu u^{(\alpha_2)}(k_2) \quad (\text{B.5})$$

To obtain the cross section it is necessary to sum over initial and average over final lepton helicities.

$$\overline{l_\lambda l_\nu^*} = \frac{1}{2} \sum_{\alpha_1 \alpha_2} \bar{u}^{(\alpha_2)}(k_2) \gamma_\mu (1 + \gamma_5) u^{(\alpha_1)}(k_1) \bar{u}^{(\alpha_1)}(k_1) (1 - \gamma_5) \gamma_\nu u^{(\alpha_2)}(k_2) \quad (\text{B.6})$$

It is helpful to use the fact that,

$$\sum_\alpha u_\xi^{(\alpha)}(k) \bar{u}_{\xi'}^{(\alpha)}(k) = \left( \frac{k_\mu \gamma^\mu + m}{2E_p} \right)_{\xi\xi'} \quad (\text{B.7})$$

Thus (the mass term falls due to  $\gamma$  matrices algebra),

$$\overline{l_\lambda l_\nu^*} = \frac{\nu^\mu \nu'^{\mu'}}{4\nu\nu'} \text{tr}\{\gamma_\lambda(1 + \gamma_5)\gamma_\mu\gamma_\nu\gamma_{\mu'}\} \quad (\text{B.8})$$

finally,

$$\overline{l_\lambda l_\nu^*} = \frac{1}{\nu\nu'} \{\nu_\lambda \nu'_\nu + \nu'_\lambda \nu_\nu \nu_\mu \nu'_\mu - i\epsilon_{\lambda\mu\nu\mu'} \nu^\mu \nu'^{\mu'}\} \quad (\text{B.9})$$

the calculation for anti-neutrino reaction is similar and gives

$$\overline{l_\lambda l_\nu^*} = \frac{1}{\nu\nu'} \{\nu_\lambda \nu'_\nu + \nu'_\lambda \nu_\nu \nu_\mu \nu'_\mu + i\epsilon_{\lambda\mu\nu\mu'} \nu^\mu \nu'^{\mu'}\} \quad (\text{B.10})$$

The general neutrino reaction cross-section requires the following expressions,

$$\overline{l_0 l_0^*} = 1 + \hat{\nu} \cdot \hat{\nu}' \quad (\text{B.11})$$

$$\overline{l_3 l_3^*} = 1 - \hat{\nu} \cdot \hat{\nu}' + 2(\hat{\nu} \cdot \hat{q})(\hat{\nu}' \cdot \hat{q}) \quad (\text{B.12})$$

$$\overline{l_3 l_0^*} = \hat{q} \cdot (\hat{\nu} + \hat{\nu}') \quad (\text{B.13})$$

$$\frac{1}{2}(\vec{l} \cdot \vec{l}^* - l_3 l_3^*) = 1 - (\hat{\nu} \cdot \hat{q})(\hat{\nu}' \cdot \hat{q}) \quad (\text{B.14})$$

$$(\vec{l} \times \vec{l}^*)_3 = S \times 2i\hat{q} \cdot (\hat{\nu} - \hat{\nu}') \quad (\text{B.15})$$

where  $q^\mu = \nu'^\mu - \nu^\mu$  is the momentum transfer.  $S$  is +1 for neutrino scattering and  $\beta^+$  decay, and -1 for anti-neutrino scattering and  $\beta^-$  decay.

# NON-RELATIVISTIC EXPANSIONS OF DIRAC SPINORS EXPRESSIONS

Dirac spinor of a mass  $M$ , takes the form:

$$u(p, \sigma) = \sqrt{\frac{E_p + M}{2E_p}} \begin{pmatrix} \chi_\sigma \\ \frac{\vec{\sigma} \cdot \vec{p}}{E_p + M} \chi_\sigma \end{pmatrix} \quad (\text{C.1})$$

where  $E_p = \sqrt{p^2 + M^2}$  is the energy of the particle. It is useful to recall that  $\bar{u} = u^\dagger \gamma_0$ . This convention leads to a normalized density, i.e.  $u^\dagger u = 1$

In this representation,

$$\gamma^0 = \begin{pmatrix} 1 & 0 \\ 0 & -1 \end{pmatrix}, \vec{\gamma} = \gamma^0 \begin{pmatrix} 0 & \vec{\sigma} \\ \vec{\sigma} & 0 \end{pmatrix}, \gamma_5 = \begin{pmatrix} 0 & 1 \\ 1 & 0 \end{pmatrix}, \quad (\text{C.2})$$

where we use  $\gamma^0 \gamma_5 \gamma^0 = -\gamma_5$  and  $\gamma^0 \gamma_5 \vec{\gamma} = -\vec{\sigma}$ .

One can now expand the needed matrix elements in the inverse mass:

$$\bar{u}(p', \sigma') \gamma^0 u(p, \sigma) = \chi_\sigma^\dagger \left( 1 - \frac{\vec{q}^2}{8M^2} + i\vec{q} \cdot \frac{\vec{\sigma} \times \vec{p}}{4M^2} \right) \chi_\sigma \quad (\text{C.3})$$

$$\bar{u}(p', \sigma') \vec{\gamma} u(p, \sigma) = \frac{1}{2M} \chi_\sigma^\dagger (\vec{P} - i\vec{\sigma} \times \vec{q}) \chi_\sigma \quad (\text{C.4})$$

$$\bar{u}(p', \sigma') \gamma_5 \gamma^0 u(p, \sigma) = -\frac{1}{2M} \chi_\sigma^\dagger (\vec{\sigma} \cdot \vec{P}) \chi_\sigma \quad (\text{C.5})$$

$$\bar{u}(p', \sigma') \gamma_5 u(p, \sigma) = \frac{1}{2M} \chi_\sigma^\dagger (\vec{\sigma} \cdot \vec{q}) \chi_\sigma \quad (\text{C.6})$$

$$\bar{u}(p', \sigma') \gamma_5 \vec{\gamma} u(p, \sigma) = -\chi_\sigma^\dagger \left( \vec{\sigma} \left( 1 - \frac{P^2}{8M^2} \right) + i \frac{\vec{q} \times \vec{p}}{4M^2} + \frac{\vec{P}(\vec{\sigma} \cdot \vec{P}) - \vec{q}(\vec{\sigma} \cdot \vec{q})}{8M^2} \right) \chi_\sigma \quad (\text{C.7})$$

where  $\vec{P} = \vec{p} + \vec{p}' = -i(\vec{\nabla} - \overleftarrow{\nabla})$  and  $\vec{q} = \vec{p} - \vec{p}'$ .

# D FEYNMAN DIAGRAMS FOR $\chi$ PT

The Feynman rules are exhausted from the interaction Lagrangian, and from the currents. This is done by expanding the complete term to first order in the pion field. The diagrams are then easily achieved.

It is valuable to remind here the pion propogator  $\frac{i}{k^2 - m_\pi^2}$ , and the nucleon propogator  $\frac{i}{\not{p} - M}$ .

## D.1 Leading Order Diagrams

The pion-nucleon interaction lagrangian to leading order in the pion field is given in Eq. (3.17). The resulting Feynman rules appear in Fig. D.1.

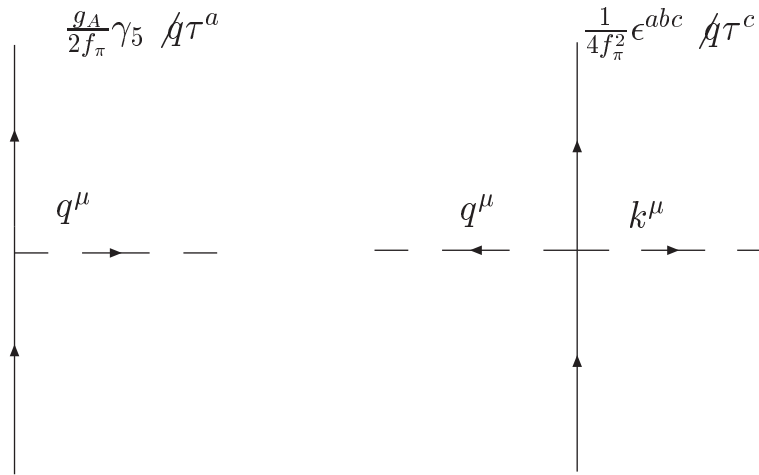


Figure D.1: The lowest order pion - nucleon Feynman diagrams. Nucleons are indicated by solid lines, whereas pions are indicated by dashed lines.

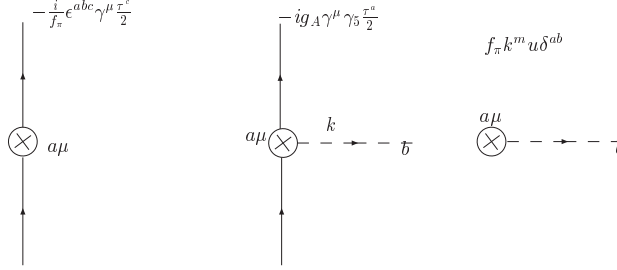


Figure D.2: Vertices in the axial current. Crossed circles indicate the attachment to the external probe.

The axial current to the same order is given in Eqs. (3.30 - 3.31), and appear in Fig. D.2.

To lowest order in the pion field, one can get the following vector vertices from Eqs. (3.27 - 3.28):

- $i\gamma^\mu \frac{\tau^a}{2}$ .
- $i\frac{g_A}{f_\pi} \epsilon^{abc} \gamma^\mu \gamma_5 \frac{\tau^c}{2}$ .
- $-\epsilon^{abc} k^\mu$ .

## D.2 Next-to Leading Order Diagrams

The NLO pion-nucleon interaction lagrangian to leading order in the pion field is given in Eq. (3.21). The resulting Feynman diagram is identical to the diagram drawn in the right part of Fig. D.1. The strength of the vertex is:

$$\frac{2i}{f_\pi^2 M} \left\{ \hat{c}_4 \epsilon^{abc} \frac{\tau_c}{2} k_\mu q_\nu \sigma^{\mu\nu} - \hat{c}_3 k_\mu q^\mu \delta^{ab} \right\} \quad (\text{D.1})$$

The NLO contribution to currents within the nuclei appear in Eqs. (3.31 - 3.28). The resulting vector current includes two pions, thus of higher order. The resulting axial

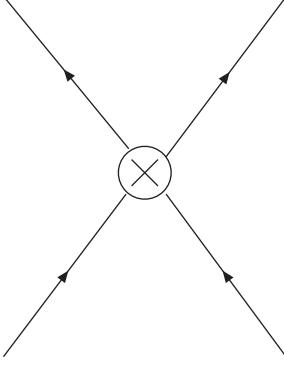


Figure D.3: Contact axial vertex in NLO.

vector diagram is identical to the one which appears in the center of Fig. D.2. The additional strength is:

$$\frac{2}{f_\pi M} \left\{ -\hat{c}_4 \epsilon^{abc} \frac{\tau_c}{2} q_\nu \sigma^{\mu\nu} + \hat{c}_3 q^\mu \delta^{ab} \right\} \quad (\text{D.2})$$

The NLO Lagrangian includes in addition contact terms, as given in Eq. (3.22). The form of the vertex is a contact term with an outgoing pion line, and the strength of the resulting vertex is  $-\frac{g_A D_1}{f_\pi} \gamma_5 \not{q} \tau_a$ .

The contact term contribution to the vector currents is zero in the non-relativistic limit. However, the contribution to the axial current diagram does not vanish  $D_1 \gamma^\mu \gamma_5 \frac{\tau_a}{2}$  with the diagram in Fig. D.3.

### D.3 Example: Single Nucleon Operators For Neutrino Scattering

One can use the Feynman diagrams of the previous section to draw neutrino scattering on a single nucleon:

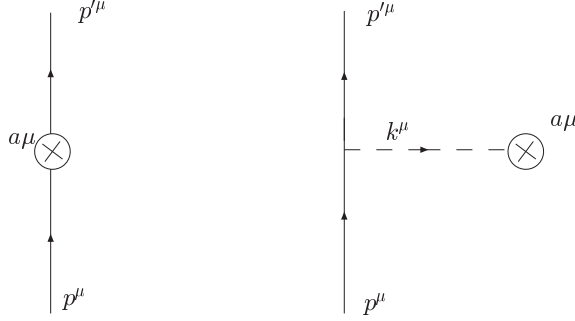


Figure D.4: Leading order 1-body axial vector current.

The resulting strength is identical to that achieved by standard nuclear physics approach (SNPA):

$$M^{a\mu}(1) = ig_A \bar{u}(p') \gamma_5 \left\{ \gamma^\mu - \not{k} \frac{k^\mu}{k^2 - m_\pi^2} \right\} \frac{\tau^a}{2} u(p) = i \bar{u}(p') \{ F_A \gamma^\mu \gamma_5 + F_P \gamma_5 k^\mu \} \frac{\tau^a}{2} u(p) \quad (\text{D.3})$$

The second equality uses the known SNPA axial form factor  $F_A = -g_A$ , and pion form factor  $F_P = -\frac{2Mg_A}{k^2 - m_\pi^2}$ . By non-relativistic expansion of the nucleon spinor, as explained in Appendix C, one gets the single nucleon scattering operators of Eqs. (3.43 - 3.46).

## D.4 Example: Axial MEC Operators For Neutrino Scattering

In order to continue to axial currents that involve two nucleons with a pion exchange, we will find the amplitude for pion production. This is done in Ananyan et al. (2002), and the resulting Feynman diagrams are given in Figure D.5. This is however wrong, as the first three diagrams (starting upper left side) include pion exchange between nucleons without any interaction of this pion with the external probe. The correct

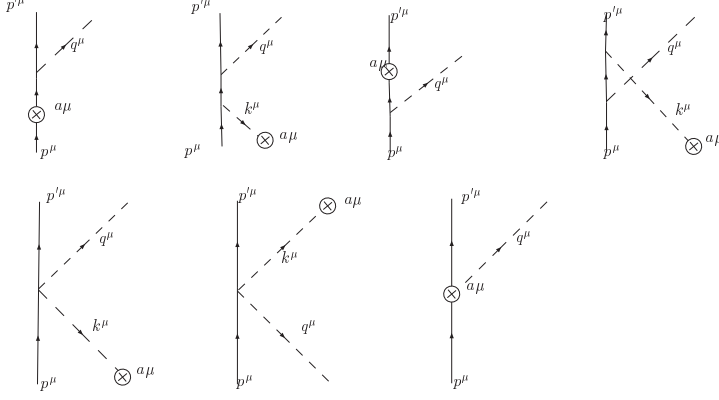


Figure D.5: Pion-production on a nucleon.

pion production amplitude is thus,

$$2f_\pi M^{ab\mu}(\pi) = \bar{u}(p') \left\{ -g_A^2 \not{q} \gamma_5 \frac{1}{(\not{p}' + \not{q} - M) \gamma_5} \not{k} \frac{k^\mu}{k^2 - m_\pi^2} \frac{\tau^b \tau^a}{2} \right. \\ \left. + i\epsilon^{abc} \frac{\tau_c}{2} \left[ (\not{k} - \not{q}) \frac{k^\mu}{k^2 - m_\pi^2} - 2\gamma^\mu \right] \right\} u(p) \quad (\text{D.4})$$

The two nucleon axial current is achieved through the exchange of a pion, as observed in Figure D.6. The amplitude is:

$$M^{a\mu}(2) = M^{ab\mu}(\pi) \frac{i}{q^2 - m_\pi^2} \frac{g_A}{f_\pi} \bar{u}(p'_2) \not{q} \gamma_5 \frac{\tau^b}{2} u(p_2) + \text{momenta permutations} \quad (\text{D.5})$$

Taking the non-relativistic limit ( $O(1/M)$ ) and the soft pion limit ( $q, k \rightarrow 0$ ), we get for the pion production,

$$2f_\pi M^{ab\mu}(\pi) \approx -i\bar{u}(p') \epsilon^{abc} \tau^c \gamma^\mu u(p) \quad (\text{D.6})$$

hence,

$$\vec{M}^a \approx \frac{ig_A}{8Mf_\pi^2} (\tau^{(1)} \times \tau^{(2)})^a (i\vec{P}_1 + \vec{\sigma}_1 \times \vec{q} + \vec{\sigma}_1 \times \vec{k}_2) \frac{\vec{\sigma}_2 \cdot \vec{k}_2}{k_2^2 + m_\pi^2} + (1 \leftrightarrow 2), \quad (\text{D.7})$$

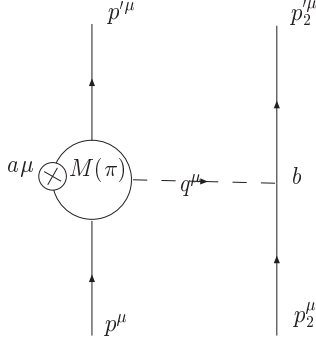


Figure D.6: Pion exchange contribution to the scattering amplitude .

$$M^{a0} \approx \frac{g_A}{4f_\pi^2} (\tau^{(1)} \times \tau^{(2)})^a \frac{\vec{\sigma} \cdot \vec{k}_2}{\vec{k}_2^2 + m_\pi^2} + (1 \leftrightarrow 2). \quad (\text{D.8})$$

where  $\vec{P}_1 = \vec{p} + \vec{p}'$ ,  $\vec{k}_i = \vec{p}_i - \vec{p}'_i$ , and  $\vec{q}$  is the neutrino's momentum.

An additional contribution to the pion production amplitude comes from NLO (calculated using the diagrams in Figure D.7):

$$M_{NLO}^{ab\mu} = -\frac{2\hat{c}_4}{f_\pi M} \epsilon^{abc} \left\{ g_\lambda^\mu - \frac{k^\mu k_\lambda}{k^2 - m_\pi^2} \right\} q_\nu \bar{u}(p') \sigma^{\lambda\nu} \frac{\tau^c}{2} u(p) + \frac{2\hat{c}_3}{f_\pi M} \epsilon^{abc} \left\{ q^\mu - \frac{k^\mu}{k^2 - m_\pi^2} k \cdot q \right\} \delta^{ab} \bar{u}(p') u(p), \quad (\text{D.9})$$

using Eq. (D.5) we can now get the NLO contribution to the pion exchange currents:

$$M_{NLO}^{a\mu}(2) = i \frac{g_A}{f_\pi^2} \left\{ -\frac{2\hat{c}_4}{M} \epsilon^{abc} \left[ g_\lambda^\mu - \frac{k^\mu k_\lambda}{k^2 - m_\pi^2} \right] \times \left( \bar{u}(p'_1) \sigma^{\lambda\nu} \frac{\tau^c}{2} u(p_1) \frac{q_\nu q_\sigma}{q^2 - m_\pi^2} \bar{u}(p'_2) \gamma^\sigma \gamma_5 \frac{\tau^b}{2} u(p_2) \right) + \frac{2\hat{c}_3}{M} \left[ q^\mu - \frac{k^\mu}{k^2 - m_\pi^2} k \cdot q \right] \frac{q_\sigma}{q^2 - m_\pi^2} \left( \bar{u}(p'_1) u(p_1) \bar{u}(p'_2) \gamma^\sigma \gamma_5 \frac{\tau^a}{2} u(p_2) \right) \right\} \quad (\text{D.10})$$

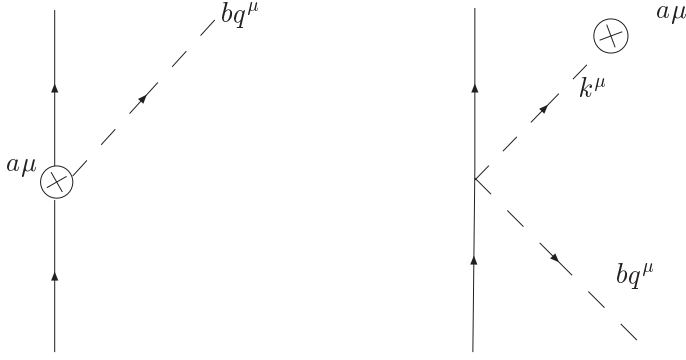


Figure D.7: Pion production contribution from NLO lagrangian.

The non-relativistic reduction leads to no contribution to the axial charge density and to the following expression for the axial current:

$$\vec{M}_{NLO}^a(2) = \frac{ig_A}{2Mf_\pi^2} \left\{ \hat{c}_4 (\vec{\tau}^{(1)} \times \vec{\tau}^{(2)}) \vec{\sigma}_1 \times \vec{k}_2 + 2\hat{c}_3 \vec{\tau}^{(2)a} \vec{k}_2 \right\} \frac{\vec{\sigma}_2 \cdot \vec{k}_2}{k_2^2 + m_\pi^2}. \quad (\text{D.11})$$

If we combine this with Eq. (D.7), we get

$$\begin{aligned} \vec{M}^a \approx & \frac{ig_A}{2Mf_\pi^2} \left\{ \frac{i}{4} (\vec{\tau}^{(1)} \times \vec{\tau}^{(2)})^a \vec{P}_1 + 2\hat{c}_3 \vec{\tau}^{(2)a} \vec{k}_2 + \right. \\ & + \left( \frac{1}{4} + \hat{c}_4 \right) (\vec{\tau}^{(1)} \times \vec{\tau}^{(2)})^a \vec{\sigma}_1 \times \vec{k}_2 + \\ & \left. + \frac{1}{4} (\vec{\tau}^{(1)} \times \vec{\tau}^{(2)})^a (\vec{\sigma}_1 \times \vec{q}) \right\} \frac{\vec{\sigma}_2 \cdot \vec{k}_2}{k_2^2 + m_\pi^2} + (1 \leftrightarrow 2), \end{aligned} \quad (\text{D.12})$$

The contribution of the contact Lagrangian vanishes for the axial charge operator in the non-relativistic limit. Its contribution to the MEC reads:

$$M_4^{a\mu} \approx iD_1 \left( \vec{\sigma}_1 \frac{\vec{\tau}^{(1)a}}{2} + \vec{\sigma}_2 \frac{\vec{\tau}^{(2)a}}{2} \right). \quad (\text{D.13})$$

In order to get the scattering operators, one has to transform to configuration space. After doing thus, one gets the final form of the MEC operators, appearing in Eq. (3.48).

# REDUCED MATRIX ELEMENTS OF DIFFERENT OPERATORS

In this chapter, I give a list of the needed matrix elements when calculating in the HH expansion, as implemented in the program. In the following  $\vec{\Sigma}$  is a spin spherical tensor operator of order 1.

## ME1

$$\begin{aligned}
 \langle K(ls)j \| j_J(qx)Y_J(\hat{x}) \| K'(l's')j' \rangle &= \\
 &= \delta_{s,s'} (-)^{J+j'+l+s} \sqrt{(2j+1)(2j'+1)} \begin{Bmatrix} l & J & l' \\ j' & s & j \end{Bmatrix} \times \\
 &\langle Kl \| j_J(qx)Y_J(\hat{x}) \| K'l' \rangle
 \end{aligned} \tag{E.1}$$

using the fact that,

$$\langle l \| Y_J(\hat{x}) \| l' \rangle = (-)^l \sqrt{\frac{(2l+1)(2J+1)(2l+1)}{4\pi}} \begin{pmatrix} l & J & l' \\ 0 & 0 & 0 \end{pmatrix} \tag{E.2}$$

We finally get,

$$\begin{aligned}
 \langle K(ls)j \| j_J(qx)Y_J(\hat{x}) \| K'(l's')j' \rangle &= \\
 &= \delta_{s,s'} (-)^{J+j'+s'} \sqrt{\frac{(2l+1)(2j+1)(2J+1)(2l'+1)(2j'+1)}{4\pi}} \times \\
 &\begin{Bmatrix} l & J & l' \\ j' & s & j \end{Bmatrix} \begin{pmatrix} l & J & l' \\ 0 & 0 & 0 \end{pmatrix} \langle Kl \| j_J(qx) \| K'l' \rangle
 \end{aligned} \tag{E.3}$$

**ME2**

We use the fact that  $\vec{\Sigma} \cdot \vec{Y}_{JLM}(\hat{x}) = [\Sigma^{(1)} \otimes Y_L]_M^{(J)}$ ,

$$\begin{aligned} \langle K(ls)j \| j_J(qx) \vec{\Sigma} \cdot \vec{Y}_{JLM}(\hat{x}) \| K'(l's')j' \rangle &= \sqrt{(2j+1)(2J+1)(2j'+1)} \\ &\times \left\{ \begin{array}{ccc} l' & s' & j' \\ L & 1 & J \\ l & s & j \end{array} \right\} \langle Kl \| j_J(qx) Y_L(\hat{x}) \| K'l' \rangle \langle s \| \vec{\Sigma} \| s' \rangle \end{aligned} \quad (\text{E.4})$$

putting now Eq. (E.2), we get

$$\begin{aligned} \langle K(ls)j \| j_J(qx) \vec{\Sigma} \cdot \vec{Y}_{JLM}(\hat{x}) \| K'(l's')j' \rangle &= (-)^l \left\{ \begin{array}{ccc} l' & s' & j' \\ L & 1 & J \\ l & s & j \end{array} \right\} \\ &\times \sqrt{\frac{(2j+1)(2l+1)(2J+1)(2L+1)(2j'+1)(2l'+1)}{4\pi}} \\ &\times \left( \begin{array}{ccc} l & L & l \\ 0 & 0 & 0 \end{array} \right) \langle s \| \vec{\Sigma} \| s' \rangle \langle Kl \| j_J(qx) \| K'l' \rangle \end{aligned} \quad (\text{E.5})$$

**ME3**

$$\begin{aligned} \langle Kl \| \vec{Y}_{JL}(\hat{x}) \cdot \vec{\nabla} \| K'l' \rangle &= (-)^{J+1} \sqrt{\frac{(2l+1)(2J+1)(2L+1)(2l'+1)}{4\pi}} \\ &\times \left[ \left\{ \begin{array}{ccc} J & l' & l \\ l'-1 & L & 1 \end{array} \right\} \frac{\left( \begin{array}{ccc} l & L & l'-1 \\ 0 & 0 & 0 \end{array} \right)}{\left( \begin{array}{ccc} l' & 1 & l'-1 \\ 0 & 0 & 0 \end{array} \right)} \frac{l'}{2l'+1} \langle Kl | \left( \frac{d}{dr} + \frac{l'+1}{r} \right) | K'l' \rangle \right. \\ &+ \left. \left\{ \begin{array}{ccc} J & l' & l \\ l'+1 & L & 1 \end{array} \right\} \frac{\left( \begin{array}{ccc} l & L & l'+1 \\ 0 & 0 & 0 \end{array} \right)}{\left( \begin{array}{ccc} l'+1 & 1 & l' \\ 0 & 0 & 0 \end{array} \right)} \frac{l'+1}{2l'+1} \langle Kl | \left( \frac{d}{dr} - \frac{l'}{r} \right) | K'l' \rangle \right] \end{aligned} \quad (\text{E.6})$$

**ME4**

$$\begin{aligned}
 \langle K(ls)j \| \vec{Y}_{JL}(\hat{x}) \cdot \vec{\nabla} \| K'(l's')j' \rangle &= \\
 &= \delta_{s,s'} (-)^{J+j+l+s} \sqrt{(2j+1)(2j'+1)} \begin{Bmatrix} l & J & l' \\ j' & s & j \end{Bmatrix} \langle Kl \| \vec{Y}_{JL}(\hat{x}) \cdot \vec{\nabla} \| K'l' \rangle = \\
 &= \delta_{s,s'} (-)^{j+l+s+1} \sqrt{\frac{(2j+1)(2l+1)(2J+1)(2L+1)(2j'+1)(2l'+1)}{4\pi}} \begin{Bmatrix} l & J & l' \\ j' & s & j \end{Bmatrix} \\
 &\times \left[ \begin{Bmatrix} J & l' & l \\ l'-1 & L & 1 \end{Bmatrix} \frac{\begin{pmatrix} l & L & l'-1 \\ 0 & 0 & 0 \end{pmatrix}}{\begin{pmatrix} l' & 1 & l'-1 \\ 0 & 0 & 0 \end{pmatrix}} \frac{l'}{2l'+1} \langle Kl | \left( \frac{d}{dr} + \frac{l'+1}{r} \right) | K'l' \rangle \right. \\
 &\left. + \begin{Bmatrix} J & l' & l \\ l'+1 & L & 1 \end{Bmatrix} \frac{\begin{pmatrix} l & L & l'+1 \\ 0 & 0 & 0 \end{pmatrix}}{\begin{pmatrix} l'+1 & 1 & l' \\ 0 & 0 & 0 \end{pmatrix}} \frac{l'+1}{2l'+1} \langle Kl | \left( \frac{d}{dr} - \frac{l'}{r} \right) | K'l' \rangle \right] \quad (\text{E.7})
 \end{aligned}$$

**ME5**

We note that

$$Y_{LM}(\hat{x}) \vec{\nabla} \cdot \vec{\Sigma} = \sum_J (-)^{L-J} \sqrt{\frac{2J+1}{2L+1}} \left[ \left[ Y_L \otimes \vec{\nabla} \right]^J \otimes \vec{\Sigma} \right]_M^L \quad (\text{E.8})$$

Thus

$$\begin{aligned}
 \langle K(ls)j \| Y_L(\hat{x}) \vec{\nabla} \cdot \vec{\Sigma} \| K'(l's')j' \rangle &= \sum_J (-)^{L-J} \sqrt{(2j+1)(2J+1)(2j'+1)} \\
 &\times \langle s \| \vec{\Sigma} \| s' \rangle \begin{Bmatrix} l' & s' & j' \\ J & 1 & L \\ l & s & j \end{Bmatrix} \langle Kl \| \vec{Y}_{JL}(\hat{x}) \cdot \nabla \| K'l' \rangle \quad (\text{E.9})
 \end{aligned}$$

## Radial Integrals

The radial matrix element to be calculated is,

$$\begin{aligned}
 & \langle (K_{N-1}l_N)K_N | \hat{O}(Lq\rho \sin \theta_N) | (K_{N-1}l'_N)K'_N \rangle = \\
 & = \mathcal{N}_n^{(\alpha\beta)} \mathcal{N}_{n'}^{(\alpha'\beta')} \int_0^{\frac{\pi}{2}} d\theta_N \sin^2 \theta_N \cos^{3N-4} \theta_N \\
 & \times \sin^{l_N} \theta_N \cos^{K_{N-1}} \theta_N P_n^{(\alpha\beta)}(\cos 2\theta_N) \\
 & \times \hat{O}(Lq\rho \sin \theta_N) \sin^{l'_N} \theta_N \cos^{K_{N-1}} \theta_N P_{n'}^{(\alpha'\beta')}(\cos 2\theta_N)
 \end{aligned} \tag{E.10}$$

where  $N = A - 1$ ,  $n = \frac{K'_N - K_{N-1} - l'_N}{2}$ ,  $\alpha = l_N + \frac{1}{2}$ , and  $\beta = K_{N-1} + \frac{3N-5}{2}$ .

$$I_0 = \langle (K_{A-1}l_N)K_N | j_J(Lq\rho \sin \theta_N) | (K_{A-1}l'_N)K'_N \rangle \tag{E.11}$$

$$I_1 = \langle (K_{A-1}l_N)K_N | j_J(Lq\rho \sin \theta_N) \frac{1}{Lq\rho \sin \theta_N} | (K_{A-1}l'_N)K'_N \rangle \tag{E.12}$$

$$I_2 = \langle (K_{A-1}l_N)K_N | j_J(Lq\rho \sin \theta_N) \frac{d}{d(Lq\rho \sin \theta_N)} | (K_{A-1}l'_N)K'_N \rangle \tag{E.13}$$

using the fact that

$$\begin{aligned}
 & \frac{d}{d \sin \theta_N} (\sin^{l_N} \theta_N \cos^{K_{N-1}} \theta_N P_n^{(\alpha\beta)}(\cos 2\theta_N)) = \\
 & = \sin^{l_N} \theta_N \cos^{K_{N-1}} \theta_N P_n^{(\alpha\beta)}(\cos 2\theta_N) \\
 & \times \left[ \frac{l_N}{\sin \theta_N} - \frac{K_{N-1} \sin \theta_N}{\cos^2 \theta_N} + \frac{2n(n+\beta)}{(2n+\alpha+\beta) \sin \theta_N \cos^2 \theta_N} - 2n \frac{\sin \theta_N}{\cos^2 \theta_N} \right] \\
 & - \frac{2(n+\alpha)(n+\beta)}{2n+\alpha+\beta} \sin^{l_N-1} \theta_N \cos^{K_{N-1}-2} \theta_N P_{n-1}^{(\alpha\beta)}(\cos 2\theta_N)
 \end{aligned} \tag{E.14}$$

We can now calculate numerically the integrals above.

## E.1 2-Body Matrix Elements

The 2-body matrix elements needed for the evaluation of the axial MEC include several operators, whose reduced matrix elements are not completely trivial.

A much needed equalities are the following reduced matrix elements, important

also for the isospin part, of pauli matrices:

$$\langle (\frac{1}{2} \frac{1}{2}) S' | | \vec{\sigma}_1 + \vec{\sigma}_2 | | (\frac{1}{2} \frac{1}{2}) S \rangle = \delta_{S,S'} \sqrt{S(S+1)(2S+1)} \quad (\text{E.15})$$

$$\langle (\frac{1}{2} \frac{1}{2}) 0 | | \vec{\sigma}_1 - \vec{\sigma}_2 | | (\frac{1}{2} \frac{1}{2}) 1 \rangle = -\langle (\frac{1}{2} \frac{1}{2}) 1 | | \vec{\sigma}_1 - \vec{\sigma}_2 | | (\frac{1}{2} \frac{1}{2}) 0 \rangle = -2\sqrt{3} \quad (\text{E.16})$$

$$\langle (\frac{1}{2} \frac{1}{2}) 0 | | \vec{\sigma}_1 \times \vec{\sigma}_2 | | (\frac{1}{2} \frac{1}{2}) 1 \rangle = \langle (\frac{1}{2} \frac{1}{2}) 1 | | \vec{\sigma}_1 \times \vec{\sigma}_2 | | (\frac{1}{2} \frac{1}{2}) 0 \rangle = -2\sqrt{3}i. \quad (\text{E.17})$$

These are used both for the spin and isospin operators.

By making use of the known spherical harmonics coupling:

$$[Y^{(l_1)} \otimes Y^{(l_2)}]_m^{(l)} = (-)^{l_1-l_2} \sqrt{\frac{[l_1][l_2]}{4\pi}} \begin{pmatrix} l_1 & l_2 & l \\ 0 & 0 & 0 \end{pmatrix} Y_m^{(l)} \quad (\text{E.18})$$

(here  $[l] = 2l + 1$ ) we can achieve the following formula,

$$\begin{aligned} & \langle (L'S') J' | | [Y_1 \otimes (\vec{\sigma}_1 \odot \vec{\sigma}_2)^{(1)}]^{(0)} Y_L | | (LS) J \rangle = \\ & = (-)^{J+J'+L+L'+S+S'} \frac{\sqrt{[L'][J'][L][L][J]}}{4\pi} \langle S' | | \vec{\sigma}_1 \odot \vec{\sigma}_2 | | S \rangle \\ & \sum_{L''} [L''] \begin{pmatrix} L'' & L & L \\ 0 & 0 & 0 \end{pmatrix} \left\{ \begin{matrix} L'' & L & L \\ J & S' & J' \end{matrix} \right\} \begin{pmatrix} L'' & 1 & L' \\ 0 & 0 & 0 \end{pmatrix} \left\{ \begin{matrix} L'' & 1 & L' \\ S' & J' & S \end{matrix} \right\} \end{aligned}$$

Thus,

$$\vec{O}_{\odot}^a \cdot \vec{Y}_{JLM} = (\vec{\tau}^{(1)} \odot \vec{\tau}^{(2)})^a [\vec{\Sigma}_{\odot} \otimes Y_L]_M^{(J)} \quad (\text{E.19})$$

$$\vec{T}_{\odot}^a \cdot \vec{Y}_{JLM} = (\vec{\tau}^{(1)} \odot \vec{\tau}^{(2)})^a \left\{ (-)^L \sqrt{4\pi[L]} \begin{pmatrix} 1 & L & J \\ 0 & 0 & 0 \end{pmatrix} [\vec{\Sigma}_{\odot} \otimes Y_1]^{(0)} Y_{JM} - \frac{1}{3} [\vec{\Sigma}_{\odot} \otimes Y_L]_M^{(J)} \right\} \quad (\text{E.20})$$

where  $\vec{\Sigma}_{\odot} = \vec{\Sigma}_1 \odot \vec{\Sigma}_2$ , for  $\odot = \times, +, -$ .

# Bibliography

- Ananyan, S. M., Serot, B. D., and Walecka, J. D.: 2002, *Phys. Rev. C* **66(5)**, 055502
- Arenhövel, H. and Fabian, W.: 1977, *Nucl. Phys. A* **292**, 429
- Arenhövel, H. and Sanzone, M.: 1991, *Few-Body Syst. Suppl.* **3**, 1
- Arkatov, Y. M. et al.: 1979, *Yad. Konst.* **4**, 55
- Bacca, S.: 2004, *Ph.D. thesis*, Università degli Studi di Trento, Italia and Johannes Gutenberg-Universität, Deutschland
- Bacca, S., Barnea, N., Leidemann, W., and Orlandini, G.: 2004, *Phys. Rev. C* **69(5)**, 057001
- Bacca, S., Marchisio, M. A., Barnea, N., Leidemann, W., and Orlandini, G.: 2002, *Phys. Rev. Lett.* **89(5)**, 052502
- Barnea, N.: 1997, *Ph.D. thesis*, Hebrew University of Jerusalem
- Barnea, N., Efros, V. D., Leidemann, W., and Orlandini, G.: 2001a, *Physical Review C* **63**, 057002
- Barnea, N., Efros, V. D., Leidemann, W., and Orlandini, G.: 2004, *FEW BODY SYST.* **35**, 155
- Barnea, N., Leidemann, W., and Orlandini, G.: 2000, *Phys. Rev. C* **61(5)**, 054001
- Barnea, N., Leidemann, W., and Orlandini, G.: 2001b, *Nucl. Phys. A* **693(3-4)**, 565

- Barnea, N. and Novoselsky, A.: 1997, *Ann. Phys. (N.Y)* **256**, 192
- Basdevant, J. L.: 1972, *Fortschr. Phys.* **20**, 283
- Berman, B. L., Faul, D. D., Meyer, P., and Olson, D. L.: 1980, *Phys. Rev. C* **22(6)**, 2273
- Bernard, V., Kaiser, N., and Meißner, U.-G.: 1995, *Nucl. Phys. B* **457**, 147
- Borie, E. and Rinker, G. A.: 1978, *Phys. Rev. A* **18(2)**, 324
- Brink, D. M.: 1957, *Nucl. Phys. A* **4**, 215
- Callan, C. G., Coleman, S., Wess, J., and Zumino, B.: 1969, *Phys. Rev.* **177(5)**, 2247
- Carlson, J. and Schiavilla, R.: 1994, *Phys. Rev. C* **49(6)**, R2880
- Chou, W.-T., Warburton, E. K., and Brown, B. A.: 1993, *Phys. Rev. C* **47(1)**, 163
- Coleman, S., Wess, J., and Zumino, B.: 1969, *Phys. Rev.* **177(5)**, 2239
- Colgate, S. A. and White, R. H.: 1966, *Astrophys. J.* **143**, 626
- Costantini, M. L., Ianni, A., and Vissani, F.: 2004, *Phys. Rev. D* **70(4)**, 043006
- Dellafore, A. and Brink, D. M.: 1977, *Nucl. Phys. A* **286**, 474
- Dellafore, A. and Lipparini, E.: 1982, *Nucl. Phys. A* **388**, 639
- Donnelly, T. W. and Walecka, J. D.: 1976, *Nucl. Phys. A.* **274**, 368
- Drell, S. D. and Hearn, A. C.: 1966, *Phys. Rev. Lett.* **16(20)**, 908
- Efros, V. D.: 1972, *Yad. Fiz.* **15**, 226, [Sov. J. Nucl. Phys. 15, 128 (1972)]
- Efros, V. D.: 1999, *Phys. At. Nucl.* **62**, 1833
- Efros, V. D., Barnea, N., Leidemann, W., and Orlandini, G.: 1999, *Few-Body Systems* **26**, 251

- Efros, V. D., Leidemann, W., and Orlandini, G.: 1994, *Phys. Lett. B* **338(2-3)**, 130
- Efros, V. D., Leidemann, W., and Orlandini, G.: 1997a, *Phys. Lett. B* **408**, 1
- Efros, V. D., Leidemann, W., and Orlandini, G.: 1997b, *Phys. Rev. Lett.* **78**, 432
- Efros, V. D., Leidemann, W., and Orlandini, G.: 1997c, *Phys. Rev. Lett.* **78(21)**, 4015
- Efros, V. D., Leidemann, W., Orlandini, G., and Tomusiak, E. L.: 2000, *Phys. Lett. B* **484**, 223
- Efros, V. D., Leidemann, W., Orlandini, G., and Tomusiak, E. L.: 2004, *Phys. Rev. C* **69(4)**, 044001
- Ellerkmann, G., Sandhas, W., Sofianos, S. A., and Fiedeldey, H.: 1996, *Phys. Rev. C* **53(6)**, 2638
- Entem, D. R. and Machleidt, R.: 2003, *Phys. Rev. C* **68(4)**, 041001
- Epelbaum, E., Glöckle, W., and Meißner, U.-G.: 2000, *Nucl. Phys. A* **671**, 295
- Epelbaum, E. and Meissner, U. G.: 2006, *On the renormalization of the one-pion exchange potential and the consistency of Weinberg's power counting*
- Epstein, R. I., Colgate, S. A., and Haxton, W. C.: 1988, *Phys. Rev. Lett.* **61(18)**, 2038
- Fabian, W. and Arenhövel, H.: 1976, *Nucl. Phys. A* **258**, 461
- Feldman, G., Balbes, M. J., Kramer, L. H., Williams, J. Z., Weller, H. R., and Tilley, D. R.: 1990, *Phys. Rev. C* **42(4)**, R1167
- Fermi, E.: 1934, *Z. Phys* **88**, 161
- Foldy, L. L.: 1957, *Phys. Rev.* **107(5)**, 1303
- Friar, L.: 1975, *Ann. Phys. (N.Y)* **95**, 170

- Fuller, G. M. and Meyer, B. S.: 1995, *Astrophys. J.* **453**, 792
- Gari, M., Hebach, H., Sommer, B., and Zabolitzky, J. G.: 1978, *Phys. Rev. Lett.* **41(19)**, 1288
- Gazit, D., Bacca, S., Barnea, N., Leidemann, W., and Orlandini, G.: 2006a, *Phys. Rev. Lett.* **96(11)**, 112301
- Gazit, D. and Barnea, N.: 2004, *Phys. Rev. C* **70(4)**, 048801
- Gazit, D. and Barnea, N.: 2007a, in prep.
- Gazit, D. and Barnea, N.: 2007b, *Nucl. Phys. A* **790(1-4)**, 356
- Gazit, D. and Barnea, N.: 2007c, *Phys. Rev. Lett.* **98(19)**, 192501
- Gazit, D., Barnea, N., Bacca, S., Leidemann, W., and Orlandini, G.: 2006b, *Phys. Rev. C* **74(6)**, 061001
- Gerasimov, S. B.: 1964, *Phys. Lett.* **13**, 240
- Gerasimov, S. B.: 1965, *Yad. Fiz.* **2**, 598, [Sov. J. Nucl. Phys. 2, 430 (1966)]
- Golak, J., Skibinski, R., Gloeckle, W., Kamada, H., Nogga, A., Witala, H., Efros, V. D., Leidemann, W., Orlandini, G., and Tomusiak, E. L.: 2002, *Nucl. Phys. A* **707**, 365
- Golak, J., Skibinski, R., Witala, H., Gloeckle, W., Nogga, A., and Kamada, H.: 2005, *Phys. Rep.* **415**, 89
- Goldstone, J., Salam, A., and Weinberg, S.: 1962, *Phys. Rev.* **127(3)**, 965
- Grdestig, A. and Phillips, D. R.: 2006, *Phys. Rev. Lett.* **96(23)**, 232301
- Haxton, W. C.: 1988, *Phys. Rev. Lett.* **60(20)**, 1999
- Heinze, W., Arenhövel, H., and Horlacher, G.: 1978, *Phys. Lett. B* **76**, 379
- Horowitz, C. J. and Schwenk, A.: 2006a, *Nucl. Phys. A* **776**, 55

- Horowitz, C. J. and Schwenk, A.: 2006b, *Phys. Lett. B* **638**, 153
- Kuhn, W.: 1923, *Z. Phys.* **33**, 408
- Lanzos, C.: 1950, *J. Res. Nat. Bur. Stand.* **45**, 255
- Landerburg, R. and Reiche, F.: 1923, *Naturwiss* **11**, 873
- Lazauskas, R. and Carbonell, J.: 2004, *Phys. Rev. C* **70**, 044002
- Levinger, J. S. and Bethe, H. A.: 1950, *Phys. Rev.* **78(2)**, 115
- Livne, E.: 2007, private communication
- Lunardini, C. and Smirnov, A. Y.: 2004, *Astroparticle Physics* **21**, 703
- Marcucci, L. E., Schiavilla, R., Viviani, M., Kievsky, A., Rosati, S., and Beacom, J. F.: 2000, *Phys. Rev. C* **63(1)**, 015801
- Meyer, B. S.: 1995, *Astrophys. J.* **449**, L55
- Mintkevich, O. and Barnea, N.: 2004, *Phys. Rev. C* **69(4)**, 044005
- Navrátil, P. and Barrett, B. R.: 1996, *Phys. Rev. C* **54(6)**, 2986
- Navrátil, P. and Barrett, B. R.: 1998, *Phys. Rev. C* **57(2)**, 562
- Navrátil, P. and Barrett, B. R.: 1999, *Phys. Rev. C* **59(4)**, 1906
- Nilsson, B. et al.: 2005, *Phys. Lett. B* **626**, 65
- Nogga, A., Kamada, H., Glöckle, W., and Barrett, B. R.: 2002, *Phys. Rev. C* **65(5)**, 054003
- Nogga, A., Kievsky, A., Kamada, H., Glöckle, W., Marcucci, L. E., Rosati, S., and Viviani, M.: 2003, *Phys. Rev. C* **67(3)**, 034004
- Nogga, A., Timmermans, R. G. E., and van Kolck, U.: 2005, *Phys. Rev. C* **72(5)**, 054006

- Novoselsky, A., Katriel, J., and Gilmore, R.: 1988, *Journal of Mathematical Physics* **29**, 1368
- O'Connor, E., Gazit, D., Horowitz, C. J., Schwenk, A., and Barnea, N.: 2007, *Phys. Rev. C* **75**, 055803
- Ohnishi, N., Kotake, K., and Yamada, S.: 2006, *Inelastic Neutrino-Helium Scatterings and Standing Accretion Shock Instability in Core-Collapse Supernovae*
- Ordóñez, C., Ray, L., and van Kolck, U.: 1994, *Phys. Rev. Lett.* **72(13)**, 1982
- Orlandini, G.: 2004, *Nucl. Phys. A* **737**, 210
- Park, T.-S., Marcucci, L. E., Schiavilla, R., Viviani, M., Kievsky, A., Rosati, S., Kubodera, K., Min, D.-P., and Rho, M.: 2003, *Phys. Rev. C* **67(5)**, 055206
- Pudliner, B. S., Pandharipande, V. R., Carlson, J., Pieper, S. C., and Wiringa, R. B.: 1997, *Phys. Rev. C* **56(4)**, 1720
- Quaglioni, S., Barnea, N., Efros, V. D., Leidemann, W., and Orlandini, G.: 2004, *Phys. Rev. C* **69**, 044002
- Rho, M.: 2006
- Schiavilla, R., Fabrocini, A., and Pandharipande, V.: 1987, *Nucl. Phys. A* **473**, 290
- Schiavilla, R., Stoks, V. G. J., Glöckle, W., Kamada, H., Nogga, A., Carlson, J., Machleidt, R., Pandharipande, V. R., Wiringa, R. B., Kievsky, A., Rosati, S., and Viviani, M.: 1998, *Phys. Rev. C* **58(2)**, 1263
- Schiavilla, R. and Wiringa, R. B.: 2002, *Phys. Rev. C* **65(5)**, 054302
- Shen, H., Toki, H., Oyamatsu, K., and Sumiyoshi, K.: 1998, *Progress of Theoretical Physics* **100**, 1013
- Shima, T., Naito, S., Nagai, Y., Baba, T., Tamura, K., Takahashi, T., Kii, T., Ohgaki, H., and Toyokawa, H.: 2005, *Phys. Rev. C* **72**, 044004

- Siegert, A. J. F.: 1937, *Phys. Rev.* **52(8)**, 787
- Suzuki, K. and Lee, S. Y.: 1980, *Prog. Theor. Phys.* **64**, 2091
- Suzuki, K. and Lee, S. Y.: 1982, *Prog. Theor. Phys.* **68**, 246
- Suzuki, K. and Lee, S. Y.: 1983, *Prog. Theor. Phys.* **70**, 439
- Suzuki, T., Chiba, S., Yoshida, T., Kajino, T., and Otsuka, T.: 2006, *Phys. Rev. C* **74(3)**, 034307
- Suzuki, Y. and Varga, K.: 1998, *Stochastic Variational Approach to Quantum Mechanical Few-Body Systems*, Springer-Verlag, Berlin
- Thomas, L. H.: 1925, *Naturwiss* **13**, 627
- van Kolck, U.: 1994, *Phys. Rev. C* **49(6)**, 2932
- Viviani, M., Kievsky, A., and Rosati, S.: 2005, *Phys. Rev. C* **71(2)**, 024006
- Walecka, J. D.: 1995, *Theoretical Nuclear and Subnuclear Physics*, Oxford Univ. Press, New York
- Weinberg, S.: 1979, *Physica* **A96**, 327
- Weinberg, S.: 1996, *The Quantum Theory of Fields, Vol. 2: Modern Applications*, Cambridge Univ. Press, Cambridge, UK
- Wells, D. P., Dale, D. S., Eisenstein, R. A., Federspiel, F. J., Lucas, M. A., Mellendorf, K. E., Nathan, A. M., and O'Neill, A. E.: 1992, *Phys. Rev. C* **46(2)**, 449
- Weng, W., Kuo, T., and Brown, G.: 1973, *Phys. Lett. B* **46**, 329
- Wiringa, R. B., Pieper, S. C., Carlson, J., and Pandharipande, V. R.: 2000, *Phys. Rev. C* **62**, 014001
- Wiringa, R. B., Stoks, V. G. J., and Schiavilla, R.: 1995, *Phys. Rev. C* **51(1)**, 38

- Woosley, S. E., Hartmann, D. H., Hoffman, R. D., and Haxton, W. C.: 1990, *Astrophys. J.* **356**, 272
- Woosley, S. E. and Hoffman, R. D.: 1992, *Astrophys. J.* **395**, 202
- Woosley, S. E. and Weaver, T. A.: 1995, *Astrophys. J. Suppl. Ser.* **101**, 181
- Yao, W.-M. et al.: 2006, *Journal of Physics G* **33**
- Yoshida, T., Kajino, T., and Hartmann, D. H.: 2005, *Phys. Rev. Lett.* **94(23)**, 231101
- Yoshida, T., Kajino, T., Yokomakura, H., Kimura, K., Takamura, A., and Hartmann, D. H.: 2006, *Phys. Rev. Lett.* **96(9)**, 091101

# ACKNOWLEDGEMENTS

---

Writing this section is always a pleasure, not only because I write it at the end of the work, but also since I treasure the help given to me by many people in the period of the PhD.

First of all, I would like to thank Nir Barnea, who has been more than a supervisor, who put his trust in me and gave me the opportunity to research with him. This gratitude stretches to the long coffee-breaks, and the even longer arguments.

I am more than grateful to Prof. G. Orlandini and Prof. W. Leidemann, for all the physics I have learned from them, and for giving me the feeling of a colleague rather than a student. I would also like to thank each and every one of the other co-authors of the papers which constitute this work: Sonia Bacca, Evan O'connor, Achim Schwenk, and Chuck Horowitz.

Third, this work would not have been such joy without the people of the Physics department, with whom every day is a new experience. Among others Yuval Birnboim deserves some kind of a prize for tolerating my changing moods; Shmulik Balberg and Eli Livne for many fruitful discussions; TT, Ami, Shimon, who made these times memorable.

Most important are of course all my family: my parents, my sisters and my grandparents. For the constant support, reassurance and encouragement, which made this difficult session more tolerable.

Last, and definitely not least, I would like to thank my wife Shani, for helping through difficult times; for taking on every burden; and of course for convincing me to take Daffy...